Flight guidance along 3D+T trajectories and space indexed traffic management

Mastura Ab Wahid

THÈSE

En vue de l'obtention du

DOCTORAT DE L'UNIVERSITÉ DE TOULOUSE

Délivré par : *l'Université Toulouse 3 Paul Sabatier (UT3 Paul Sabatier)*

Présentée et soutenue par :
MASTURA AB WAHID
le *8/12/2015*
Titre:

FLIGHT GUIDANCE ALONG 3D+T TRAJECTORIES AND SPACE INDEXED TRAFFIC MANAGEMENT

École doctorale er discipline ou spécialité
ED MITT : Domaine Mathématiques : Mathématiques appliquées

Unité de recherche :
Laboratoire de Mathématiques Appliquées, Informatique et Automatique pour l'Aérien (MAIAA), ENAC

Directeurs de Thèse :
FÉLIX MORA-CAMINO (Directeur)
ANTOINE DROUIN (Co-Directeur)

Jury :

FRANCISCO JAVIER SAEZ NIETO	Rapporteur
DAVID ZAMMIT-MANGION	Rapporteur
BENOÎT DACRE-WRIGHT	Examinateur
CHRISTIAN BÈS	Examinateur
DANIEL CHOUKROUN	Examinateur

INTENTIONALLY LEFT BLANK

ACKNOWLEDGMENT

Firstly I would like to give my gratitude to the Ministry of Education Malaysia and Universiti Teknologi Malaysia (UTM) for giving me a scholarship to pursue my studies in France for both Master and PhD degrees from 2010 to 2015. Secondly, I am thankful to my Supervisor Prof. Dr. Felix Mora-Camino for accepting me in MAIAA laboratory as his PhD student and for being attentive with me. I have learned a lot under his guidance and his many ideas have helped me to complete this thesis. Thank you. Thirdly, I want to thank my second supervisor, Dr. Antoine Drouin who helped me with the numerical simulation part. Also, I want to thank my colleague, now Dr. Hakim Bouadi, who has given me assistance during my first year of internship. I found his thesis to be very useful as a basis for my own research. Also, not forgetting the important people in my life, my husband, both my parents and in-laws and my sisters who have given me moral support, for that I thank you. Last but not least, I would like to give my sincerest gratitude to all my friends here in this lab, in Toulouse and Malaysia. The discussion that we had either about the research or other things have given me ideas, helped me find solutions and also helped me unwind during my PhD years. Thank you All.

To my loving husband Suffyan…

To my supportive parents Ab Wahid, Norbiha…

ABSTRACT

With the increase in air traffic, surely a question of flight efficiency (delays), environment impact and safety arise. This calls for improvements in accuracy of spatial and temporal trajectory tracking. The first main objective of this thesis is to contribute to the synthesis of a space-indexed nonlinear guidance control law for transportation aircraft presenting enhanced tracking performances and to explore the performances and feasibility of a flight guidance control law which is developed based on a space-indexed reference to track a 3D+T reference trajectory using nonlinear dynamic inversion control. The proposed guidance control law present reduced tracking errors and able to meet more easily overfly time constraints. Before presenting the main approaches for the design of the 3D+T guidance control laws; the modern flight guidance and flight dynamics of transportation aircraft, including explicitly wind components are first introduced. Then, a description of the current and modern air traffic organization including the organization of air traffic in high density flow will be shown and this will lead to a description of the Airstreams concept. This proposed concept is to organize main traffic flows in congested airspace along airstreams which are characterized by a three dimensional (3D) common reference track (ASRT). Finally, a scenario to perform basic maneuvers inside the airstream following a 3D+T trajectory using a common space-indexed will be developed and will be used to illustrate the traffic management along an airstream.

Keywords: Airstreams, 3D+T trajectory tracking, flight guidance, space-indexed nonlinear control.

RESUME

Avec la forte augmentation actuelle et future du trafic aérien, les questions relatives à la capacité, la sécurité et les effets environnementaux du transport aérien vont se poser de façon chaque fois plus critique. L'objectif général de cette thèse est de contribuer à l´amélioration de l'opération et de l´organisation du trafic aérien dans cette perspective de croissance.

Le premier objectif spécifique de cette thèse est de faire la synthèse d'une loi de commande permettant aux avions de transport de suivre avec précision une trajectoire 3D+T.

Le deuxième objectif spécifique de cette thèse est d´introduire une organisation particulière des corridors aériens, les airstreams, compatible avec la loi de guidage développée et permettant d´utiliser au mieux la capacité du corridor.

Ainsi dans une première étape est introduite la dynamique de guidage des avions de transport, ainsi que les systèmes de guidage et de gestion du vol des avions modernes. Ensuite les principaux éléments de l´organisation de la gestion et du contrôle du trafic aérien sont introduits. La loi de guidage 3D+T est développée, simulée et ses performances sont analysées. L´étude d´une manœuvré de changement de voie dans un airstream est alors menée et mise en œuvre dans le cadre de la gestion du trafic à l'intérieur de celui-ci. Finalement les conclusions et perspectives de cette étude sont présentées.

Mots-clés: Airstream, suivi de trajectoire 3D+T, guidage du vol, commande non linéaire indexées espace.

CONTENTS

Acknowledgment i

Abstract v

Résumé vii

Contents ix

List of Figures xiii

List of Tables xvii

Nomenclature xix

CHAPTER 1 General Introduction 1

CHAPTER 2 Transportation Aircraft Flight Dynamics 7

2.1 Introduction 9

2.2 The reference frames 9

2.3 Frame Transformations 12

2.4 Aircraft Speeds and Wind Speed 14

2.5 Flight path angle 18

2.6 The Standard Atmosphere 18

2.7 Flight dynamic equations 20

2.7.1 Forces 22

2.7.2 Moments 24

2.8 A State Representation of Flight Dynamics 25

2.9 Global view of Flight Equations 27

2.10 Conclusion 28

CHAPTER 3 Modern Flight Guidance SystemS 29

3.1 Introduction 31
3.2 The Flight Management Systems 32
3.2.1 Flight Management Functions 32
3.2.2 Horizontal Flight Plan Composition and Construction 33
3.2.3 Vertical Flight Plan composition and construction 35
3.2.4 Pilot's Flight Plan modification capability 38
3.3 Flight Guidance Systems (FGS) 39
3.3.1 Classification of Flight guidance modes 39
3.3.2 Flight Guidance laws 43
3.4 Flight Guidance Protections 44
3.5 Conclusion 48
CHAPTER 4 Modern Organization Of Traffic Management 49
4.1 Introduction 51
4.2 Current Traffic Management Space Organization 52
4.3 Modern Traffic Management Space Organization 57
4.3.1 Performance Based Operations (PBO) 57
4.4 Free Flight 61
4.4.1 Definition and objectives 61
4.4.2 Traffic Separation Systems for Free Flight 62
4.4.3 Free Flight Implementation 64
4.5 SESAR and NEXTGEN Objectives 66
4.5.1 Projects' objectives 66
4.5.2 Implementations of TBO 68
4.6 Conclusion 69
CHAPTER 5 New Organizations for High Density Traffic Flows 71
5.1 Introduction 73
5.2 Flow Corridors 73

5.2.1 Flow corridors organizations 74
5.2.2 Estimating safety within flow corridors 77
5.3 Airstreams 79
5.3.1 Definition of airstream 80
5.3.2 Reference Tracks and Frames 81
5.3.3 Local Axial Reference Frames 82
5.3.4 Coordinates transformation 83
5.3.5 Slot Characteristics 88
5.3.6 Expected benefits and challenges from airstream 89
5.4 Conclusion 90
CHAPTER 6 3D+T Guidance 91
6.1 Introduction 93
6.2 Space-Indexed versus Time-Indexed Dynamics 94
6.3 Tracking control objectives 96
6.4 Considered aircraft Guidance Dynamics 101
6.5 Inverting guidance dynamics 104
6.6 Simulation results 109
6.6.1 Rejection of perturbations 110
6.6.2 Tracking of trajectories 111
6.6.3 Comparison of time and spatial laws 113
6.7 Conclusion 114
CHAPTER 7 Feasibility of the proposed approach 115
7.1 Introduction 117
7.2 Data accuracy 117
7.2.1 Current Performance of onboard sensors 118
7.2.2 Performance Analysis of the tracking system with data inaccuracy 120
7.3 Robustness to parameters errors 123

7.4 Compatibility with current auto-pilots 125
7.5 Invertibility 127
7.5.1 Invertibility analysis 127
7.6 Conclusion 129
CHAPTER 8 Towards Traffic Management along airstreams 131
8.1 Introduction 133
8.2 Configuration inside the airstream 133
8.3 Reference shift maneuver between lanes 134
8.3.1 Reference shift trajectories between lanes 135
8.3.2 Characterization of the reference trajectory 136
8.4 Traffic management along an airstream 139
8.4.1 Heuristic Assignment 140
8.4.2 Illustration of traffic assignment 142
8.5 Conclusion 145
CHAPTER 9 Conclusion and Perspectives 147
REFERENCES 153
APPENDIX A Nonlinear Dynamic Inversion 165
APPENDIX B Research Civil Aircraft Model (RCAM) Data 173

LIST OF FIGURES

Figure 2.1: Earth Centered Inertial Frame and Earth-Ceterd Earth-Fixed Frame [Fr.mathworks.com, 2015] 10
Figure 2.2: Local Earth Frame 11
Figure 2.3: Aircraft body axis frame 11
Figure 2.4: Wind axis (w), Stability axis (s) and Body axis (b) 12
Figure 2.5: Transformation from inertial frame to the body frame [Mora-Camino, 2014] 13
Figure 2.6: Relative wind 15
Figure 2.7: Angles relating the orientation of the airspeed Va with respect to Local Earth and Body frame respectively 15
Figure 2.8: International Standard Atmosphere 20
Figure 2.9: International Standard Atmosphere 20
Figure 2.10: Aerodynamic Forces 22
Figure 2.11: Global view of flight equations [Mora-Camino, 2014] 27
Figure 3.1: Overall classical structure of flight control systems [Mora-Camino, 2014] 32
Figure 3.2: Flight Management System (FMS) Block Diagram [Collinson, 2011] 33
Figure 3.3: Multifunction Control Display Unit (MCDU) [Wikipedia, 2015d] 34
Figure 3.4: Example of lateral (track) flight plan 35
Figure 3.5: Vertical Flight Profile [Collinson, 2011] 37
Figure 3.6: Primary Flight Display (PFD) – Boeing term[Wikipedia, 2015c] 40
Figure 3.7: Navigation Display (ND) – Boeing term. Indicates the aircraft track, waypoints / pseudo-waypoints and other navigation information [Wikipedia, 2015a] 40
Figure 3.8: Flight Control Unit (FCU) – Airbus term: Mode engagement and target selection capability [Meriweather, 2013] 41

Figure 3.9: Example architecture of FMS/FGS in A320 [Bouadi, 2013] 43
Figure 3.10: GPWS thresholds modes with the aural and visual warning[GPS, 2001].....46
Figure 4.1 : General Airspace Classification [FAA, 2013].....53
Figure 4.2: Example of routes segregation and convergent of traffic at the entry [EUROCONTROL, 2014] 56
Figure 4.3: Good design practice proposed by ICAO for departure (DEP) and arrival (ARR) vertical constraints [EUROCONTROL, 2010].....56
Figure 4.4: From classical to RNAV operation [Todorov, 2009] 58
Figure 4.5: RNP-X definition means that navigation system must be able to calculate its position to within a circle with a radius of X nautical miles. The 2 x RNP containment limit represents the level of assurance of the navigation performance with a 99.999% percent probability per flight hour 59
Figure 4.6 : Navigation specification for RNP and RNAV.....59
Figure 4.7: Corresponding RNP designation to the TSE value [AIRBUS, 2009].....60
Figure 4.8: Definition of NSE, FTE and PDE [AIRBUS, 2009] 60
Figure 4.9: US expected evolution of traffic management [Barraci, 2010] 62
Figure 4.10: Overview of the traffic separation system 63
Figure 4.11 : The Aircraft Protection Zone.....63
Figure 4.12: Countries that have fully/partially implemented FRA as of end 2014 [EUROCONTROL, 2015c].....65
Figure 4.13: Example of continuous descent approach (CDA) and continuous climb operation (CCO).....68
Figure 5.1: Nominal design of Corridor Building block [Yousefi et al., 2010].....74
Figure 5.2: Separation Requirements 75
Figure 5.3: Speed-Dependent Track – designated by nominal Mach number [Wing et al., 2008].....75
Figure 5.4: Speed independent track[Wing et al., 2008].....76
Figure 5.5: Conflict resolution: Speed of aircraft A is 250m/s while aircraft B is 230 m/s. Both aircraft make a slight left and right turn to achieve required separation.....78
Figure 5.6 : Example of cross-section of an airstream 80
Figure 5.7: Guidance along an aircraft reference trajectory.....82

Figure 5.8 : The local airstream frame at point *S* 82
Figure 5.9 : Reference point in cross section plane 83
Figure 5.10: Track speed along the ASRT 85
Figure 6.1: Organization of traffic around a common reference track (ASRT) 94
Figure 6.2: Projection of airspeed along ASRT 94
Figure 6.3: Piloting and Guidance Dynamics 96
Figure 6.4: Aircraft following the center of a moving slot. 100
Figure 6.5: Simulation settings 109
Figure 6.6: Perturbation rejection property of the guidance law 110
Figure 6.7: Wind gust rejection during a constant velocity horizontal trajectory 111
Figure 6.8: Tracking of a 3D+T trajectory consisting in a change of velocity at constant altitude and heading 112
Figure 6.9: Tracking of a 3D+T trajectory consisting in a change of altitude at constant velocity 112
Figure 6.10: Tracking of a 3D+T lane change trajectory 113
Figure 6.11: Pertubation rejection of a traditional time-indexed NLI guidance law 113
Figure 6.12: Pertubation rejection of the space-indexed NLI guidance law 113
Figure 7.1: Non-invertibility situations 128
Figure 7.2: Non-invertibility situations in cruise 128
Figure 8.1: Standard shift maneuver in an airstream 134
Figure 8.2: Standard shift maneuver between lanes in an ASRT 136
Figure 8.3: Example of transient (blue) flights and assigned (green) flight along an ASRT 140

LIST OF TABLES

Table 2.1: ISA assumes the conditions at mean sea level (MSL) 19
Table 2.2: Variation of TLR according to altitude 19
Table 3.1: Lateral Guidance Modes [Tribble et al., 2002] 41
Table 3.2: Vertical Guidance Modes [Tribble et al., 2002] 42
Table 4.1: Separation Minima 54
Table 4.2: Horizontal Separation Minima for non-radar area between two aircraft 55
Table 7.1: Attitude Performance of inertial navigation systems (INS) with GPS-updating [Schwarz, 1996] 118
Table 7.2: Velocity performance of inertial navigation systems (INS) with GPS-updating [Schwarz, 1996] 118
Table 7.3: ICAO GNSS Signal-in-Space Performance Requirements [Spitzer, 2001] 119
Table 7.4: Actual GNSS Signal-in-Space Performance [Spitzer, 2001] 119
Table 7.5: A typical air-data computer accuracy requirements [Kayton and Fried, 1997] 119
Table 8.1: Initial situation in ARST 144
Table 8.2: First ranking between transient flights 144
Table 8.3: Final proposed assignment and performance 145
Table B.0.1: Aircraft Configuration 175
Table B.0.2: Aerodynamic Data 175

NOMENCLATURE

3D+T	3 Dimensional Plus Time
A/THR	Auto-Throttle
AP	Auto-Pilot
ASAS	Airborne Separation Assurance System
ASRT	Airstream Reference Track
ATC	Air Traffic Control
ATC	Air Traffic Controller
ATFM	Air Traffic Flow And Capacity Management
ATM	Air Traffic Management
ATS	Air Traffic Services
CNS/ATM	Communications, Navigation, And Surveillance/Air Traffic Management
ECEF	Earth-Centered Earth-Fixed
ECI	Earth-Centered-Inertial Axis
FAA	Federal Aviation Association
FANS	Future Air Navigation Systems
F_B	Body-Reference Frame
FCU	Flight Control Unit
FGS	Flight Guidance Systems
FMS	Flight Management Systems
F_s	Stability Reference Frame
F_W	Wind Reference Frame
GNSS	Global Navigation Satellite Systems
GS	Ground Speed
ICAO	International Civil Aviation Organization
LEF	Local Earth Frame

MCDU	Multifunction Control Display Unit
ND	Navigational Display
NEXTGEN	Next Generation Air Transportation System
PBN	Performance Based Navigations
PBO	Performance Based Operations
PDF	Primary Flight Display
RNAV	Area Navigation
RNP	Required Navigation Performance
SESAR	Single European Sky Atm Research
TBO	Trajectory Based Operations
TCAS	Traffic Collision Avoidance System
TLR	Temperature Lapse Rate
TMA	Terminal Maneuvering Area
$\dot{x}$	Aircraft Inertial Velocity In X-Direction
$\dot{y}$	Aircraft Inertial Velocity In Y-Direction
$\dot{z}$	Aircraft Inertial Velocity In Z-Direction
$\bar{c}$	Mean Aerodynamic Chord
α_i	Gain For $i \in \{x, y, z\}$
ω_{si}	Space Natural Frequency For $i \in \{x, y, z\}$
ω_{ni}	Time Natural Frequency For $i \in \{x, y, z\}$
$m_{j^*}^f$	Merging Trajectory
$\dot{()}$	Rate Of The Concerned Variables
ω	Angular Rate
ψ	Yaw Angle
θ	Pitch Angle
ϕ	Roll Angle
γ	Flight Path Angle
ψ	Heading Angle
α	Angle Of Attack
β	Side Slip Angle
ρ	Axial Distance

σ	Azimuth Angle
ε	Tracking Error
ρ_a	Air Density
δ_e	Elevator Deflection
δ_r	Rudder Deflection
δ_{TH}	Thrust Command
C_D	Aerodynamic Drag Coefficient
C_L	Aerodynamic Lift Coefficient
C_{LM}	Yawing Moment Coefficient
C_M	Pitching Moment Coefficient
C_N	Rolling Moment Coefficient
C_Y	Aerodynamic Side Force Coefficient
D	Aerodynamic Drag Force
F	Forces
g	Gravity
J_a	Set Of Assigned Aircraft
J_T	Set Of Non-Assigned/Transient Aircraft
L	Longitude Angle
L	Aerodynamic Lift Force
M	Latitude Angle
m	Mass
M_j	Set Of Conflict Free Trajectories
p	Roll Rate
q	Pitch Rate
R	Distance To The Center Of The Earth
r	Yaw Rate
S	Area Of The Wing
s	Curvilinear Abscissa
t	Time
u	Aircraft Body Velocity In X-Direction
$\underline{V}$	Speed
v	Aircraft Body Velocity In Y-Direction
$\underline{V_a}$	Airspeed

w	Aircraft Body Velocity In Z-Direction
$\underline{W}$	Wind Components In Body Frame
$\underline{w}$	Wind Components In Body Frame
Y_F	Aerodynamic Side Force
X	Direction Along X-Axis
Y	Direction Along Y-Axis
Z	Direction Along Z-Axis

SUBSCRIPT

W	Components Wind Axis
b	Components Body Axis
E	Components Local Earth Frame
S	Components Stability Frame
g	Gravitational Forces
T	Thrust Forces
a	Components Of Aerodynamic Forces
s	Position On The Curvilinear Abscissa S
ASRT	Along Airstream Reference Track
c	Input Command

CHAPTER 1
GENERAL INTRODUCTION

Chapter 1: General Introduction

It is forecasted that by the year 2035, both Europe and United States will be handling up to 1.4 billion air travellers/passengers [IATA, 2014], [STATFOR, 2013] and consequencely increasing the air traffic volume. With the increase in air traffic, inevitably questions about flight efficiency (delays), impacts on the environment and safety will arise. To face these issues, improvements in accuracy and reliability of spatial and temporal trajectory tracking by transportation aircraft are expected. Already in 1993, the Special Committee on Future Air Navigation Systems (FANS) provided a recommendation called Communications, Navigation, and Surveillance/Air Traffic Management (CNS/ATM) for the design of new on-board systems. These CNS/ATM systems were to ease the handling and transfer of information, improve aircraft surveillance using latest technology (Automatic Dependent Surveillance Systems) and increase aircraft navigational accuracy (Area Navigation (RNAV) and Global Navigation Satellite Systems (GNSS)).

The demand from CNS/ATM to modernize the future air navigation resulted in worldwide research and more recently in two pioneer projects: the Single European Sky ATM Research (SESAR) project and the american Next Generation Air Transportation System (NextGen) project. The main improvements expected from Future Air Navigation systems were:

- Strategic data link services for sharing of information;
- Negotiation of planning constraints between ATC (Air Traffic Control) and aircraft in order to ensure planning consistency;
- The use of the 3D+T aircraft trajectory information in the Flight Management System for ATC operations.

An exigency of future ATM systems is to have a safe, efficient and predictable flight through a continuous accurate knowledge of the aircraft position [Christopher et al., 2013, De Prins et al., 2013]. Then flight plans should become 3D+T (3 space dimensions and time) objects allowing what is called today Trajectory Based Operations (TBO) [Cate, 2013, Doc9750-AN/963, 2002, Ashford, 2010, Bowen, 2014, Hayman, 2009]. TBO appears to be a key to manage very large volumes of air

traffic in restrained space and time. Also, TBO integrates advanced Flight Management System (FMS) capabilities with ground automation to manage aircraft trajectories in latitude, longitude, altitude, and time in order to dynamically adapt the aircraft flight path to new ATC directives. As a consequence, TBO would allow aircraft to fly safely in high density air flows while adopting efficient trajectories in the context of Free Flight [Kotecha and Hwang, 2009, Ye et al., 2014, Yousefi et al., 2010]. Free Flight and Corridor Flows are some of the research and development projects contribution to TBO [Bowen, 2014, Enea and Porretta, 2012, NextGEN, 2010].

The current air transportation aircraft guidance systems generate in real time corrective actions to maintain the flight trajectory as close as possible to the flight plan or to comply with the spatial or temporal directives issued by ATC. Wind remains one of the main causes for guidance errors and flight inefficiency [Miele, 1990, Psiaki and Park, 1992, Stengel and Psiaki, 1985]. Today the the current navigation systems on board commercial aircraft present a high accuracy and reliability through the fusion of air data, inertial data and satellite information . With classical control techniques, the corresponding guidance errors are still large even with the adoption of time-based guidance control laws [Mulgund and Stengel, 1996]. The recent introduction of space-indexed guidance control laws provides a new perspective for improved tracking performances and enhanced track predictability, even in the presence of wind [Bouadi and Mora-Camino, 2012, Bouadi et al., 2012]. High density air traffic situations will lead to guidance requirements where aircraft are to follow with accuracy a 3D+T trajectory to ensure traffic safety. This leads to the concept of space-indexed control which has been initially developed in 2D+T for vertical guidance in [Bouadi et al., 2012].

Therefore, the first objective of this thesis is to contribute to the synthesis of a space-indexed nonlinear guidance control law for transport aircraft presenting enhanced 3D+T tracking performances.

The second objective of this thesis is to explore the performance and feasibility of a flight guidance control law designed to make the aircraft follow a 3D+T trajectory within a high density traffic corridor. The case of an airstream (introduced

in Chapter 5) with synchronized slots along lanes and nominal lane change trajectories will be more particularly considered in Chapter 8.

The relevent background, the adopted methodology and the main findings of this research are presented in this report dissertation . The first chapters describe the principal object of this study, i.e. the transportation aircraft and its flight dynamics, then the current technological and methodological environment is introduced either when considering on-board systems or considering air traffic management and control. Current developments and prospective organizations for high density traffic are analyzed. Then a new 3D+T guidance approch is developed and illustrated while its limitations are discussed. Trajectory tracking within an airstream is then considered, showing the interest for this space indexed organization for high density traffic. The detailed chapters organization of the report is as follows:

Chapter Two introduces the flight dynamics of transport aircraft with the main reference frames for wind, forces and motion, with a special interest for guidance dynamics. The evolution of the position of the aircraft, its translational speed, its angular attitude and rotational speed are then expressed through a 12 order nonlinear state representation. The distinction between fast and slow dynamics allows the identification on one side the piloting dynamics and on the other side the guidance dynamics.

Chapter Three describes the main characteristics, modes and functions developed by modern flight guidance systems on board transport aircraft. Then the composition and construction of traditional flight plans by Flight Management Systems (FMS) are described. This flight plan generates the main guidance references used by the flight guidance system unless some ATC directive is received or some guidance protection is activated.

Chapter Four discusses the recent evolution of the air traffic organization towards the future air traffic system. The required Navigation Performances (RNP) from the arrival/approach areas, the Terminal Maneuvering Area (TMA) and the En-Route area are introduced. Then a general presentation of modern traffic management concepts such as Performance Based Operation and Free Flight is performed. These concepts lead to the Trajectory Based Operation (TBO) approach envisioned by both NextGen and SESAR projects.

Chapter Five introduces first the concept of an air corridor which is envisioned by the United States to absorb in a safe way high density traffic within the Trajectory Based Operations (TBO) concept. Then the concept of Airstream is described, where traffic is distributed on lanes located around a geometric (3D) reference track (Airstream Reference Track-ASRT). In that case traffic on each lane is assigned in a synchronized way along moving slots.

Chapter Six formulates the 3D+T guidance problem around a reference trajectory. The tracking error requirements are given using a space indexed performance which is converted to a time-based tracking error performance. Then a normal nonlinear dynamic inversion is performed to generate the control inputs to be applied to the guidance dynamics. The fast dynamics under the inner loop of the flight control system (auto-pilot) is supposed to behave in a standard way and the design of the auto-pilot law is not considered, concentrating on the design of a generic auto-guidance law.

Chapter Seven analyzes the limitations of the control design approach presented in chapter six. Issues regarding the effect of on-board sensors inaccuracy and parameter errors on the guidance performances are considered. Also potential numerical problems are investigated and the compatibility of this new guidance function with existing guidance systems is discussed.

Chapter Eight introduces the space-indexed parameterization of a 3D+T trajectory performing the transfer from a synchronized lane to another within an airstream. This 3D+T trajectory will serve as reference for aircraft shifting from one lane to another. The management of traffic within an airstream is then considered.

Chapter Nine, the final chapter, gives a general conclusion on the main efforts developed in this research work and concludes whether the objectives are achieved. Finally a general perspective of the work and potential issues to pursue the current research are given.

CHAPTER 2
TRANSPORTATION AIRCRAFT FLIGHT DYNAMICS

Chapter 2: Transport Aircraft Flight Dynamics

2.1 Introduction

This chapter describes and analyzes the flight dynamics of transport aircraft as we are interested in designing a new guidance system for them. Once reference frames as well as the main relevant variables to describe atmospheric flight are introduced, the flight dynamics equations are established following main principles of mechanics and aerodynamics. These flight equations are shown to be composed on one side, by the fast dynamics related with rotational motion and angular attitude of the aircraft, and on the other side; by the slow dynamics related with the trajectory of the center of gravity of the aircraft. In this thesis we will be more interested with these slow dynamics, as "guidance dynamics" which are directly related with our control objective.

2.2 The reference frames

Reference frames are used to describe the motions of the aircraft with respect to the Earth and the local atmosphere. **Earth-Centered Inertial (ECI)** is defined to be stationary or moving at a constant velocity. It is inertial. This reference frame is used for the calculation of a satellite's position and its velocity; also inertial sensors produce measurement relative to the inertial frame. Its origin is located at the center of the Earth. Z_i axis points along the nominal axis of rotation. X_i lies in the equatorial plane and point towards vernal equinox. Y_i axis is orthogonal to both axes.

The Earth-Centered Earth-Fixed (ECEF) has the same origin and Z-axis as the ECI frame, but it rotates with the Earth around its North-South axis at an angular rate, ω_{IE}. It is denoted by (X,Y and Z) This is a basic coordinate frame for navigation and satellite-based radio navigation systems often used the ECEF coordinates to calculate satellite and aircraft positions.

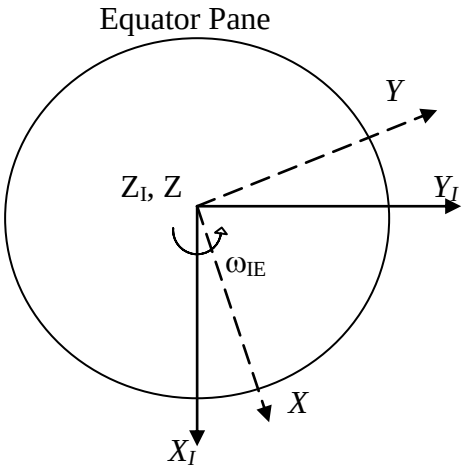

Figure 2.1: Earth Centered Inertial Frame and Earth-Ceterd Earth-Fixed Frame [Fr.mathworks.com, 2015]

The **Local Earth Frame (LEF)** shown in figure Figure 2.2 defines the angular altitude of the aircraft with respect to the Earth. The LEF is composed of X_E – axis points towards true north, the Z_E-axis is perpendicular towards the ground and the Y_E – axis completes the right-handed coordinate systems.

The Body-Axis Frame (F_B) shown in Figure 2.3 expresses the speed components (translational and rotational) with respect to the aircraft main inertial axis. Normally the sensitive axes of the accelerometer sensors are made to coincide with the axes of the moving platform in which the sensors are mounted [Noureldin et al., 2013]. The X_b axis lies in the symmetry plane of the aircraft and points forward. The Z_b axis also lies in the symmetry plane, but points downwards. (It is perpendicular to the X_b axis.) The Y_b axis can again be determined using the right-hand rule. The inertial speed in the body frame is $\underline{V}=(u,v,w)'$

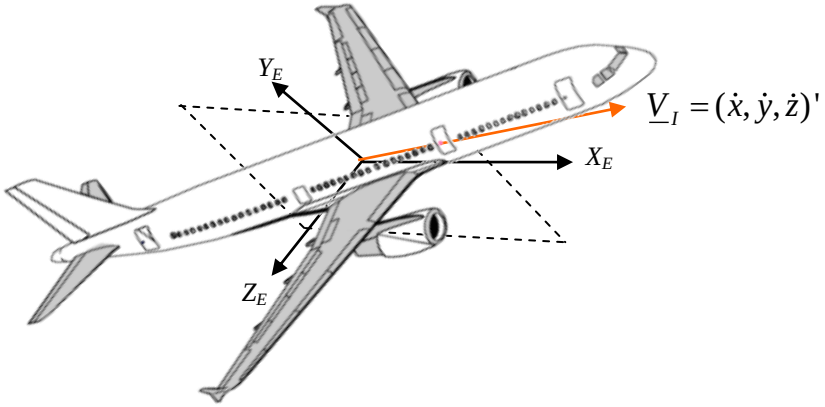

Figure 2.2: Local Earth Frame

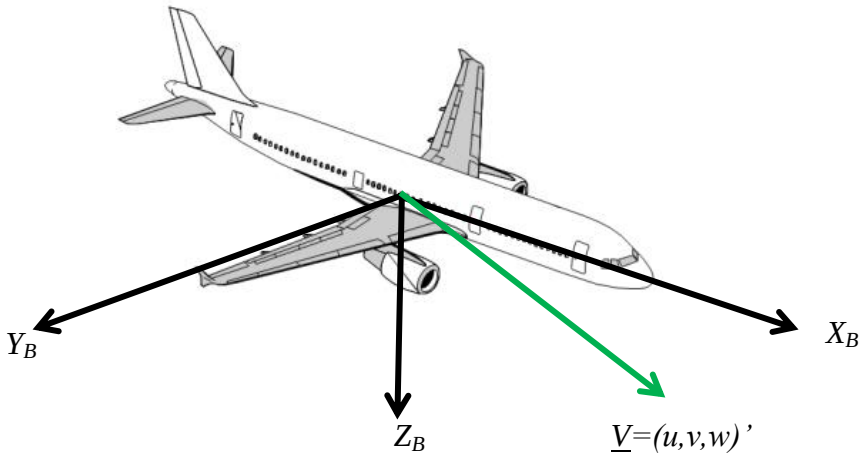

Figure 2.3: Aircraft body axis frame

The Stability Reference frame (F_S) is a body-carried coordinate system. The *Xs* axis is taken as the projection of the velocity vector of the aircraft relative to the air mass, $\underline{Va}$ into the aircraft plane of symmetry. The angle of attack α is defined as the angle between X_S and X_B. The Z_S axis lies in the plane of symmetry and Y_S axis is equal to the Y_B axis. This frame is considered as an intermediate frame equidistant to the transformation between the wind frame and the body-fixed axis system.

The Wind Reference frame (F_w) combined with the stability frame (F_S) is used to express the aerodynamic forces and moments acting on an aircraft. X_W axis is in the direction of the velocity vector of the aircraft relative to the air mass, $\underline{Va}$. The Z_W axis

is aligned to the Z_S axis and the Y_W axis can now be found using the right-hand rule. The side slip angle, β is the angle between the *Xs* and *Xw*.

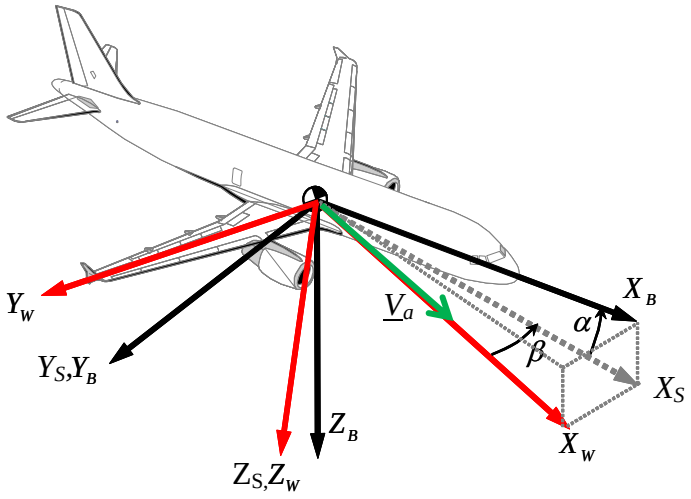

Figure 2.4: Wind axis (w), Stability axis (s) and Body axis (b)

2.3 Frame Transformations

According to the physical phenomenon considered it is more convenient to work with one frame than the other. Here the notation for a transformation is R_{IJ}, where *I* is the final frame and *J* is the initial frame.

The transformation from Local Earth Frame to the Body Frame can be done using three Euler's angles. First we have to rotate over the yaw angle, ψ, around the Z axis. Afterward we rotate over the pitch angle, θ, about the subsequent Y axis. Finally, the new resulting reference frame is then rotated over the roll angle ϕ - around its X axis. Figure 2.5 shows the transformation. The resulting equation is:

$$R_{LB}(\phi,\theta,\psi) = R^{B}_{v2}(\phi)R^{v2}_{v1}(\theta)R^{v1}_{L}(\psi) = \begin{bmatrix} c(\theta)\cdot c(\psi) & c(\theta)\cdot s(\psi) & -s(\theta) \\ s(\phi)\cdot s(\theta)\cdot c(\psi) - c(\phi)\cdot s(\psi) & s(\phi)\cdot s(\theta)\cdot s(\psi) + c(\phi)\cdot c(\psi) & c(\theta)\cdot s(\phi) \\ c(\phi)\cdot s(\theta)\cdot c(\psi) + s(\phi)\cdot s(\psi) & c(\phi)\cdot s(\theta)\cdot s(\psi) - s(\phi)\cdot c(\psi) & c(\phi)\cdot c(\theta) \end{bmatrix} \quad (2.1)$$

where $c(\cdot)$ stands for $\cos(\cdot)$ and $s(\cdot)$ stands for $\sin(\cdot)$. As this rotation matrix is orthonormal, the transformation from the Local Earth Frame to the Body Frame is obtained by inverting the above matrix or taking the transpose.

$$R_{BL}(\phi,\theta,\psi) = R_L^{v1}(-\psi)R_{v1}^{v2}(-\theta)R_L^{v1}(-\phi) = \begin{bmatrix} c(\theta)\cdot c(\psi) & s(\phi)\cdot s(\theta)\cdot c(\psi) - c(\phi)\cdot s(\psi) & c(\phi)\cdot s(\theta)\cdot c(\psi) + s(\phi)\cdot s(\psi) \\ c(\theta)\cdot s(\psi) & s(\phi)\cdot s(\theta)\cdot s(\psi) + c(\phi)\cdot c(\psi) & c(\phi)\cdot s(\theta)\cdot s(\psi) - s(\phi)\cdot c(\psi) \\ -s(\theta) & c(\theta)\cdot s(\phi) & c(\phi)\cdot c(\theta) \end{bmatrix} \tag{2.2}$$

In order to avoid angular ambiguities and to comply with transportation aircraft operations the following limits are considered:

$$-\pi < \phi < \pi,\ -\pi/2 < \theta < \pi/2, \text{ and } -\pi < \psi < \pi$$

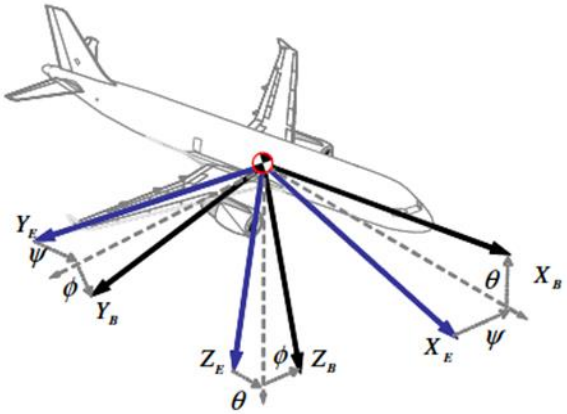

Figure 2.5: Transformation from inertial frame to the body frame [Mora-Camino, 2014]

Another transformation matrix is from the Wind Reference Frame to the Body-Axis Frame. It is used to express the aerodynamic forces and moments in the Body-Axis Frame. The aircraft is first aligned along the wind vector and then rotation through the side slip angle β is performed to reach the Stability Frame before finally a rotation by an angle α.

$$R_{WB} = R_1^B(\alpha)R_W^1(-\beta) = \begin{bmatrix} \cos\beta\cos\alpha & -\sin\beta\cos\alpha & -\sin\alpha \\ \sin\beta & \cos\beta & 0 \\ \cos\beta\sin\alpha & -\sin\beta\cos\alpha & \cos\alpha \end{bmatrix} \tag{2.3}$$

This rotation matrix is also orthonormal; therefore inversing the matrix to transform back to the Wind Frame is also achieved by transposing this matrix.

$$R_{BW} = R_W^1(\beta)R_1^B(-\alpha) = \begin{bmatrix} \cos\beta\cos\alpha & \sin\beta & \cos\beta\sin\alpha \\ -\sin\beta\cos\alpha & \cos\beta & -\sin\beta\cos\alpha \\ -\sin\alpha & 0 & \cos\alpha \end{bmatrix} \tag{2.4}$$

For the navigation purposes, we need to transform the LEF to the ECEF frame. The rotation between the ECEF and LEF frames is described by two single axis rotation matrices, and only by the longitude angle, λ, and latitude angle μ as the LEF frame is constrained to have its *z*-axis to always be perpendicular to the reference ellipsoid. The rotation matrix is given by:

$$R_{EL} = \begin{bmatrix} -\sin(\mu)\cdot\cos(\lambda) & -\sin(\lambda) & -\cos(\mu)\cdot\cos(\lambda) \\ -\sin(\mu)\cdot\sin(\lambda) & \cos(\mu) & -\cos(\mu)\cdot\sin(\lambda) \\ \cos(\mu) & 0 & -\sin(\mu) \end{bmatrix} \tag{2.5}$$

2.4 Aircraft Speeds and Wind Speed

To determine the distance an aircraft has travelled, continuous and accurate information of the ground speed *GS* should be available to the pilot and other shareholders such as the ATC and the destination airport. An aircraft ground speed *GS* can be greatly enhanced or diminished by the wind. Therefore the consideration of two speeds: wind speed $\underline{W}$ and airspeed V_a must be considered. Airspeed is the speed of an aircraft in relation to the surrounding air. Ground speed is the horizontal inertial speed of an aircraft relative to the ground given by:

$$GS = \sqrt{\dot{x}^2 + \dot{y}^2} \tag{2.6}$$

The components of the wind, $\underline{W} = (W_x, W_y, W_Z)'$ in the Local Earth Frame can be represented in the Body Frame using the transformation matrix R_{LB}:

$$\begin{pmatrix} w_x \\ w_y \\ w_z \end{pmatrix} = R_{LB} \begin{pmatrix} W_x \\ W_y \\ W_z \end{pmatrix} \tag{2.7}$$

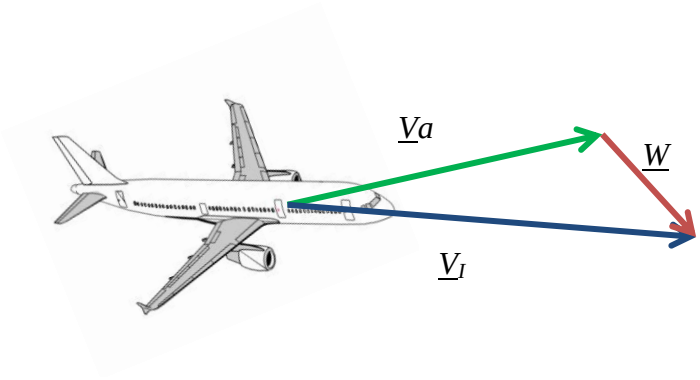

Figure 2.6: Relative wind

The relationship between the inertial speed $\underline{V}_I$, wind speed $\underline{W}$ and air speed $\underline{V}_a$ is given by:

$$\underline{V}_I = \underline{V}_a + \underline{W} \tag{2.8}$$

The inertial speed $\underline{V}_I$ can be expressed both in the Body Frame and the Local Earth Frame. Before moving into the presentation of each inertial speed $\underline{V}_I$, understanding the orientation of the aircraft airspeed $\underline{V}_a$ with respect to Body Frame and the Local Earth Frame needs to be done (Figure 2.7). The orientation of the aircraft airspeed $\underline{V}_a$ in the Local Earth Frame can be expressed by flight path angle γ and heading angle ψ while the orientation of the airspeed in the Body Frame can be defined by angle of attack α and side slip angle β:

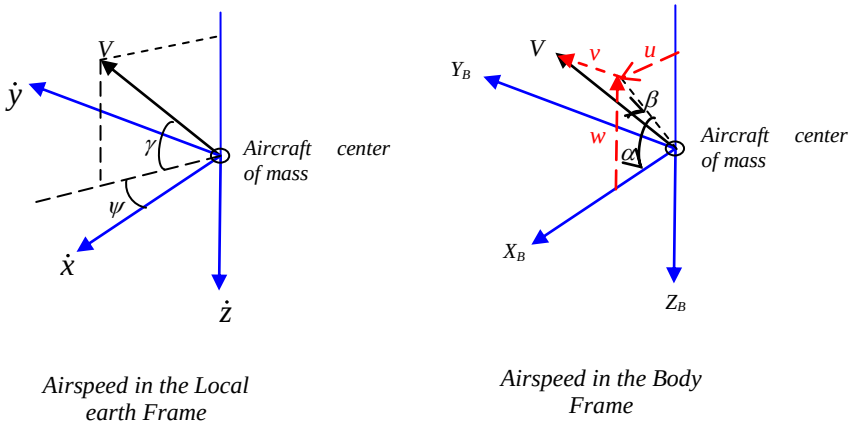

Figure 2.7: Angles relating the orientation of the airspeed Va with respect to Local Earth and Body frame respectively

Firstly, considering that there is no wind, from equation 2.8 the inertial speed $\underline{V_I}$ is the same as the aircraft airspeed $\underline{V_a}$. Hence the inertial speed in the Local Earth Frame ($\underline{V_I}$) and in the Body Frame ($\underline{V_B}$) can be defined from the observation of Figure 2.7. Then, the aircraft inertial speed in the Local Earth Frame $\underline{V_I}$ is given by:

$$\underline{V}_I = \begin{pmatrix} \dot{x} \\ \dot{y} \\ \dot{z} \end{pmatrix} = \begin{pmatrix} V_a \cos\gamma \cos\psi \\ V_a \cos\gamma \sin\psi \\ -V_a \sin\gamma \end{pmatrix} \tag{2.9}$$

and the inertial speed in the Body Frame, $\underline{V_B}$ is given by:

$$\underline{V}_B = \begin{pmatrix} u \\ v \\ w \end{pmatrix} = \begin{pmatrix} V_a \cos\alpha \cos\beta \\ V_a \sin\beta \\ V_a \cos\alpha \sin\beta \end{pmatrix} \tag{2.10}$$

Following a simple trigonometric the airspeed, V_a can be given by:

$$V_a = \sqrt{(u)^2 + (v)^2 + (w)^2} \qquad \text{or} \qquad V_a = \sqrt{(\dot{x})^2 + (\dot{y})^2 + (\dot{z})^2} \tag{2.11}$$

The angles, flight path angle γ, heading angle ψ, side slip angle β and angle of attack α can be found by:

$$\gamma = \sin^{-1}\left(\frac{-\dot{z}}{V}\right) \tag{2.12}$$

$$\psi = \sin^{-1}\left(\frac{\dot{y}}{\sqrt{\dot{x}^2 + \dot{y}^2}}\right) \tag{2.13}$$

$$\alpha = \arctan\left(\frac{w}{u}\right) \tag{2.14}$$

$$\beta = \arcsin\left(\frac{v}{V_a}\right) \tag{2.15}$$

Now we will consider when the wind speed is not zero, the inertial speed will not be the same as the airspeed. From equation 2.8 the inertial speed represented in equation 2.9 will become:

$$\underline{V}_I = \begin{pmatrix} \dot{x} \\ \dot{y} \\ \dot{z} \end{pmatrix} = \begin{pmatrix} V_a \cos\gamma \cos\psi \\ V_a \cos\gamma \sin\psi \\ -V_a \sin\gamma \end{pmatrix} + \begin{pmatrix} W_x \\ W_y \\ W_z \end{pmatrix} \tag{2.16}$$

while the airspeed, flight path angle and heading angle will be:

$$V_a = \sqrt{\left(\dot{x} - W_x\right)^2 + \left(\dot{y} - W_y\right)^2 + \left(\dot{z} - W_z\right)^2} \tag{2.17}$$

$$\gamma = \sin^{-1}\left(\frac{-(\dot{z} - W_z)}{V}\right) \tag{2.18}$$

$$\psi = \sin^{-1}\left(\frac{(\dot{y} - W_x)}{\sqrt{(\dot{x} - W_x)^2 + (\dot{y} - W_y)^2}}\right) \tag{2.19}$$

Then inertial speed with respect to Body Frame can be found through the conversion from Local Earth Frame to Body Frame. Recalling the transformation matrix in equation 2.1, the inertial speed in the body frame $\underline{V}_B$ can be expressed with the following relation:

$$\underline{V}_B = R_{LB} \cdot \underline{V}_I \tag{2.20}$$

or

$$\begin{pmatrix} u \\ v \\ w \end{pmatrix} = R_{LB}\left(\begin{pmatrix} V_a \cos\gamma \cos\psi \\ V_a \cos\gamma \sin\psi \\ -V_a \sin\gamma \end{pmatrix} + \begin{pmatrix} W_x \\ W_y \\ W_z \end{pmatrix}\right) \tag{2.21}$$

and the angle of attack α and sideslip β can be obtained by substituting equation 2.21 into equation 2.14 and 2.15.

2.5 Flight path angle

The flight path angle gives the information to the pilot where the aircraft is heading to in the verticle plane. Flight path angle (angle between the local horizontal plane and the considered speed) can be affected by the wind. From [Mora-Camino, 2014], it was shown that the inertial and air flight path angle (γ_I and γ_a respectively) can be written as:

$$\gamma_I = -\arcsin\left[\frac{V_a}{V_I}(-\sin\theta\cos\alpha\cos\beta + \sin\varphi\cos\theta\sin\beta + \cos\varphi\cos\theta\sin\alpha\cos\beta) + \frac{W_z}{V_I}\right] \tag{2.22}$$

and

$$\gamma_a = -\arcsin\left[\frac{V_a}{V_I}(-\sin\theta\cos\alpha\cos\beta + \sin\varphi\cos\theta\sin\beta + \cos\varphi\cos\theta\sin\alpha\cos\beta)\right] \tag{2.23}$$

If there is no wind and both bank angle, ϕ and sideslip angle β is zero, the classic formula is obtained:

$$\gamma_I = \gamma_a = \theta - \alpha \tag{2.24}$$

2.6 The Standard Atmosphere

The performance of an aircraft is dependent on the properties of the atmosphere. Since the real atmosphere never remains constant at any particular time or place, it is impossible to determine aircraft performance parameters precisely without defining the state of the atmosphere. Therefore a hypothetical model called the standard

atmosphere will be used as an approximation to the real atmosphere. The standard atmospheric model used today was introduced in 1952 and is known as International Standard Atmosphere (ISA) model. With this model the air is assumed to be devoid of dust, moisture, and water vapor and is at rest with respect to the Earth. Three main characteristics of air that are important to understand flight in the atmosphere are the pressure, temperature and density.

Table 2.1: ISA assumes the conditions at mean sea level (MSL)

Properties	SI units
Pressure	P_o = 101 325 N/m^2
Density	ρ_o = 1.225 kg/m^3
Temperature	T_o = 288.15^{o}K
Speed of sound	a_o = 340.294 m/s
Acceleration of gravity	g_o = 9.80665 m/s^2
Gas constant	R = 287.04 J/kg K

The temperature, pressure and density along with the altitude. The modeling of the three main characteristic of air is as follows. The pressure variation modeling in ISA is calculated using the hydrostatic equations, perfect gas law and the temperature lapse rate (L_R) equations. L_R is defined as rate of atmospheric temperature increase with increasing altitude.

Table 2.2: Variation of TLR according to altitude

Atmospheric Level	Altitude Range (Geopotential) [km]	Temperature Lapse Rate,L_R (dT/dH) [K/m]
Troposphere	0-11	-0.0065
Troposphere	11-20	0
Stratosphere II	20-32	+0.001
Stratosphere III	32-47	+0.0028
Stratopause	47-51	0

The derivation of ISA can be found from [Cavcar, 2000, Daidzic, 2015, Anderson, 2005]. The change in temperature, pressure and density with altitude within the troposphere are given by the following equations:

$$\frac{p}{p_o} = \left(\frac{T}{T_o} \right)^{-g_0/(L_R R)} \tag{2.25}$$

$$\frac{\rho_a}{\rho_o} = \left(\frac{T}{T_o} \right)^{-\{[g_0/(L_R R)]+1\}} \tag{2.26}$$

$$T = T_1 + L_R(h - h_1) \tag{2.27}$$

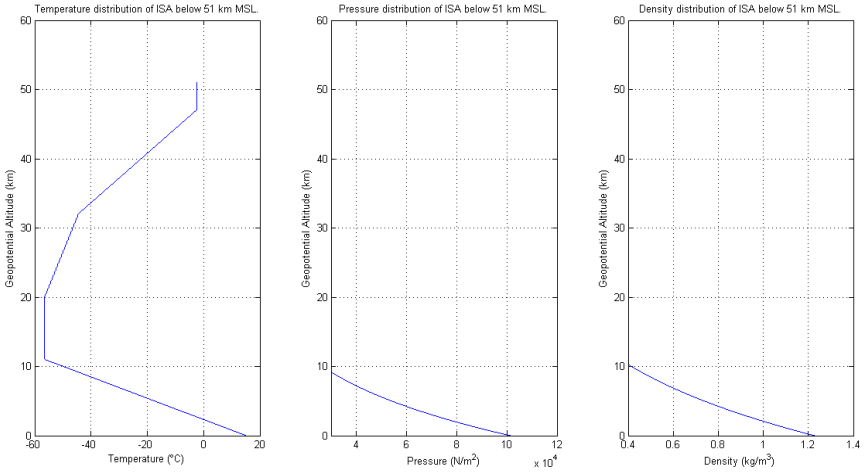

Figure 2.9: International Standard Atmosphere

This standard atmosphere is a generalization of the standard atmosphere. The lapse rate is assumed constant for each layer however some variation along the altitude may exist and also the gravitational force is not constant. However, this model is fairly accurate up to about 11km and most flight operation is limited to the troposphere and the stratosphere.

2.7 Flight dynamic equations

The many assumptions done in general for establishing the flight dynamics equations in view of the control of the flight of an aircraft and more specifically in view of the control of its trajectory using the control techniques are [Etkin and Reid, 1996] :

- The aircraft is assumed to be a rigid body
- The mass of the aircraft is taken as constant during a short period of time.
- The atmospheric parameters (static temperature and pressure, viscosity, volumic mass) are supposed to follow the standard atmospheric model.

- The modulus of the gravity vector is taken as constant in its direction towards the local vertical line.

A detailed computation of flight dynamics equations can be obtained from [Etkin and Reid, 1996],[Nelson, 1998],[Cook, 2013] and [Stevens and Lewis, 2003]. The rigid body assumption leads to consider the Euler equations relating the rotational speed components in the body frame to the rate of change of the attitude angles $\Phi = (\phi, \theta, \psi)'$ given in equation 2.28.

$$\dot{\Phi} = \mathrm{E}(\Phi)\omega_{bE} \tag{2.28}$$

$$\mathrm{E}(\Phi) = \begin{bmatrix} 1 & \sin\phi\tan\theta & \cos\phi\tan\theta \\ 0 & \cos\phi & -\sin\phi \\ 0 & \tan\theta & \dfrac{\cos\phi}{\cos\theta} \end{bmatrix} \tag{2.29}$$

The flight dynamic equations are governed by the force and moment equations according to Newton's law:

$$\text{Force equations: } F = m\dot{\underline{V}}_B + m\omega_{bE} \times \underline{V}_B \tag{2.30}$$

$$\text{Moment equations: } M = I\dot{\omega}_{bE} + \omega_{bE} \times I\omega_{bE} \tag{2.31}$$

where the moments of inertia of the aircraft I is such as:

$$I = \begin{bmatrix} I_x & 0 & -I_{xz} \\ 0 & I_y & 0 \\ -I_{xz} & 0 & I_z \end{bmatrix} \tag{2.32}$$

m is the aircraft mass and I is the aircraft inertial matrix in which the aircraft is assumed to be symmetrical (ie. $I_{xy}=I_{yx}$ and $I_{yz}=I_{zy}$ are zero). $\underline{V}_B=(u,v,w)'$ is the velocity of the center of gravity of the aircraft expressed in Body Frame. , ω_{bE} = $(p,q,r)'$ is the angular rotation vector of the body about the center of mass of the aircraft.

F and M respectively are the summation of external forces and moments respectively. The forces came from gravity, engine thrust and aerodynamic forces, while the moments are from the engine thrust and the aerodynamic forces.

2.7.1 Forces

2.7.1.1 Gravity and Engine Thrust

As said before, the aircraft forces are made up by weight, thrust and also the aerodynamic forces. The Gravitational force, *mg* is directed normal from the earth surface, and is considered constant over the altitude envelope.

$$F_G = mg \begin{pmatrix} -\sin\theta \\ \sin\phi\cos\theta \\ \cos\phi\cos\theta \end{pmatrix} \tag{2.33}$$

As for the engine thrust, *T*, it is parallel to the aircraft body x-axis and the engine is mounted such that the thrust lies on the body-axes *XZ*-plane, offset from the center of gravity by Z_{TP} along the z-axis. These gives:

$$F_T = \begin{pmatrix} T \\ 0 \\ 0 \end{pmatrix} \tag{2.34}$$

2.7.1.2 The Aerodynamic forces

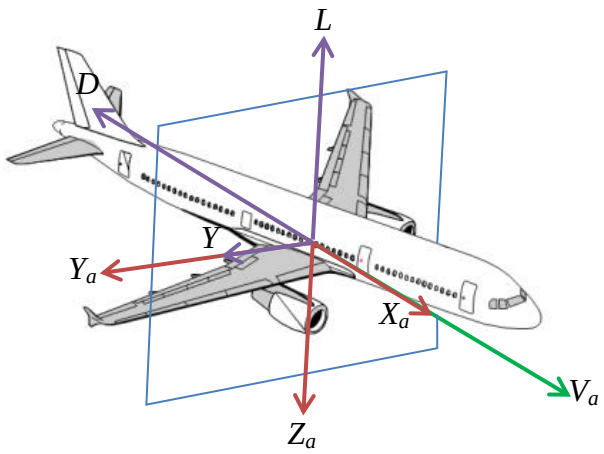

Figure 2.10: Aerodynamic Forces

The aerodynamic forces depend on other variables, like the angular rates (*p*, *q*, *r*) and the time derivatives of the aerodynamic angles ($\dot{\alpha}, \dot{\beta}$). The movements and positions

of control surfaces $(\delta_a,\delta_e,\delta_r)$ and thrust command (δ_{Th}) also influence these aerodynamic forces.

From figure 2.10, it can be seen that the aerodynamic components, Lift (L), Drag (D) and Side Force (Y_F) are resolved in the aerodynamic frames (X_a,Y_a,Z_a). The components of the aerodynamic forces can be defined through the transformation matrix R_{WB} such as:

$$\begin{pmatrix} F_X \\ F_Y \\ F_Z \end{pmatrix} = R_{WB} \begin{pmatrix} -D \\ Y_F \\ -L \end{pmatrix} \tag{2.35}$$

Where D is the drag force, Y_F is the lateral aerodynamic force and L is the lift force. These aerodynamic forces are related to the dynamic pressure, the airspeed and the aircraft wing surface area through the following equation:

$$D = \frac{1}{2}\rho_a(x,y,z)\,V_a{}^2 S C_D \tag{2.36}$$

$$L = \frac{1}{2}\rho_a(x,y,z)\,V_a{}^2 S C_L \tag{2.37}$$

$$Y_F = \frac{1}{2}\rho_a(x,y,z)\,V_a{}^2 S C_Y \tag{2.38}$$

where C_D, C_Y and C_L are respectively the dimensionless aerodynamic coefficients of the drag, the side force and the lift which depend mainly on the angle of attack α and the side-slip angle β, and through the Mach number, on the airspeed and the flight level. The accepted expression of the aerodynamic forces coefficients are [Duke et al., 1988],[Etkin and Reid, 1996]:

$$C_L = C_{L_0} + C_{L\alpha}\alpha + C_{Lq}\frac{q}{V_a} + C_{L_{\delta_E}}\delta_e \tag{2.39}$$

$$C_Y = C_{Y_0} + C_{Y\beta}\beta + C_{Yr}\frac{rb}{2V_a} + C_{Yp}\frac{pb}{2V_a} + C_{Y_{\delta r}}\delta_r \tag{2.40}$$

$$C_D = C_{D_0} + C_{D\alpha}\alpha + C_{D_{\alpha^2}}\alpha^2 \tag{2.41}$$

From equation 2.30, the force equations in the body-axis reference frame can be written as:

$$\dot{u} = rv - qw - g\sin\theta + \frac{1}{m}(F_x + F_T) \tag{2.42}$$

$$\dot{v} = pw - ru + g\cos\theta\sin\phi + \frac{1}{m}(F_y) \tag{2.43}$$

$$\dot{w} = qu - pv + g\cos\phi\cos\theta + \frac{1}{m}(F_z) \tag{2.44}$$

2.7.2 Moments

As for the moments, the moment due to the thrust that lies on the body-axes XZ-plane, offsets from the center of gravity by Z_{TP} along the z-axis as given by:

$$M_E = \begin{pmatrix} 0 \\ T \cdot Z_{TP} \\ 0 \end{pmatrix} \tag{2.45}$$

The aerodynamic moment $M_A=(L_M,M,N)$ is expressed directly in the aircraft Body-Axis Frame. The aerodynamic moments are also dependent on multiple variables as states for the aerodynamic forces. The moment of the aircraft is dependent on the airspeed, the dynamic pressure and also the aircraft reference chord length, $\bar{c}$, and reference span, *b*. The accepted expressions of the aerodynamic moments are given by [Duke et al., 1988],[Etkin and Reid, 1996]:

$$L_M = \frac{1}{2}\rho_a(x,y,z)\,V_a{}^2 S \cdot b \cdot C_{L_M} \tag{2.46}$$

$$M = \frac{1}{2}\rho_a(x,y,z)\,V_a{}^2 S \cdot \bar{c} \cdot C_M \tag{2.47}$$

$$N = \frac{1}{2}\rho_a(x,y,z)\,V_a{}^2 S \cdot b \cdot C_N \tag{2.48}$$

And the contributing factor to the yawing moment C_{LM}, pitching moment C_M and rolling moment C_N coefficients are:

$$C_{L_M} = C_{lo} + C_{l_\beta}\beta + C_{lr}\frac{rb}{2V_a} + C_{lp}\frac{pb}{2V_a} + C_{l_{\delta a}}\delta_a + C_{l_{\delta r}}\delta_r \tag{2.49}$$

$$C_M = C_{mo} + C_{m_\alpha}\alpha + C_{m\dot{\alpha}}\frac{\dot{\alpha}\bar{c}}{2V_a} + C_{mq}\frac{q\bar{c}}{2V_a} + C_{m_{\delta e}}\delta_e + C_{m_{\delta th}}\delta_{th} \tag{2.50}$$

$$C_N = C_{no} + C_{n_\beta}\beta + C_{nr}\frac{rb}{2V_a} + C_{np}\frac{pb}{2V_a} + C_{n_{\delta a}}\delta_a + C_{n_{\delta r}}\delta_r \tag{2.51}$$

From equations 2.30 and 2.31 moment equations in the body-axes reference frame can be written as:

$$\dot{p} = \frac{1}{I_x I_z - I_{xz}{}^2}\left(\{r[(I_y - I_z)I_z - I_{xz}{}^2] + [(I_x - I_y + I_z)I_{xz}]p\}q + I_z\underline{L} + I_{xz}\underline{N}\right) \tag{2.52}$$

$$\dot{q} = \frac{1}{I_y}\left(pr(I_z - I_x) + I_{xz}(p^2 - r^2) + \underline{M} + F_T \cdot Z_{TP}\right) \tag{2.53}$$

$$\dot{r} = \frac{1}{I_x I_z - I_{xz}{}^2}\left(\{p[(I_x - I_y)I_x + I_{xz}{}^2] - [(I_x - I_y + I_z)I_{xz}]r\}q + I_z\underline{N} + I_{xz}\underline{L}\right) \tag{2.54}$$

2.8 A State Representation of Flight Dynamics

All these equation can be rewritten as a 12th order state representation considering the state variables $p,q,r,\phi,\theta,\psi,u,v,w,x,y$ and z. These equations are composed of:

a) The aircraft rotational accelerations:

$$\dot{p} = \frac{1}{I_x I_z - I_{xz}^{\ 2}}\left(\{r[(I_y - I_z)I_z - I_{xz}^{\ 2}] + [(I_x - I_y + I_z)I_{xz}]p\}q + I_z \underline{L} + I_{xz}\underline{N}\right) \quad (2.55a)$$

$$\dot{q} = \frac{1}{I_y}\left(pr(I_z - I_x) + I_{xz}(p^2 - r^2) + \underline{M} + F_T \cdot Z_{TP}\right) \quad (2.56b)$$

$$\dot{r} = \frac{1}{I_x I_z - I_{xz}^{\ 2}}\left(\{p[(I_x - I_y)I_x + I_{xz}^{\ 2}] - [(I_x - I_y + I_z)I_{xz}]r\}q + I_z \underline{N} + I_{xz}\underline{L}\right) \quad (2.57c)$$

b) The aircraft Euler equations:

$$\dot{\phi} = p + \tan\theta(q\sin\phi + r\cos\theta) \quad (2.58a)$$

$$\dot{\theta} = q\cos\phi - r\sin\phi \quad (2.59b)$$

$$\dot{\psi} = \frac{q\sin\phi + r\cos\phi}{\cos\theta} \quad (2.60c)$$

c) The acceleration components of the center of gravity in the body frame:

$$\dot{u} = rv - qw - g\sin\theta + \frac{1}{m}(F_x + F_T) \quad (2.61a)$$

$$\dot{v} = pw - ru + g\cos\theta\sin\phi + \frac{1}{m}(F_y) \quad (2.62b)$$

$$\dot{w} = qu - pv + g\cos\phi\cos\theta + \frac{1}{m}(F_z) \quad (2.63c)$$

d) The speed components of the center of gravity of the aircraft in the LEF frame:

$$\begin{pmatrix}\dot{x}\\ \dot{y}\\ \dot{z}\end{pmatrix} = \begin{bmatrix} c(\theta)\cdot c(\psi) & s(\phi)\cdot s(\theta)\cdot c(\psi) - c(\phi)\cdot s(\psi) & c(\phi)\cdot s(\theta)\cdot c(\psi) + s(\phi)\cdot s(\psi) \\ c(\theta)\cdot s(\psi) & s(\phi)\cdot s(\theta)\cdot s(\psi) + c(\phi)\cdot c(\psi) & c(\phi)\cdot s(\theta)\cdot s(\psi) - s(\phi)\cdot c(\psi) \\ -s(\theta) & c(\theta)\cdot s(\phi) & c(\phi)\cdot c(\theta) \end{bmatrix}\begin{pmatrix}u\\ v\\ w\end{pmatrix} + \begin{pmatrix}W_x\\ W_y\\ W_z\end{pmatrix} \quad (2.64)$$

The input parameters are composed of controlled parameters:

1. The total thrust of the engines (all engines are targeted to work identically)
2. The deflection of the main aerodynamic surfaces actuators (e.i. aileron, rudder, elevator)

3. The deflection of the secondary aerodynamic surfaces actuators (e.i. flaps, slats, spoiler, speed break) define the aerodynamic configuration of the aircraft on the medium term.

The uncontrolled parameters composed mainly of the wind components (W_x, W_y, W_z) which can change with the atmosphere.

2.9 Global view of Flight Equations

As can be seen from the previous sections, the flight equations appear as a very complex system. However this complex system can be analyzed through the decoupling between the longitudinal and lateral motion and from the causal relationship between fast and slow dynamic modes. A subset of the aircraft flight dynamics system state's variables are predominantly characterized by "fast dynamics" that is short time constants, high natural frequencies and bandwidth, and the "slow dynamics" with slow natural modes and longer transient response.

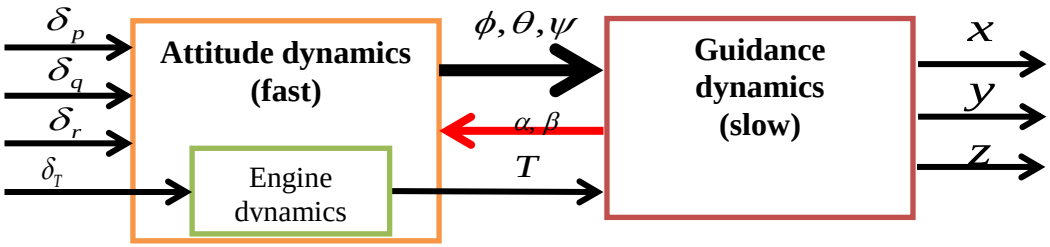

Figure 2.11: Global view of flight equations [Mora-Camino, 2014]

As shown in Figure 2.11, typically the piloting dynamics are faster than the guidance dynamics and they are the input to the guidance dynamics. In this thesis, the guidance dynamics will be addressed in order to design controllers to track specific aircraft reference trajectories. While it is assumed that the piloting dynamics are properly controlled by the autopilot.

The guidance dynamics are then given by:

a) The acceleration components of the center of gravity in the body frame:

$$\begin{bmatrix} \dot{u} \\ \dot{v} \\ \dot{w} \end{bmatrix} = \begin{bmatrix} rv - qw - g\sin\theta + \frac{1}{m}(F_x + F_T) \\ pw - ru + g\cos\theta\sin\phi + \frac{1}{m}(F_y) \\ qu - pv + g\cos\phi\cos\theta + \frac{1}{m}(F_z) \end{bmatrix} \quad (2.65a)$$

b) The speed components of the center of gravity of the aircraft in the LEF frame:

$$\begin{pmatrix} \dot{x} \\ \dot{y} \\ \dot{z} \end{pmatrix} = \begin{bmatrix} c(\theta)\cdot c(\psi) & s(\phi)\cdot s(\theta)\cdot c(\psi) - c(\phi)\cdot s(\psi) & c(\phi)\cdot s(\theta)\cdot c(\psi) + s(\phi)\cdot s(\psi) \\ c(\theta)\cdot s(\psi) & s(\phi)\cdot s(\theta)\cdot s(\psi) + c(\phi)\cdot c(\psi) & c(\phi)\cdot s(\theta)\cdot s(\psi) - s(\phi)\cdot c(\psi) \\ -s(\theta) & c(\theta)\cdot s(\phi) & c(\phi)\cdot c(\theta) \end{bmatrix} \begin{pmatrix} u \\ v \\ w \end{pmatrix} + \begin{pmatrix} W_x \\ W_y \\ W_z \end{pmatrix} \quad (2.65b)$$

Equation 2.65 is composed of nonlinear ordinary differential equations and they are complex. Each equation consists of coupled state vectors. For simple analysis such as flight trimming and analysis of flight response on the longitudinal and lateral motions, these equations can be decoupled but this will not be discussed in this thesis. It can be found by further reading on the literature from [Nelson, 1998] and [Blakelock, 1991]. This thesis is only concern with the nonlinear ordinary differential equations.

2.10 Conclusion

From the above analysis, it appears that the guidance dynamics can be summarized by equations 2.65a and 2.65b. Once an autopilot system is available to control the attitude dynamics of the aircraft with short response time with respect to the guidance dynamics, the effective controller inputs of the guidance dynamics become the reference values for the pitch and bank angles and the total thrust of the engines, while the wind has indirect (equation 2.65a) and direct (equation 2.65b) effects. From the control point of view, the guidance dynamics form a strongly coupled nonlinear system where aircraft parameters (mass, configuration) have important influence.

CHAPTER 3
MODERN FLIGHT GUIDANCE SYSTEMS

Chapter 3: Modern Flight Guidance Systems

3.1 Introduction

In this chapter a description and analysis of flight guidance systems on board modern air transport aircraft is performed. In the text, the terminologies are taken from Airbus aircraft but an equivalent Boeing aircraft also existed. The flight guidance function on board modern aircraft is designed to drive the aircraft along a safe and efficient trajectory. This function is embedded in the Flight Management System (FMS) and operates in close relation with the Navigation functions. Flight plans are generated by the Flight Management System (FMS) in accordance with tactical choices of the airline operating that aircraft. In general, a flight plan combines lateral and vertical parts composed of different segments. Each segment corresponds in general to some local objective with respect to the guidance variables. This induces a sequence of different guidance modes along the flight from initial climb to landing. A flight plan can be followed automatically by the flight guidance system where the FMS provides the successive decisions with respect to the shift from one guidance mode to the next and to the choice of the guidance target parameters. In that case, the guidance system is managed by the FMS. In other situations, the pilot takes over the control of the flight guidance systems, imposing a different sequence of modes (selected mode) and guidance parameters. This second situation happens normally at take-off and when the ATC produces injunctions with respect to the trajectory of the aircraft. This can also happen when the pilot reacts to a guidance alarm, including or not a resolution advice.

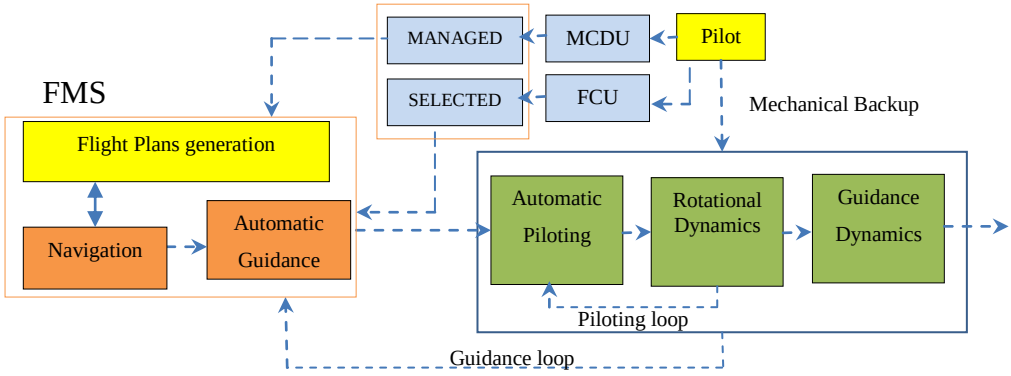

Figure 3.1: Overall classical structure of flight control systems [Mora-Camino, 2014]

So in this chapter, to understand better the organization and operation of the flight guidance systems, first, a description of up-to-date FMSs and the main characteristics of the generated flight plans which must be achievable by the flight guidance system will be introduced.

3.2 The Flight Management Systems

3.2.1 Flight Management Functions

Today the Flight Management System integrates closely related functions to allow the aircraft and its pilot to perform a safe and efficient flight. These related functions are:

- The navigation function which allows to appreciate any difference between the current position of the aircraft and its planned one, possibly for correction through the guidance function.
- The trajectory predictive function which provides information and predictions about the actual flight, allowing for instance to check if delays resulting from late departure or different winds than forecasted can be compensated.
- The flight planning function which helps the pilot to choose the horizontal track to be followed all along the flight.
- The performance function which computes for a particular flight characteristic parameters such as take-off speed and an optimized vertical profile to be fed to the guidance system.
- and finally the flight guidance function.

It appears rather difficult to distinguish the flight guidance system from the other systems imbedded in the flight management system, especially when, as is generally the case with modern aircraft where all these functions are developed

within a single computer (coupled in general with another one operating in dual mode) such as the Flight Management and Guidance Computer of different aircraft.

Then from the point of view of the system, the Flight Management Systems consists of navigation radio receivers, inertial reference systems, air data systems, navigation, interfaces (Multipurpose Control Display Unit-MCDU) and instrument displays (the Navigation Display-ND) for the pilot in the cockpit, flight control systems, engine and fuel system, and data link. These subsystems are managed and processed by the Flight Management Computer (FMC) as shown in Figure 3.2 [Herndon, 2012].

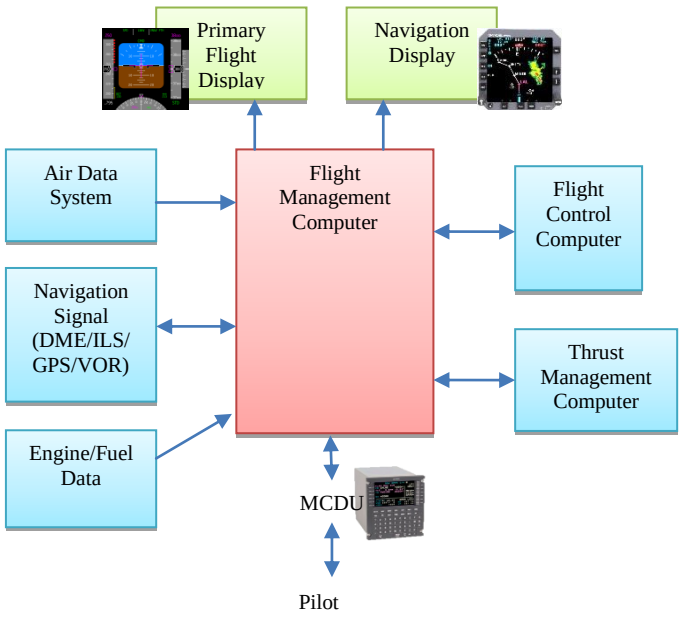

Figure 3.2: Flight Management System (FMS) Block Diagram [Collinson, 2011]

3.2.2 Horizontal Flight Plan Composition and Construction

The flight plan is composed of segments and waypoints for the aircraft to follow starting from departure to destination airport. The flight plan is separated into two parts which are the lateral flight plan and the vertical flight plan. The construction of the lateral flight plan can be done in three ways:

1. Inserting company route: the flight plan is generated from the computers in the airline center and is given to the flight crew to be uploaded to the FMS.

The pilot needs to enter the name of the route and this action enters the element of the flight plan related to this route.

2. Pilot input: This is done by the pilot by inserting the origin and the destination city in the MCDU and manually selecting the departure, waypoints, airways, approaches and so on.

3. Flight Plan uplink: The ground can upload the active flight plan from the airline to the aircraft if there is a request from the flight crew.

Figure 3.3: Multifunction Control Display Unit (MCDU) [Wikipedia, 2015d]

After these data entries, FMS will compute the flight profile along with the optimum speed, climb/descend rate, altitude and predicted fuel consumption. The entry must be confirmed by the pilot to ensure that no restriction from the ATC is breached. The lateral flight plan will include the following elements:

1. Take-off Runway

2. Departure Standard Instrument Departure (SID)/ Engine Out (SID) procedures

3. En-route waypoints and Airways

4. Standard Terminal Arrival Route (STAR)

5. Landing runway with selected approach and approach via

6. Missed-Approached
7. Alternate Flight Plan
8. Alternate Destination

These elements can be described in the following figure.

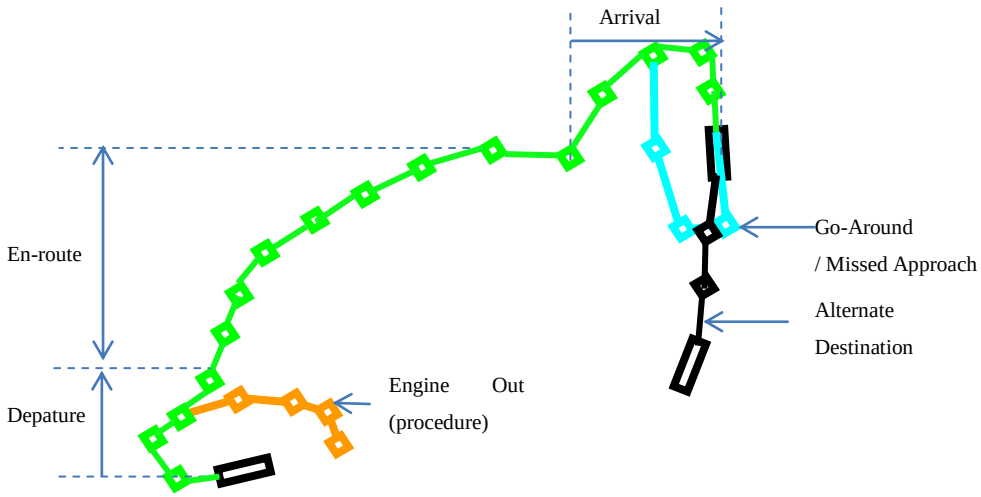

Figure 3.4: Example of lateral (track) flight plan

3.2.3 Vertical Flight Plan composition and construction

To complete the flight plan, it is essential to have the vertical flight plan. This vertical flight plan defines the speed, altitude and time constraint at each waypoint based on the Lateral flight plan, winds, temperature, aircraft weight, atmospheric pressure, aircraft performance, cost index and flight predictions. The cost index is subjected to the airline policy and it is used to compute the best trip cost which evidently affects the speed (ECON Speed/Mach) and altitude (OPT ALT) computation in the vertical flight plan. It is given by:

$$\text{Cost Index}(CI) = \frac{\text{Time Cost}}{\text{Fuel Cost}} \tag{3.1}$$

This cost index is related to the following variable cost:

1. Cost of fuel / kg,

2. Time-related cost per minute of flight (hourly maintenance cost, flight crew and cabin crew cost, marginal depreciation or leasing cost),

3. Flight time.

So the objective is to optimize the choice of cost index to achieve an optimized flight plan. Whereas for the prediction of the flight plan, 3 categories of data are presented:

1. Strategic data where the input is entered by the pilot and it applies to all flight phases. They include:

    - Zero Fuel Weight,
    - Zero Fuel Centre of Gravity,
    - Block fuel,
    - Airline Cost Index,
    - Flight Condition which include the flight level, wind, temperature.

2. Weather data obtained either by the entered data from the pilot in case they encounter weather changes outside the forecasted information or from the air data computed by the FMS. Example:

    - Wind and temperature in the flight phases
    - Sea level atmospheric pressure (QNH) at destination
    - Surface temperature (TEMP) at destination airport
    - The tropopause altitude

3. Tactical data on each flight phase which include the speed and altitude constraints and transition between waypoints and between flight phases. Example in the tactical data:

    - Switching between waypoints or pseudo waypoints:
        - Entering cruise level (top of climb (T/C)),
        - Entering descent phase (top of descent (T/D)),

- Reaching acceleration altitude (accel alt).

• Speed limitations:

  - Take-off speed, V2,
  - Economy climb speed (ECON CLB SPD/MACH),
  - Economy cruise speed (ECON CRZ MACH),
  - Economy descent speed (ECON DES MACH/SPD).

These predictions will be continuously updated throughout the flight and it includes any modification by the flight crew, the actual positions of the aircraft with respect to the profile and current guidance modes selected. As what was described, the process of computing the flight profile is a continuous process and it reflects the limitation and constraint subjected by the ATC and airlines, the flight envelope based on the limitation of altitude and speed, the current condition of the flight and position of the aircraft controlled by the flight guidance system (FGS). A description of the flight guidance system will be described in the next sections. An example of the vertical flight profile (Figure 3.5):

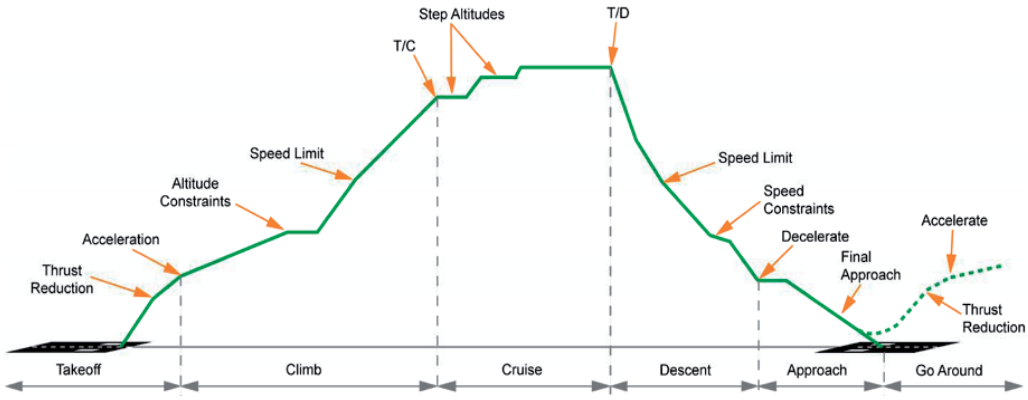

Figure 3.5: Vertical Flight Profile [Collinson, 2011]

3.2.4 Pilot's Flight Plan modification capability

Even with the computation of the flight plan from the FMS, the pilot is allowed to modify both the lateral and vertical flight plan. This is done in order to react to ATC demand and tactical and strategic demand. Some revisions that are allowed on the flight plan are:

Lateral flight plan:

1. Delete and adding a waypoint,
2. Give a command to change waypoint of the active leg using for example Direct to (DIR TO), direct to a beam (DIR To A BEAM), Direct or Intercept (DIR TO/INTERCEPT),
3. Insert and replacement of procedures such as SID, STAR, approach procedure and also missed approach procedure,
4. Create and insert a temporary flight plan as a revision to the active flight plan when the flight crew modifies several waypoints of an airway or procedure at once.

Vertical flight plan:

1. Modify speed and altitude constraint,
2. Modify the time constraint,
3. Modify of enter a step climb or step descent,
4. Adding new wind data.

Here even though the flight plan is defined into two parts, they are not at all decoupled from each other. They are coupled through the ground speed parameter since for example this parameter is used in the calculation of the turn radius in lateral flight profile and the calculation of average speed and level segments in the vertical profile. From these computed vertical and lateral flight profiles the flight guidance system (FGS) will control the aircraft to react to the difference in the aircraft current position to the flight plan.

3.3 Flight Guidance Systems (FGS)

The flight guidance system (FGS) is in charge of making the aircraft follow the flight plan as the guidance directives given by the pilot. For that, the flight guidance system (FGS) compares the actual aircraft position to the desired position or flight profile and invokes a flight control law to manipulate the flight path and orientation of the aircraft so as to minimize the position error. It generates commanded pitch and roll values to the autopilot (AP) and thrust reference values to the auto-throttle (A/THR) modifying the modulus and orientation of the speed vector to minimize the difference between the measured and desired positions. The flight guidance system can be operated in two modes - the selected mode and the managed mode. The selected mode is accessible by the pilot from the flight control unit (FCU). The FCU is the main interface between the pilot and the auto-guidance system for short-term tactical guidance (i.e. for immediate guidance) while the MCDU is the main interface between the pilot and the flight management system (i.e. for current and subsequent flight phases) which is in charge of the Flight Guidance System (FGS) in the managed mode.

3.3.1 Classification of Flight guidance modes

The different guidance modes are able to guide the aircraft all along the flight plan or according to the pilot guidance directives. These guidance modes are divided into lateral and vertical guidance modes. Which lateral and vertical guidance modes are activated or armed is determined by flight mode logic in accordance with the succession of flight plan segments as pilot's guidance directives. The division of the guidance modes is given below:

1. Managed Modes: The aircraft is guided along the flight plan by the FMS. This mode reduces the workload for the pilot since the flight guidance task is performed by an automated system. Therefore in managed navigation modes, the FMS will guide the aircraft and the pilot will monitor the situation of the action from the navigation Display (ND) unit.

2. Selected Mode: The aircraft is guided to acquire and maintain the targets (heading speed, altitude and vertical speed) set by the crew from the FCU. The modes are armed, activated and deactivated by push buttons on the FCU. The input from the FCU will be used by the auto-pilot and auto-throttle to send a command to the flight control channels. The Selected mode might be used in diverting from the reference flight plan considering ATC directives, or bad weather conditions. This will be entirely up to the crew.

Some of the components used as interfaced between the pilot and AP/A-THR are shown in the following figure:

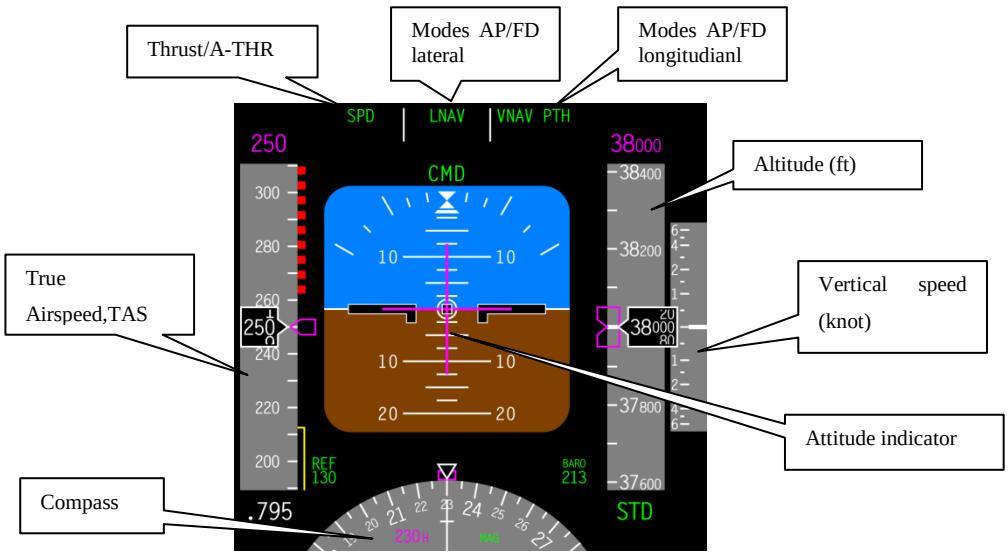

Figure 3.6: Primary Flight Display (PFD) – Boeing term[Wikipedia, 2015c]

Figure 3.7: Navigation Display (ND) – Boeing term. Indicates the aircraft track, waypoints / pseudo-waypoints and other navigation information [Wikipedia, 2015a]

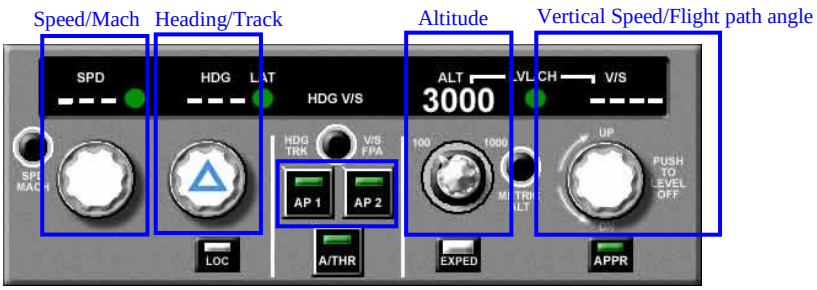

Figure 3.8: Flight Control Unit (FCU) – Airbus term: Mode engagement and target selection capability [Meriweather, 2013]

Further these guidance modes can be broken down to the lateral guidance modes and the vertical guidance modes. The lateral mode controls the horizontal motion of the aircraft by adjusting the roll. The vertical mode controls the vertical motion of the aircraft by adjusting the pitch. The Speed or Mach and thrust are controlled by the throttle command. The tables below show typical lateral and vertical modes of operation. In general, generic modes such as “navigation”, “climb” are typically managed modes while other modes such as “heading”, “altitude hold” can be either managed or selected modes. Table 3.1 and Table 3.2 give a short description of the modes (terms used are Airbus terminology but and equivalent Boeing terminology exist) available in the lateral and vertical guidance modes:

Table 3.1: Lateral Guidance Modes [Tribble et al., 2002]

Mode	Description
Runway (RWY) [MANAGED]	Activated after pilot set thrust levers to FLX or TOGA. Divided into two: RWY mode - Activated to maintain the runway middle. RWY TRK mode - activated after take-off and passes 30 ft radio altitude (RALT).
Navigation (NAV)[MANAGED]	This mode is used for en-route navigation and non-precision approaches. It will capture and track the lateral guidance.
Approach (APPR) [MANAGED]	In the lateral guidance, this mode captures and tracks the lateral guidance for ILS localizer (LOC) and VOR non-precision approaches. This mode is selected manually by pressing the APPR button on the flight control panel (FCP), first it will arm APP NAV mode. It is similar to NAV mode and guide the aircraft to a target flight path. If there is no Final approach Fixed (FAF) point defined in the flight plan before next airport, LOC mode is activated.
Go Around (GA) [MANAGED]	GA TRK - This mode generates command to track a heading reference. Only activate during a Go Around
Heading Track (HDG-TRK) [SELECTED]	This mode generates command to capture and maintain a selected heading reference. The heading reference can be adjusted by the pilot.
Roll Out [MANAGED]	It guides the aircraft along runway following an automatic landing

These modes corresponding to lateral guidance mode and vertical guidance mode are controlled by the Auto-Pilot and Flight Director (AP/FD), then the Auto-Throttle (A/THR) will control the target Speed/Mach (SPD/MACH) and fix thrust to react to the AP/FD mode selected. The interaction between the A/THR and AP/FD are based on the pitch mode controls. If the AP/FD pitch modes controls the vertical trajectory or the pitch mode is not engaged then the A/THR modes controls the target SPD/MCH. However if the pitch mode controls a target speed or Mach then the A/THR controls the thrust. Typical thrust control by the A/THR is during the engagement to the Climb and Descent Modes.

The modes that were described can be used in the managed or the selected mode. An example of the usage of these modes can be shown in the diagram below. Figure 3.9 shows a typical classification of guidance mode for an A320.

Table 3.2: Vertical Guidance Modes [Tribble et al., 2002]

Mode	Description
Speed Reference (SRS) [MANAGED]	It commands the aircraft pitch in order to maintain a speed target and guides the aircraft during take-off, initial climb and after a Go-Around.
Climb (CLB) to Descent (DES)	To change altitude, the auto-throttle commands constant thrust and aircraft pitch to maintain the aircraft speed. This mode is also known as the Pitch Mode. There are many types for these modes: • OP CLB and OP DES [SELECTED]: Open climb or open descent such that it reach an altitude without considering the altitude constraints. • CLB and DES [MANAGED]: The aircraft will level off at an altitude constraint. • EXP CLB and EXP DES [SELECTED]: Similar to OP CLB and OP DES but differ in the speed target the aircraft assumes.
Altitude (ALT)	The aircraft will maintain the pressure altitude. This mode has multiple modes depending on the circumstances. • ALT and ALT* [SELECTED]: * means the capture mode. These modes are activated once the altitude target is reached and one of climb or descent mode is active or VS mode is active. ALT* activated first and once reaching level-off the ALT mode engages. • ALT CRZ [MANAGED]: Similar to the previous ALT mode except that the selected altitude must be at or above Cruise altitude define in MCDU. • ALT CST and ALT CST* [MANAGED]: This mode considers the altitude constraint.
Approach (APPR) [MANAGED]	Final Mode: Aircraft guide along the vertical flight path as defined in the flight plan. If the flight plan contains no Non-precision part of for the airport and ILS in tuned-in, the G/S* mode is engages to capture the glide slope of the ILS and then transition to G/S mode once the glide slope is sufficiently capture.
Vertical Speed (V/S) / Flight Path Angle (FPA) [SELECTED]	The aircraft will maintain the specified vertical speed (climb or descent) reference, defined by the vertical speed dial on the FCP or a Flight Path Angle. These modes will be a pitch mode and once the altitude is read this mode will change to ALT

FLARE [MANAGED]	Mode engages at 40ft. The aircraft is aligned with runway centerline on yaw axis where the FD bars are replaced by the yaw bar and flare on the pitch axis such that the AP/FD commands a suitable pitch angle for the flare.

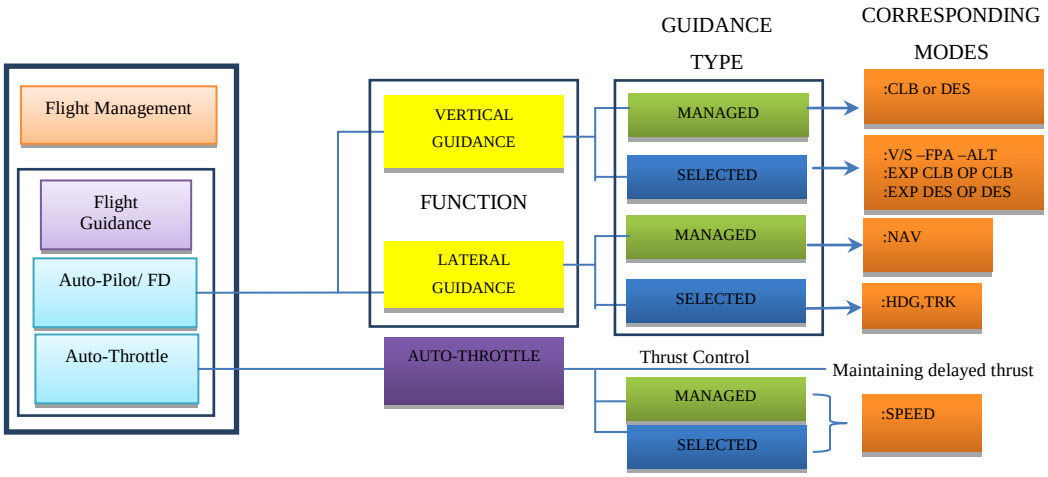

Figure 3.9: Example architecture of FMS/FGS in A320 [Bouadi, 2013]

Each flight guidance modes will dictate what Flight Guidance Control Laws to execute. The development of the Flight Guidance Control Laws is very intricate and it is a multi-disciplinary development process. The control laws are complex in order to cope with the complexity of the control task itself. The basic implementation of the control laws will be detailed in the next section.

3.3.2 Flight Guidance laws

The design of the flight guidance law has significantly improved since the beginning of the first Fly-By-Wire aircraft. The combination of the guidance control laws is very complex but the basic implementation of the early approach of the control law design is based on PID techniques. Here are given the basic design of the guidance laws for the following modes:

- Longitudinal channel with altitude hold at Z_c

$$\delta_e = K_q q + K_\theta \int (\theta_c - \theta) dt \quad \text{with} \quad \theta_c = \lim_{-15^o}^{+30^o} \{K_z (Z_c - Z) - K_{Vz} V_Z\} \tag{3.2}$$

where K_z and K_{vz} are the gains.

- For the roll channel in heading mode, the aileron deflection can be given by:

$$\delta_a = K_{p\phi}(\phi_c - \phi) + K_{I\phi}\int(\phi_c - \phi)dt + K_{D\phi}p \quad \text{with} \quad \phi_c = \lim_{-35°}^{+35°}\left\{K_{\psi}(\psi_c - \psi)\right\} \quad (3.3)$$

where $K_{p\phi}$, $K_{I\phi}$ and $K_{D\phi}$ are the gains.

- For the yaw control, the rudder deflection it is related to the bank angle by a proportional gain given by:

$$\delta_r = K_r(r - (g/V)\sin\phi) \quad (3.4)$$

where K_r is the proportional gain.

From this early design approach, the synthesis of the control laws has been expanded to better suit the latest and modern aircraft which is equipped with modern avionics systems. Today, adopting a state representation approach of flight dynamic around trim conditions, the guidance laws, mixed with the piloting and stabilizing laws appears under a feedback – feedforward form such as:

$$\underline{u} = -G\underline{x} + H\underline{y}_c \quad (3.5)$$

where $\underline{x}$ is the state, $\underline{u}$ is the controlled input vector, $\underline{y}_c$ is the output reference vector, G is the feedback gain matrix and H is the feedforward gain matrix. These matrices are chosen according to model and robust control techniques [Nelson, 1998],[Stevens and Lewis, 2003].

3.4 Flight Guidance Protections

When considering flight guidance systems, it is also necessary to consider flight guidance protection as a necessary complement to maintain safety. The flight guidance protection is a means to alert the flight crew when hazardous situation is near to the aircraft line of flight. They are used to ensure the flight navigation is smooth throughout its operations. There are 3 guidance protections programmed in the FMS.

- Terrain Awareness and Warning System – TAWS,
- Weather radar and wind shear alert,
- Traffic Collision Avoidance System – TCAS.

1. Terrain Awareness And Warning System (TAWS) :

Terrain Awareness Warning System (TAWS) aims to prevent controlled flight into terrain (CFIT) accidents. The current systems used are called the Ground Proximity Warning System (GPWS) and Enhanced Ground Proximity warning Systems (EGPWS). TAWS is developed to provide a warning of a possible terrain conflict by taking into account aircraft inputs such as position, attitude, air speed, glideslope, and an internal terrain, obstacles and airport database. TAWS is classified into three types.

- TAWS Class-A defines a class of equipment is required for turbine-powered airplanes operated under part 121 (airline) and part 135 (charter) of 10 or more passenger seats [Novacek, 2006].
- TAWS Class-B defines a class of equipment is required for turbine-powered airplanes operated under part 91 with six or more passenger seats and for turbine-powered airplanes operated under part 135 with six to nine passenger seats [Novacek, 2006].
- TAWS Class C defines a voluntary class of equipment intended for small general aviation airplanes that are not required to install Class B equipment which includes includes minimum operational performance standards intended for piston-powered and turbine-powered airplanes, when configured with fewer than six passenger seats, excluding any pilot seats. [Wikipedia, 2015e].

Figure 3.10 shows the aural and visual warning for a basic Ground Proximity warning Systems .

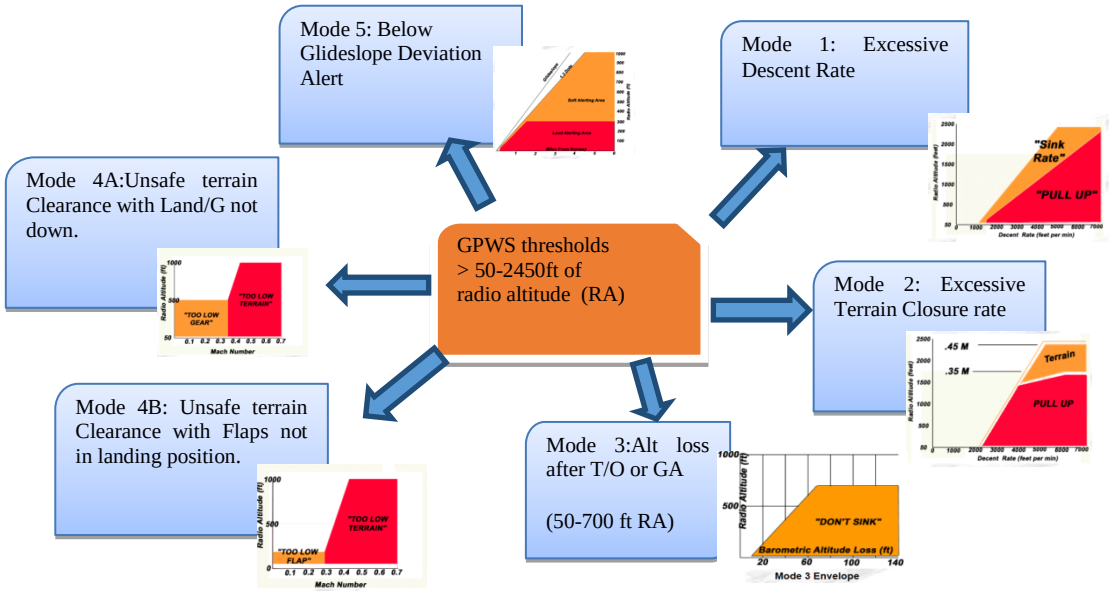

Figure 3.10: GPWS thresholds modes with the aural and visual warning[GPS, 2001]

2. Weather radar and wind shear alert

Wind shear is defined as a sudden change of wind velocity and/or direction. Wind shear conditions usually are associated with the following weather situations:

- Jet streams,
- Mountain waves,
- Frontal surfaces,
- Thunderstorms and convective clouds,
- Microbursts.

The Airborne wind shear detection and alert system, fitted in an aircraft, detects and alerts the pilot both visually and aurally of a wind shear condition. There are two cases of wind shear detection:

- Reactive: The detection takes place when the aircraft penetrates a wind shear condition of sufficient force, which can pose a hazard to the aircraft.
- Predictive: The detection takes place, if such wind shear condition is ahead of the aircraft.

Wind shear warnings are accompanied by wind shear on the attitude indicator and voice aural alert. The wind shear alerts are prioritized based on the level of hazard and the required flight crew reaction time. Predictive wind shear alerts are inhibited by an actual wind shear warning (airplane in wind shear), look-ahead terrain alerts, or radio altitude based alerts.

For the reactive detection (airplane in wind shear), the aural alert will be a two-tone siren followed by "WINDSHEAR" while the visual alert shows a red WINDSHEAR on both attitude indicators. This warning is detected by GPWS and it is enabled below 1500 ft radio altimeter and the GPWS Wind shear detection begins at rotation.

3. Traffic Collision Avoidance System (TCAS)

TCAS alerts the crew of possible conflicting traffic and it is a short-term avoidance system. TCAS operation is independent of ground-based air traffic control. It gathers the information such as the altitude and relative bearing from the surrounding traffic by sending signals to the vicinity and listens for the transponder replies. From there TCAS will determine the closest point of approach (CPA) and the time-to-go to the CPA. TCAS will issue the traffic advisory (TA) 20 to 48 seconds before CPA and the resolution advisory (RA) 15 to 35 seconds before CPA. RA is the vertical avoidance maneuver recommended to the pilot. Information regarding the TCAs traffic information is shown inside the Navigational Display (ND) and the required pitch angle or vertical speed for the maneuver is shown in the primary flight display (PFD). The standard deviation accuracy of TCAS must not exceed 50 feet.

- TCAS traffic advisory (TA): TCAS identifies a 3 dimensional airspace around the airplane where a high likelihood of traffic conflict exists. It will obtain the range, bearing and altitude of the other possible conflicting aircraft. A TA is generated when the other aircraft is approximately 40 seconds from the point of closest approach.

- TCAS Resolution advisory (RA): This alert will be generated if the other airplane is approximately 25 seconds from the point of closest approach. The RA provides aural warning and guidance as well as maneuver guidance to maintain or increase separation from the traffic.

3.5 Conclusion

From the above facts it appears that today's flight guidance systems are designed to make the aircraft follow a flight plan composed of different vertical and lateral segments. Specific flight guidance modes and associated limitations are attached between them. Therefore, it can be said that these flight guidance systems are "mode-selected" 3D guidance devices. Also, tactical moves with respect to the value of the adopted cost index by the flight management system during the flight will provide some temporal capability by allowing to satisfy at some reference point overfly time constraints. Recent studies with respect to future flight and traffic management systems consider the flight as a whole, introducing concepts such as free flight and trajectory based operations (TBO). With the implementation of these concepts, the guidance function of 3D+T trajectory tracking function all over the flight can be assigned. Then the mode-based approach for the design of flight guidance systems will be insufficient to cope with this task. So in the next chapters this question will be tackled and a solution will be proposed for the design of 3D+T guidance systems.

CHAPTER 4
MODERN ORGANIZATION OF TRAFFIC MANAGEMENT

Chapter 4: Modern Organization of Traffic Management

4.1 Introduction

In this chapter the modern organization of traffic management is defined and analysed since the expected performance of new guidance systems will be dependent in this new context. Early air navigation did not demand a complete surveillance of the airspace and with only few flights in comparison to the current traffic capacity, organization of the traffic was not strained and the activity of the Air traffic control was insignificant. In the fifties, the organization of air traffic along air traffic service (ATS) routes were enough to provide safety. More recently with the current high intensity of air traffic in many airspaces and with the expected growth of air passengers up to 1.4 million in 2035 for Europe and US, the ATS routes and in fact the world air traffic organization needs more than an upgrade. The current air traffic organization in en-route, departures and arrivals including the terminal area operations have already today many short-falls whether in terms of capacity or in terms of operation efficiency to cope safely with the current demand levels and structure. These short-falls already affect the profit of the airlines, airport and passenger convenience by generating recurrent delays. With the current development of communication systems, navigation systems and surveillance systems, high accuracy, reliability and dependability of information regarding aircraft position in space and time can be established and many potential improvements can still be implemented in the current air traffic management. The free flight concept is an answer to the above named short falls – a concept where aircraft are allowed to fly their optimal route (from the airline points of view) with self-merging and self-separation capability. In this chapter, a brief overview of the evolution of the air traffic organization methods will be discussed along with the new concepts proposed by the large European and American research development projects (SESAR and NEXTGEN respectively).

4.2 Current Traffic Management Space Organization

The current traffic management organization is described and discussed in many publications, [Amy Cavaretta and Westervelt, 2013], [Donohue et al., 2000], [EUROCONTROL, 2013] and [Lee et al., 2008]. The current air traffic management (ATM) is designed to integrate and handle air traffic. There are many variables to be handled regarding air traffic and airspace such as the routes, airspace sector, flight navigation, management of traffic flows and many others. These variables are combined to fit three elements within the ATM which are:

1. Airspace Management (ASM): To manage and maximize the airspace usage structure by (dynamic) allocation and segregation of airspace.

2. Air Traffic Services (ATS): To maintain safe separation amongst aircraft and between aircraft and obstacles. Air Traffic Control services belong to this element.

3. Air Traffic Flow and Capacity Management (ATFM): To manage and optimize the capacity of traffic flow according to air traffic control capacity.

In order to understand why the air traffic management needs to be modernized, an overview of the current operations is described. For each flight phase from departure to landing, the air traffic is organized and handled differently. The airspace today is classified into 7 classes (Figure 4.1). These airspace classes are designated by letters from A to G. Class A to E are controlled airspace by Air Control Center (ACC) and class F and G are not. Class F is not always available as it is depend on the country or region. This class is considered to be a special airspace. Figure 4.1 shows the classification of airspace in the US. Since the airspace is a wide area ranging from one country or region to others, it is divided into smaller areas called sectors.

	A	B	C	D	E	F	G
Controlled	Yes	Yes	Yes	Yes	Yes	No	No
IFR	Yes	Yes	Yes	Yes	Yes	Yes	Yes
VFR	No	Yes	Yes	Yes	Yes	No	No
ATC Clearance	Required	Required	Required	Required	Required for IFR	Advisory Only	Not Provided
Separation	All flights	All flights	For IFR flights only	Provided for IFR and between IFR-IFR	Provided for IFR and between IFR-IFR	Provided for IFR and between IFR-IFR if possible	Not Provided
Traffic Information	Not Available	Not Available	Provided for all IFR and VFR	Provided for all IFR and VFR	Provided for all IFR and VFR flights where possible	Provided where possible if requested	Provided where possible if requested

Figure 4.1 : General Airspace Classification [FAA, 2013]

The size of these sectors is such that they can be handled by a team of air traffic controllers (ATC). They are responsible to manage traffic and ensuring safe separation of aircraft within their sector and they hand-off the aircraft to the next air traffic controllers when the aircraft leave their sectors. The maximum number of aircraft allowed within a sector defines the sector workload capacity. The organization of traffic within these airspaces can be categorized into airport, terminal, en-route and oceanic;

1. En-route / Oceanic Airspace

In these airspaces, aircraft must fly along the center-line of an airway or direct course between NAVAIDs or Fixes if there is no airway. An airway is a corridor that connects the aircraft between two points and it is designed at specific altitude having its own requirement before an aircraft can fly along it. The airways are designated by letters and flight level to define which altitude the airways are. Each airway has a designated width that defines the allowable navigation errors of the aircraft. En-routes in altitude higher than 1200ft above ground level in a controlled airspace are controlled by Area Control Centers (ACC). They are responsible in ensuring safe separation between aircraft according to classes of airspace and the available means to manage the traffic flow within the airways or routes. There are separation minima that need to be followed by the aircraft. The separation minima is composed of lateral, vertical and horizontal minimum distances or time that defines an aircraft safe distance from other aircraft. This is to ensure aircraft safety and to define the maximum capacity of aircraft allowed in a given airspace. The separations minima is divided into two categories, radar separation minima and non-radar separation minima depending whether the airspace is covered by radar surveillance or not.

Table 4.1: Separation Minima

<table>
<tr><td>Type</td><td colspan="2">Radar</td><td colspan="2">Non-Radar</td></tr>
<tr><td rowspan="2">Horizontal</td><td colspan="2">3NM within 40 nm radius of radar antenna</td><td colspan="2" rowspan="2">Refer Table 4.2</td></tr>
<tr><td colspan="2">5nm beyond 40nm radius of radar antenna</td></tr>
<tr><td rowspan="4">Vertical</td><td><FL290</td><td>1000ft</td><td rowspan="2"><FL290</td><td rowspan="2">1000ft</td></tr>
<tr><td>FL290- FL410</td><td>2000ft (non-RVSM)
1000ft (RVSM)</td></tr>
<tr><td>FL410 – FL630</td><td>2000ft</td><td rowspan="2">>FL290</td><td rowspan="2">2000ft</td></tr>
<tr><td>>FL630</td><td>5000ft</td></tr>
<tr><td>Lateral</td><td colspan="2">5NM</td><td colspan="2">8NM</td></tr>
</table>

The horizontal separation minima for non-radar oceanic airspace or en-route are shown in Table 4.2. These aircraft must comply with the minimum navigation performance specifications.

Table 4.2: Horizontal Separation Minima for non-radar area between two aircraft

Separation	Description
15 minutes	Flying at the same speed along the route
10 minutes	Their position and speed can be quickly determined by radio navigation aids
10 minutes	Flying the same route in opposite directions and having to cross the level of the other aircraft
5 minutes	The preceding aircraft flies at a true speed at least 20kt higher than the following aircraft
3 minutes	The preceding aircraft flies at a true speed at least 40kt higher than the following aircraft
20NM	Fly the same track or two tracks converging with an angle lower or equal to 90°, in communication with the ATC and provided that a distance measurement is available on the same DME and at the same time. Both aircraft flying at same speed.
10NM	Fly the same track or two tracks converging with an angle lower or equal to 90°, in communication with the ATC and provided that a distance measurement is available on the same DME and at the same time. The preceding aircraft flying 20kts or more then the following aircraft

An aircraft can change to another airway at a designated waypoint that the original airway intersects. For airways on the oceanic airspace, this track may be fixed or flexible to adapt to wind changes.

2. Terminal Maneuvering Area (TMA) and airports

Terminal maneuvering Area is the airspace above an airport and its surrounding where the departure and arrival of traffic is handled. The Standard Instrument Departure Route (SID) and Standard Arrival Route (STAR) procedures are included in this airspace. This airspace maximum altitude is below 10,000 ft. The lateral minima separation between aircraft is 3NM and the vertical minima separation in 1000ft. Once an aircraft reaches the airport, the control of the aircraft will be transferred to the Air Traffic Tower control. The SID and STAR are published procedures that provide the routes with lateral, altitude and speed constraint that the aircraft needs to follow for departure and arrival respectively. These procedures have been established at certain airports to simplify clearance delivery procedures by ATC. The design of SID and STAR procedures takes into account criteria such as:

- Segregation of Routes and Entry/Exit point,
- Minimize the number of crossing points Plan for vertical separation,
- Gradually converge inbound flows,
- Group similar inbound flows in Entry Gates,
- The horizontal and vertical routes spacing constraints.

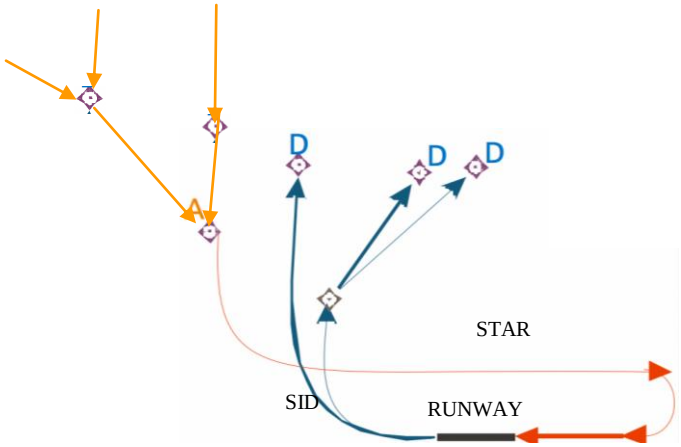

Figure 4.2: Example of routes segregation and convergent of traffic at the entry [EUROCONTROL, 2014]

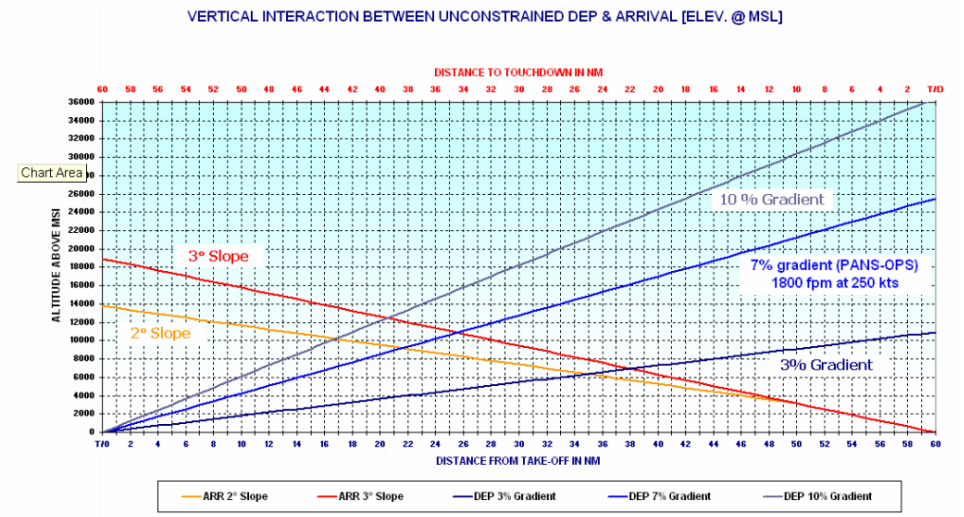

Figure 4.3: Good design practice proposed by ICAO for departure (DEP) and arrival (ARR) vertical constraints [EUROCONTROL, 2010]

4.3 Modern Traffic Management Space Organization

4.3.1 Performance Based Operations (PBO)

The previous traffic organization components were developed around sets of standards developed by Federal Aviation Association (FAA), International Civil Aviation Organization (ICAO) and other aviation organizations. These specified standard equipment performance for global ATM systems are safe to use, but nonetheless the process of changing the standards to match current technology and the implementation was time consuming. Thus, major aviation organization and providers are slowly shifting to performance based systems for setting standards and procedures. Based on Performance Based Operations (PBO), the standards and procedures are developed to achieve outcomes rather than a list of detailed procedures. As long as the procedures, processes or equipment can comply with the specified performance it can be integrated into the aviation system. PBO is being developed in areas of communications, navigations, surveillance and air traffic management [Nolan and Ballinger, 2015]. Here, the application is more interested towards the development in the navigations context.

The current airspace navigation is transitioning to new performance based navigation (PBN) concepts of area navigation (RNAV) and required navigation performance (RNP). These concepts would transform the ground-based systems and fixed navaid systems to a system where the aircraft can select which technologies (VOR, DME, GNSS or ILS) to use for en-route and terminal phases of flight.

The PBN concept is based on 3 main components, which are:

1. The Navigation Aids (NAVAIDs) Infrastructure which is connected with the ground-based and space-based aids,
2. The Navigation Specifications which relates with Area Navigation (RNAV) and Required Navigation Performance (RNP). These two navigation techniques will give the position of the aircraft with a certain level of accuracy described in RNP and RNAV specifications,

3. The Navigation Application is achieved by using both the first and second components.

Most modern aircraft are equipped with Area Navigation (RNAV) system capability. RNAV is a navigation function which gives the aircraft flexibility to fly a chosen route within a network of NAVAIDS without having to fly from on waypoints / fixes to the other. Now RNAV is part of navigation techniques of the Performance-Based-Navigation (PBN). A description of RNAV is shown in Figure 4.4.

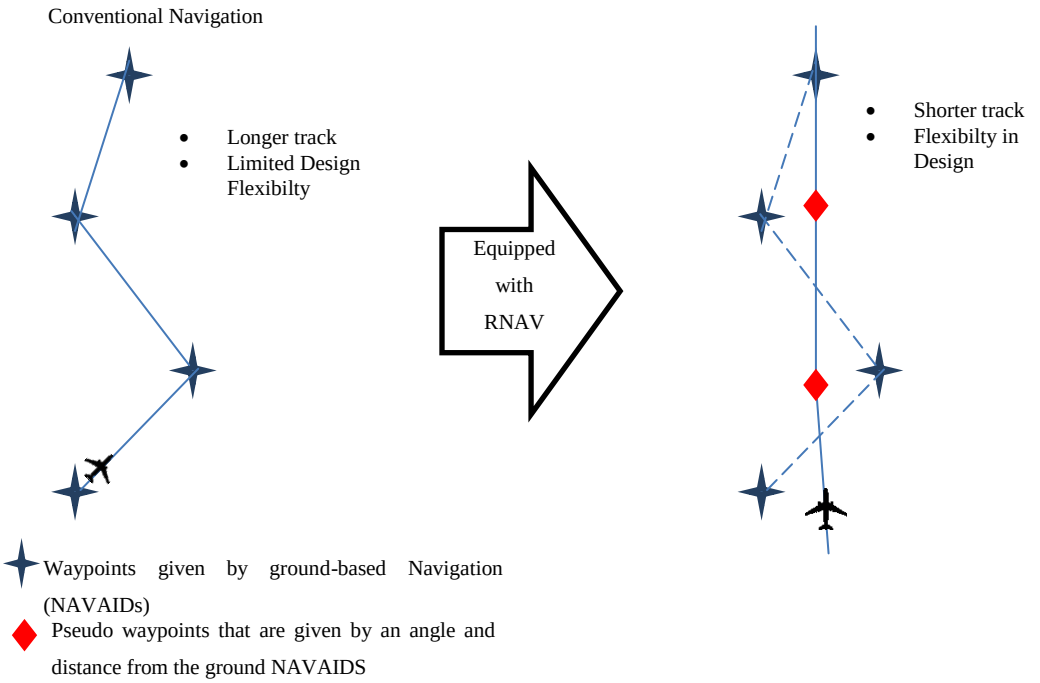

Figure 4.4: From classical to RNAV operation [Todorov, 2009]

RNP is a statement on navigation performance accuracy which allows airspace designers to specify airspace and operation requirements without referring to specific equipment or systems. RNP requires on-board performance monitoring and alerting as part of the avionic functionality. This means that the aircraft equipped with RNP can be positioned closer than those equipped only with RNAV. In the PBN manual eleven navigation specifications have been included. Each RNP and RNAV specification is designated by their type given by RNP-X and RNAV-X where X refers to the lateral navigation accuracy in nautical miles, which is expected to be achieved at least 95% of the flight time by the population of aircraft operating within the airspace, route or procedure. The containment limit quantifies the navigation

performance where the probability of total system error (TSE) greater than 2 x RNP is less than 1 x 10^{-5}. The RNP RNAV containment region helps with the safety assessments for separation and obstacle clearance in the development of routes, areas, and procedures. An example of RNP-X is shown in Figure 4.5.

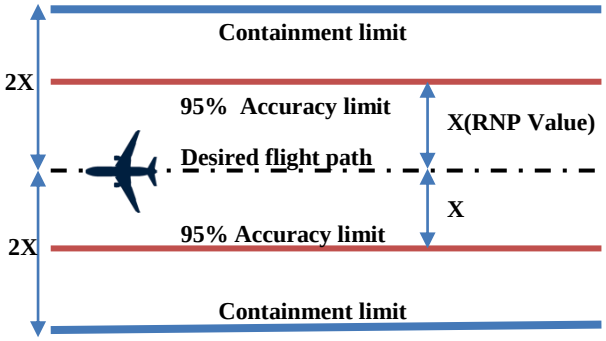

Figure 4.5: RNP-X definition means that navigation system must be able to calculate its position to within a circle with a radius of X nautical miles. The 2 x RNP containment limit represents the level of assurance of the navigation performance with a 99.999% percent probability per flight hour

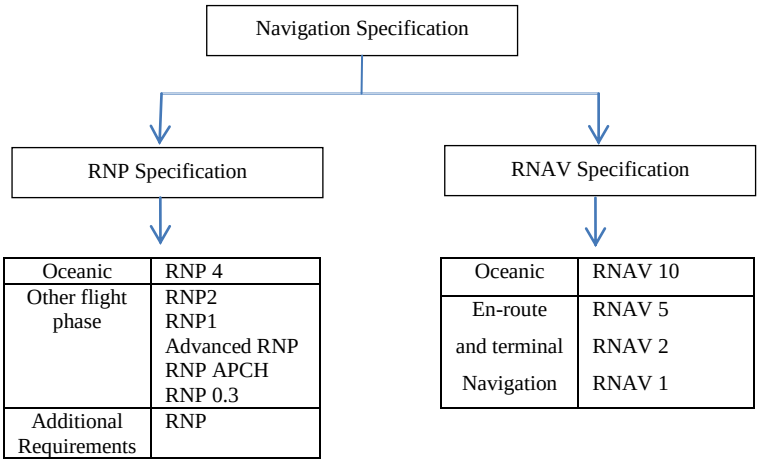

Figure 4.6 : Navigation specification for RNP and RNAV

The performance of RNP systems is quantified by the Total System Error (TSE). Total System Error (TSE) is defined as statistical sum of the component errors due to Navigation System Error (NSE), Flight Technical Error (FTE) and Path Definition Error (PDE). It is usually denoted as $\sim 2\times\sigma$ where σ being the statistical standard deviation of the TSE distribution.

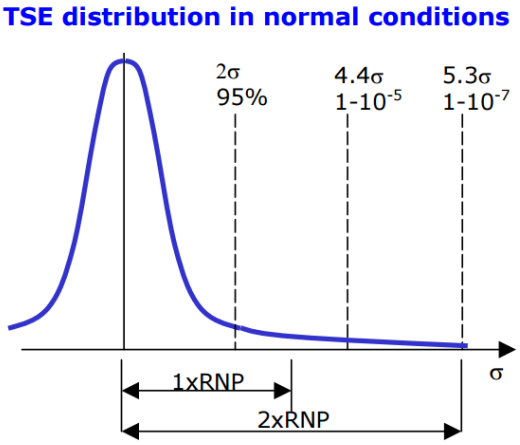

Figure 4.7: Corresponding RNP designation to the TSE value [AIRBUS, 2009]

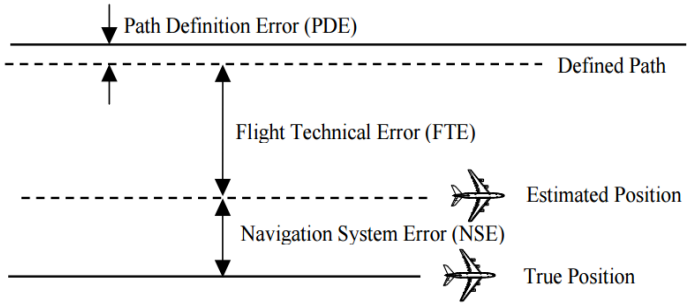

Figure 4.8: Definition of NSE, FTE and PDE [AIRBUS, 2009]

NSE value represents the capability of the navigation avionics to determine position, relative to the aircraft's actual position. FTE value represents the ability of the aircraft guidance system to follow the computed flight path and it is normally given by the aircraft manufacturer based on flight trials. Finally, PDE is the difference between the defined path/waypoints and the desired path/waypoints at a given place and time.

This total system error is used for both the lateral and vertical navigation performance evaluation. The total system error can be calculated using a general equation given by:

$$TSE = \sqrt{(FTE)^2 + (NSE)^2 + (PDE)^2} \tag{4.1}$$

From the implementation of PBN in navigation, the combination of Ground-Based and of Space-Based Navigation Aids is proven to increase the navigation

flexibility and airspace capacity [Walter, 2014]. Exploiting these systems to the fullest would lead to the concept of free flight. Free flight is a concept that gives the flight crew full responsibility in managing their flight navigation such as to take advantage of wind and optimal route.

4.4 Free Flight

4.4.1 Definition and objectives

In the early eighties, The Council of International Civil Aviation Organization (ICAO) had established a Special Committee on Future Air Navigation Systems (FANS) with the objective to study, identify and assess new technologies to recommend future development of air navigation for the next 25 years. The Special Committee on FANS came up with a concept which is known as Communication Navigation and Surveillance/Air Traffic Management (CNS/ATM). In 1995 the Radio Technical Commission for Aeronautics (RTCA) proposed based on the FANS concept an incremental approach from the current ATC to an ATM system enabling free flight. Figure 4.9 shows in the case of USA, the progress and aim towards the future air navigation proposed by FANS where the implementation of free flight is envisaged for all flight domains.

The free flight main objective is to allow the aircraft under the IFR to fly its optimal route (‘direct routing’) and the traffic separation is moved from ground control to cockpit control (‘airborne separation’)[Hoekstra et al., 2001],[John H. et al., 1998]. In free flight operation, the cockpit crew is now responsible in maintaining separation with the assistance of the Airborne Separation Assurance System (ASAS) and the final conflict resolution is given by Traffic Collision Assurance System (TCAS). The responsibility of the controller will be reduced and they will be responsible in ensuring that the traffic density does not exceed the maximum allowable capacity inside that airspace and the entry/exit point.

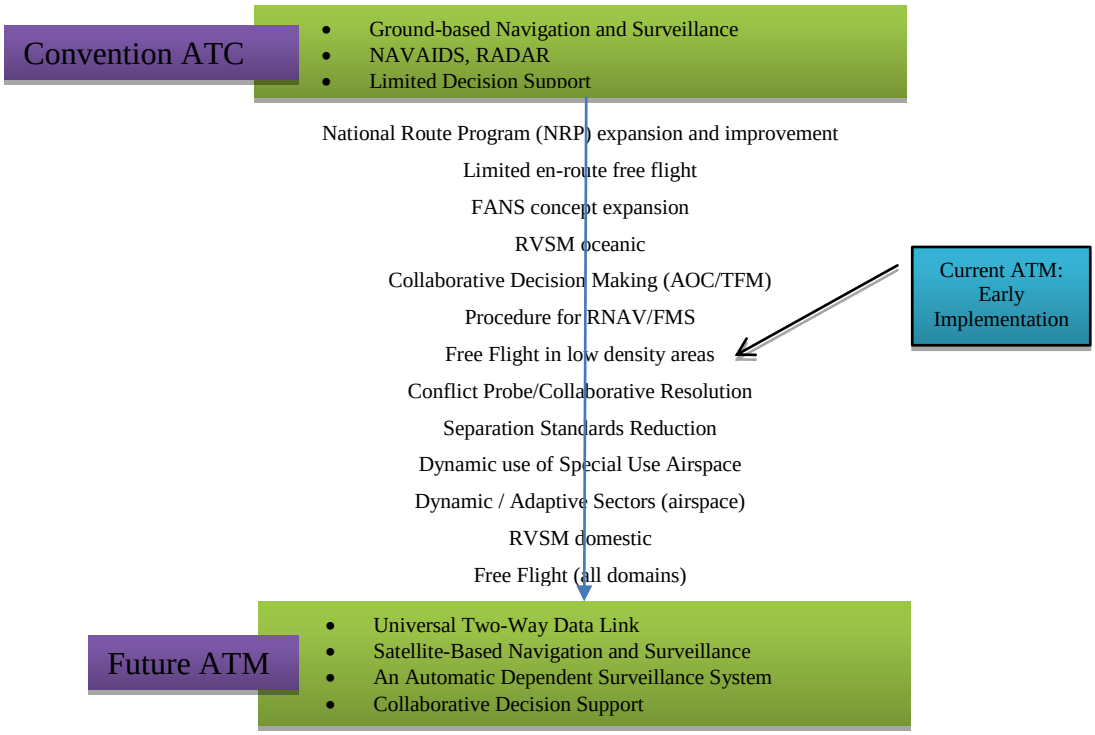

Figure 4.9: US expected evolution of traffic management [Barraci, 2010]

4.4.2 Traffic Separation Systems for Free Flight

In Airborne Separation Assurance Systems (ASAS), information sharing between aircraft is essential since the position, speed, heading, altitude and aircraft identification should be known and will be taken into consideration to calculate the probability of a collision. The ASAS concept is similar to Airborne Collision Avoidance System/Traffic Collision Avoidance System (ACAS/TCAS) but the difference is that ACAS/TCAS is an independent safety net function and short-term collision avoidance system since any last-minute maneuver of the aircraft would cause discomfort to passengers. Its purpose is to prevent collision when the primary means of separation provision has failed. ASAS assumes the responsibility of predicting a collision and it is comprised of the following system:

1. Airborne Surveillance and Separation Assurance Processing (ASSAP). From the information shared by aircraft in an area, the ASSAP processes the data received to form current estimates of position and velocity for each target aircraft, and makes these available for the pilot.

2. The Cockpit Display of Traffic Information (CDTI) display the information processed by the ASSAP

3. The Alerting System to notify the pilot for any conflict.

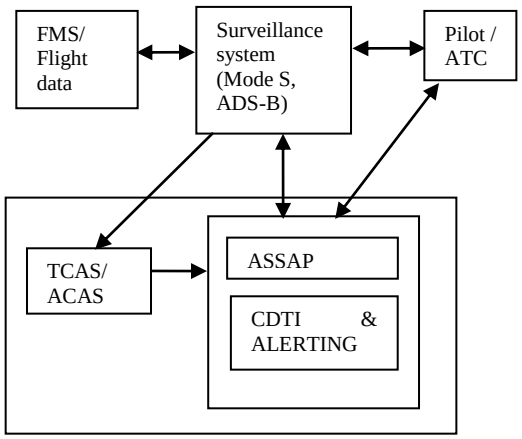

Figure 4.10: Overview of the traffic separation system

To implement the free flight, the design of efficient conflict resolution function is the utmost priority; the aircraft is designed to have its protected zone that acts as a conflict-safe zone given in Figure 4.11.

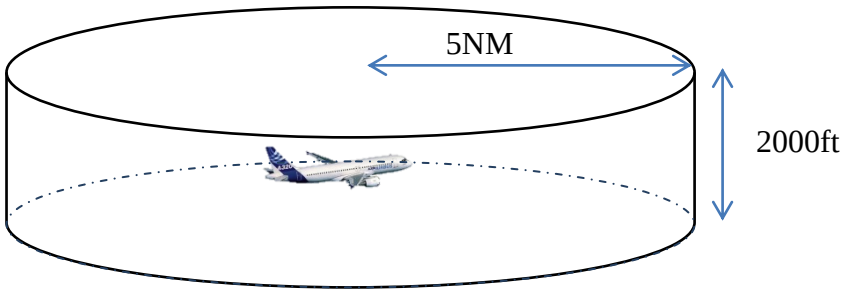

Figure 4.11 : The Aircraft Protection Zone

The Prediction Method proposed by [Paielli and Erzberger, 1997] is based on two concepts which are:

1. The State-Based Conflict Detection where the aircraft and the surrounding traffic position and velocity are used to detect conflicts.

2. The Intent-Based Conflict Detection which is a bit different in which the first methods in terms of the target path or flight plan is taken into account to detect any conflicts.

Many literatures such as [Barraci, 2010], [Durand et al., 1999], [Kim et al., 2013], [Paielli and Erzberger, 1997] discussed conflict-resolution algorithms to cope with this problem. In general the suggested maneuver is the vertical maneuver. The ASAS is used to maintain separation but the ACAS/TCAS will remain the final conflict resolution if the other conflict avoidance methods do not succeed or the standard safe separation is lost. ACAS/TCAS main objective is to ensure that the aircraft do not come into contact with each other and it will issue a traffic advisory (TA) between 20 to 48 seconds before closest point of approach (CPA) and a resolution advisory (RA) between 15 to 35 seconds before (CPA).

4.4.3 Free Flight Implementation

In Europe, a Free Route Airspace (FRA) Concept was introduced in 2009 and it was implemented step-by-step starting from Sweden. As of May 2014, 26 air traffic control centers (ACCs) have taken the initiatives to implement FRA where six of them are fully implementing the FRA inside the airspace and the other ACCs are partially implementing it [EUROCONTROL, 2015a]. Free Route Airspace (FRA) comprises specific airspace within which users can freely plan their routes between an entry point and an exit point without reference to the ATS route network as long as it does not enter any restricted airspace. This Free Route Airspace is conducted in Airspace Class C. Within this airspace, flights remain at all times subjected to air traffic control and to any overriding airspace restriction. The transition between the fixed ATS to the FRA is performed through a set of waypoints.

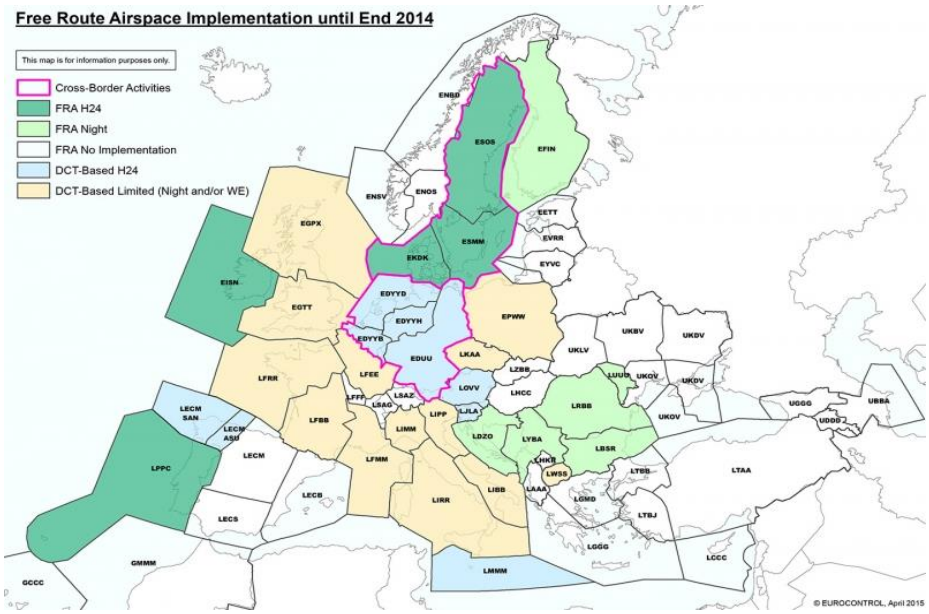

Figure 4.12: Countries that have fully/partially implemented FRA as of end 2014 [EUROCONTROL, 2015c]

Free Route Airspace (FRA) is a major step towards free flight. However there are still limitations to implement fully Free Route Airspace (FRA). Some of the foreseen limitations are [EUROCONTROL, 2015b]:

1. Time Limited: Currently Free Route Airspace (FRA) are implemented on a period basis and a slow transition towards fixed implementation is still in progress.

2. Structurally Limited: To avoid unfavorable effect (conflict and capacity) of free route operations in complex airspace, free route airspace must be structurally defined to increase predictability of the flights.

Even though free flight grants the aircraft to fly its optimal route, the structure on the airspace can be expected to look chaotic. The lack of structure of free flight may offer difficulty to the ground-controlled separation when the traffic density is high. Based on [Foreman, 1998] a question of shared loads for the pilot between maintaining separation and other critical tasks could be raised. During free flight, self-separation can be done quite simply in a low speed and low density traffic, but during high density traffic, frequent conflicts can occur and this leads to frequent changes of flight path. The implementation of free flight in free route airspace is still developing and a lot of improvements will be seen in the future. The concept of free

flight takes high attention into the ASAS system. This self-separation operation concept requires high accuracy and dependability in the aircraft real-time position and therefore research and implementation of Trajectory Based Operation (TBO) is currently conducted by two main projects – SESAR and NEXTGEN. These two projects will implement technologies to allow free flight to be operated in a safe and secure manner. Their purpose is to transform the air transport system by changing technology, infrastructure and procedures. In the next section, both SESAR and NEXTGEN TBO projects will be discussed.

4.5 SESAR and NEXTGEN Objectives

SESAR stands for Single European Sky ATM Research while NEXTGEN stands for Next Generation Transportation System. Both SESAR and NEXTGEN are programs that were created to tackle the current Air Traffic Management deficiencies in order to maintain safe airspace utilization and to modernize the current ATM to face the expected growth of air traffic during the next decades. Even though the methods used in these two programs are different, their goals are similar: to expand the capacity of the airspace, to get a global aviation harmonization, to ensure safety, to protect environment and to improve service for air transport customer. The key concept to these two programs is the 3D+T Trajectory-based Operations (TBOs).

4.5.1 Projects' objectives

According to FAA, Trajectory Operations (TOps) is such that every flight under the control of an Air Navigation Service Provider (ANSP) is managed through representations of its four-dimensional trajectory (3D+T) (3 dimensional space and time). Every managed aircraft known to the system has a 3D+T either provided by the user or derived from a flight plan or a type of operation. TOps represent a mid-term implementation strategy to improve capacity and efficiency [FAA, 2012]. Whereas for Trajectory Based Operations (TBO) it is defined as the extend trajectory operations and provides separation, sequencing, and merging and spacing of flights based on a combination of their current and future positions. TBO operates gate-to-gate, extending benefits to all phases of flight operations. TBO uses the 3D+T to both

strategically manage and tactically control ground and airborne operations. Flights are handled considering their 3D+T trajectory and ANSP automation provides TBO [FAA, 2012].

Since the current style of flight navigation is based on aircraft routes, TBO will transform from fixed aircraft routes and ATC-clearance based to a negotiation and updated flight trajectories between flight crews and ATC. Therefore, the backbones to the TBO concept are Business Trajectory and Ownership Trajectory. The first defines the intended trajectory that an operator has decided and the ATM needs to ensure that this intended trajectory is kept mostly throughout the flight. The latter is the owner of the flight which is responsible of this intended trajectory. The owner is given the power to change their intended trajectories but at the same time they are obliged to share their flight information, reacting to requests and following clearances issued by ATM.

Onboard automation has allowed the aircraft to fly more precisely and predictably, reducing the routine tasks of controllers. The sharing of aircraft trajectory data amongst the various participants in the ATM will lead to negotiating the trajectory and decision making in order to form a reference trajectory for the aircraft to follow before the flight. The expected benefits of TBO are:

1. Greater capacity and higher efficiency in terms of traffic flow and capacity inside the airspace since the reference trajectories are given by position and also time-constraints,

2. Predictability of the flight is increased due to the usage of both ground-based and satellite based navigation that could lead to the improvement of flight safety,

3. Any interventions to the flight trajectory such as flight path change due to weather or conflict avoidance are within the full knowledge of the downstream effects and hence it will be possible to choose the option causing the least amount of trajectory distortion,

4. By flying with accurate guidance, the uncertainties around the trajectory are reduced and this will make it possible to fit more aircraft into a given volume of airspace,

5. Since the best optimal path will most likely to be used, fuel burn and CO_2 emission will be reduced, leading to a healthier environment.

4.5.2 Implementations of TBO

Two projects concerning the improvement of flight efficiency through trajectory based operations are Continuous Descent Approach (CDA) and Continuous Climb operation (CCO). The variations of these operations (CDA/CCO) are now being conducted in some countries and it was proven that by implementing these technique it reduces the CO_2 emissions [Cao et al., 2011, ICAO, 2013]. Some of the benefits of CDO/CCO are lower pilot/controller workload, shorter time in sector, reduced radio transmission, reduced fuel consumption, reduced departure delays and more departure lanes and exit points to the en-route airspace.

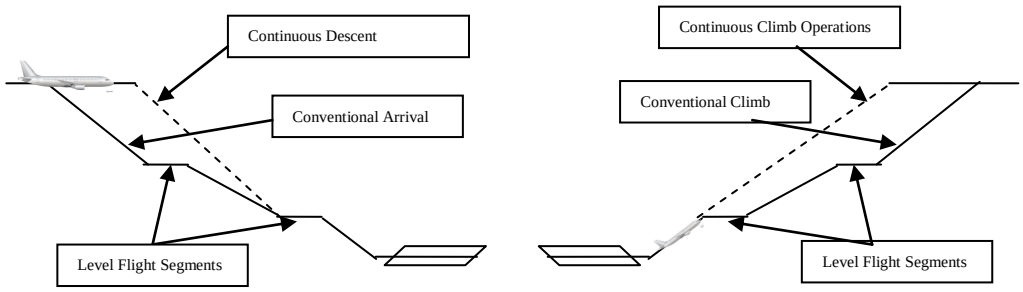

Figure 4.13: Example of continuous descent approach (CDA) and continuous climb operation (CCO)

Other than the flight technique above, an initial 4 dimension (I-4D) operations was conducted to synchronize trajectory information between Air Traffic Control (ATC) and Aircrafts (Flight Crews and their supporting avionics systems) so that the arrival sequence can be optimized. This I-4D Trajectory Management concept relies on time-based operation but it is also a major progress towards Trajectory Based Operations (TBO). Initial 4D operations consist of information of time constraint at a merging point to each aircraft, in order to sequence the traffic for arrival. Example of merging point is Initial Approach Fix (IAF) point. The first trial was conducted between Toulouse, France and Stockholm Arlanda, Sweden on 10 February 2012. The flight test was successful in demonstrating the operational and technical feasibility from an airborne and an integrated air / ground perspective [Mutuel et al., 2013, SESARJU, 2013].

4.6 Conclusion

The air traffic organization and management is currently being revolutionized to meet the demand predictions of air traffic for the very next decade. Concepts such as free flight and TBO are introduced to meet this increased demand. These concepts do not disregard the current air traffic management and technology but try to take a direct benefit of advanced technologies such as ADS-B, Satellite Based Navigation to redesign the air traffic management worldwide. The main objective is to maximize the use of the capacity promoted by the airspace while maintaining high safety standards. Free Flight is a very attractive concept but in the case of high traffic density regions, the adoption of free flight may result, even through 3D+T trajectory negotiation processes with ATM, in an increasing number of conflicts which are solved by modifying these aircraft trajectories. The development of fully automatic on-board conflict resolution devices [Ramamoorthy et al., 2004] will ease in some way the traffic control task but the resulting traffic may be in a permanent reconfiguration and its monitoring by ATC should become more and more difficult [Blom et al., 2006]. Now, the nearest concept that will be implemented is TBO. With more accurate guidance and higher predictability of flight, it can be expected that the traffic density will be allowed to increase. Recent projects and research studies related to the management of air traffic in high density traffic flow will be presented in the next chapter.

CHAPTER 5
NEW ORGANIZATIONS FOR HIGH DENSITY TRAFFIC FLOWS

Chapter 5: New Organizations for High Density Traffic Flows

5.1 Introduction

New flight guidance systems should be compliant with the new organization of traffic management and should be able to guide safely and efficiently aircraft in high density traffic. With the arrival of new technologies such as ADS-B and digital data communication between ATC and aircraft that fall within communication, navigation and surveillance (CNS) systems which are expected to give high accuracy in the aircraft position [SESARJU, 2013]. This leads to the reduction in the separation minima and consequently increases the air traffic density. A concept envision by NextGen TBO is the flow corridor. Flow corridor objective is to absorb as many flights as possible in the high density traffic flow while guaranteeing the time of departure and arrival. Flow corridors are called by many terms such as tube network, tube structure and highway in sky. This concept will be elaborated in the next section. A new concept called Airstreams concept, will be introduced which is a more structured corridor in the perspective of the flow corridor. The objective of the Airstream concept is to cope with high density traffic and ease the traffic management and surveillance. This concept introduces a reference trajectory to organized high density traffic flow and the position of the aircraft is expressed in the local axial coordinates system.

5.2 Flow Corridors

A flow corridor is described generally as a long and narrow air highway intended for use by aircraft to fly from an entry to the end with minimal interference from other traffic. Inside the corridor, flights in the same direction, opposite direction and crossing of traffic are being controlled by the Air Navigation Service Provider (ANSP). The flow corridor intention is to absorb the traffic to reduce ATC workload and increase traffic capacity at the same time maintaining a safe flight and observing

the time constraint. The implementation of flow corridor is in conjunction with its objectives:

1. Enabling high density flow by the introducing reduced separation requirements and multiple parallel traffic,
2. Diminishing controller workload due to the onboard capabilities of the aircraft such as ASAS,
3. Rerouting around weather hazards and congestion. The flow is flexible to account for any weather conditions.

5.2.1 Flow corridors organizations

Extensive research has been conducted to see how to design and implement flow corridors. In the flow corridor, there are multiple closely spaced parallel lanes. The corridor is separated from other traffic and to enter or exit the corridor, aircraft needs to use an air ramps. Only aircraft equipped with required navigation performance (RNP), a self-separation capability and an automated separation assurance system are allowed to fly inside a corridor. Figure 5.1 shows an example of the proposed flow corridor building block.

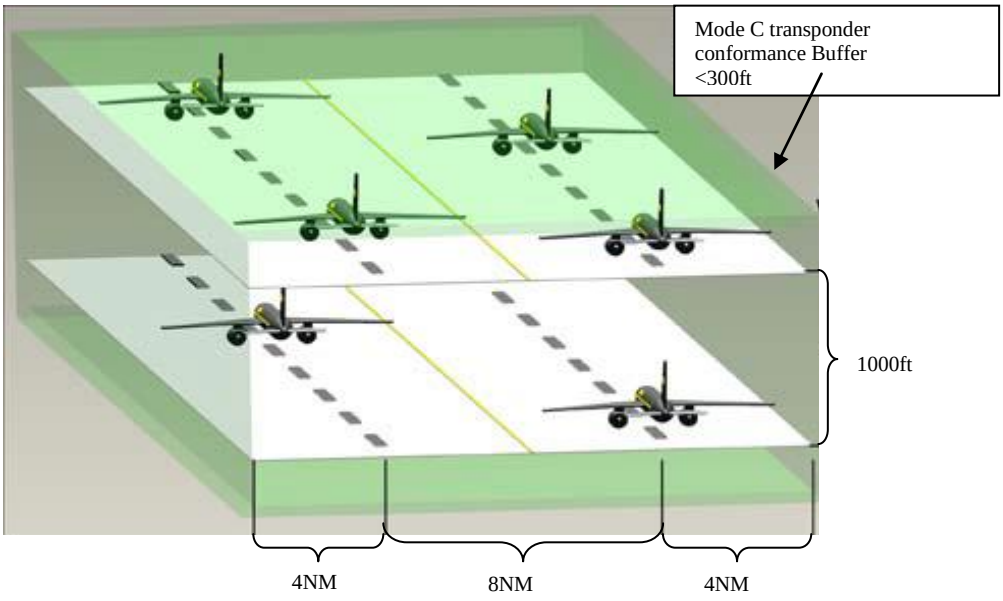

Figure 5.1: Nominal design of Corridor Building block [Yousefi et al., 2010]

The flow corridor is proposed to use the Q-Routes airways. Q-Routes are routes between FL180 and FL 450 and only RNAV equipped aircraft can use it. From [Takeichi et al., 2012], the minimum separation between aircraft inside the flow corridor is 5NM and 0.2*5NM as a safety buffer shown in Figure 5.2.

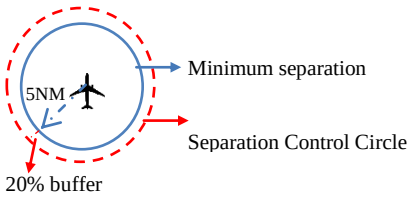

Figure 5.2: Separation Requirements

The separation standard proposed to improve the Q-Routes is 8 nautical miles (NM) between the centerlines so that two routes can be placed in a similar volume of airspace as a current High Altitude Jet Route. It is expected that separation responsibilities fall to the aircraft. They are responsible in their own separation including passing another aircraft.

The attribute and the procedures of the traffic inside a flow corridor have been discussed by [Wing et al., 2008]. The design configuration of the track inside the flow corridor is based on employing speed-dependent and speed-independent configurations. The first configuration is that the track is designated with a nominal speed or Mach number, as for the second configuration, speed change is allowed inside the corridor as a change of lane is required for a fast aircraft to overtake the slower aircrafts.

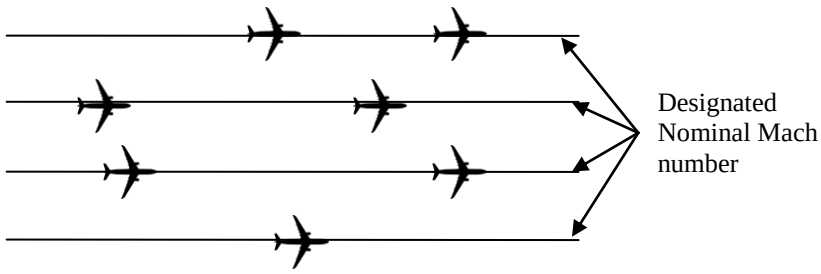

Figure 5.3: Speed-Dependent Track – designated by nominal Mach number [Wing et al., 2008]

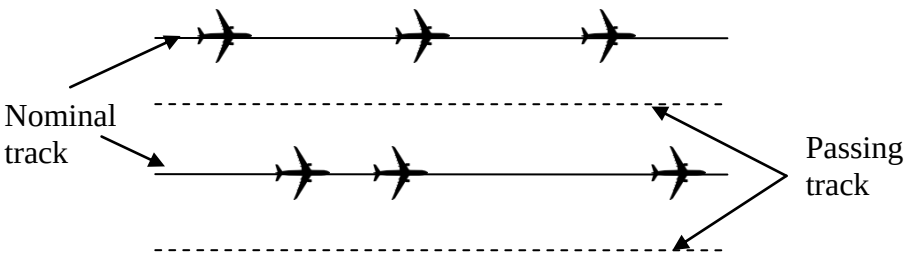

Figure 5.4: Speed independent track[Wing et al., 2008]

5.2.2 Flow corridor capacity

Papers from [Kotecha and Hwang, 2009],[Yousefi and Zadeh, 2013] and [Xue and Kopardekar, 2009] proposed an extensive review on the development of flow corridors. The design of the corridors is usually based on the highest density of traffic flow from major airports/city and from there methods such as Hough transform, Graph theory and Clustering of the Velocity Vector Field to a Sliding Window Framework have been used to find the best placement of a network of flow corridors.

The Hough Transform method suggested by [Xue and Kopardekar, 2009] is to cluster the great circle trajectories as the candidate for the flow corridors. These great circle trajectories are transformed into points in the Hough space. The clustering criterion is the minimal excess flight distance. From the initial result, a genetic algorithm is applied to refine the clustering such that it moves the center of tubes to obtain better clustering and the best corridors network. From the simulation, it was found that this method can absorb about 44% of total flight between 25 airports/cities considering about 5% increase in flight deviation from the original path.

In [Kotecha and Hwang, 2009], the authors proposed a weighted centroid approach to assign the tube points and the weight used was the number of operations (NOPs) of an airport. Then, by using the graph theory and Dijkstra's algorithm, the optimum path of the flow corridor between two points can be found. This method ensures that only high density routes are included into the flow corridor network. From this study, about 54% of the total operations between 34 cities can be absorbed inside a corridor. Finally the proposition given in [Yousefi and Zadeh, 2013]

suggests of the clustering of velocity vector field of the user's preferred trajectories between city pairs. From the clustering, the resulting vector produces the optimal routing of the Flow Corridor. Through this algorithm it was found that the 60% of the flights between ten coast-to-coast flights can be absorbed and it reduces the delay by also 60%.

From these finding, it can be seen that about 50% of the total flight operations can be absorbed inside the flow corridor. However, from [Xue and Kopardekar, 2009] and [Yousefi and Zadeh, 2013], it was found that a small number of flow corridors are enough to increase the number of flights inside the corridor without compromising the delay flight time and path deviation. From [Wing et al., 2008], it is expected that implementing the flow-corridor would also reduce the sector loads and wide delay of National Airspace System (NAS) in United States.

5.2.2 Estimating safety within flow corridors

In order to ensure safety within the flow corridor, airborne separation and assurance function need to be designed. From [Wing et al., 2008] and [Yousefi et al., 2010], the separation assurance is handled by the pilots. From [Zhang, 2014] the separation rules for aircraft inside the flow corridor are based on 4 factors which are:

1. Minimum separation – Lateral separation between aircraft is 5 nautical miles but within the flow corridor it can be reduced.

2. Separation buffer in order to give extra safety allowance, the buffer is about 20%.

3. Separation threshold is the sum of both minimum and separation buffer.

4. Relative velocity threshold: This is the threshold to see whether the trailing aircraft relative speed can pass a slower aircraft or reduce the aircraft speed to follow the leading aircraft speed. If the relative speed is greater than the threshold then the trailing aircraft is allowed to change lane if possible.

The conflict resolution algorithm based on speed and aircraft heading is introduced in [Takeichi et al., 2012]. The approach to conflict resolution is applied

for the case where the aircraft follow a uniform speed distribution between 230 m/s and 250 m/s and the initial cross-track positions and headings are also random variables. The conflict resolution maneuver is to have the aircraft turn to the opposite direction. The maneuver is shown in Figure 5.5. The results obtained show that the algorithm can achieve the conflict free operation with a large traffic amount.

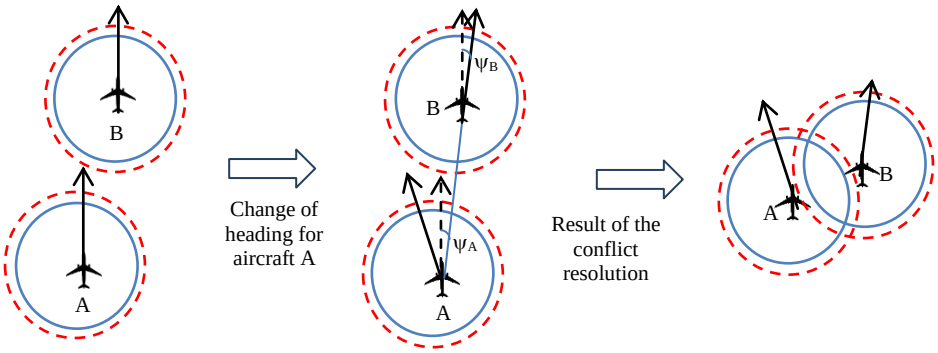

Figure 5.5: Conflict resolution: Speed of aircraft A is 250m/s while aircraft B is 230 m/s. Both aircraft make a slight left and right turn to achieve required separation.

From these studies, the conflict resolution is considered mostly between a pair of aircraft. The conflict resolution is done one at a time and it may happen that further conflict could be encountered after performing the first resolution. This could lead to increase in the workload of pilot.

Below is the summary of some design criteria of the flow corridor. The main design perspectives of flow corridors are as follows:

1. Configuration:
    - Only one direction of flow is allowed within the corridor. It is designed based on designation of flight level and parallel lanes,
    - Speed adjustments are allowed within the corridor,
2. Entering and exiting the corridor through on-ramps and off-ramps respectively
    - This can be activated or deactivated according to demand during the day,
    - Can be dynamically changed to take benefit of the wind or to avoid severe weather conditions,

- It is not constrained to higher flight level but fully functional on higher flight level.

3. Separation and Maneuver:

    - Minimum separation is 5NM laterally,
    - Aircraft are allowed to change lanes to pass by slower aircraft,
    - Separation is based on separation thresholds and relative speed thresholds.

Even though, the flow corridor is an appealing method to reduce ATC workload and flight capacity within the corridor and subsequently reduce the flight delay, flight inside the corridor can be speed based or non-speed based. For flights having a non-speed base track frequent speed adjustment need to be done which may lead to a dynamic spacing between aircraft. In the next section, a concept to organized flights in high density traffic is discussed where it employs space based slots and a local space indexed axial coordinates system to reference the aircraft to a reference trajectory.

5.3 Airstreams

For high density traffic, air corridor concept and time-based flow management have recently been proposed. In this section, a new structured corridor is proposed to organize main traffic flows in congested airspace along **airstreams** which are characterized by a **three-dimensional (3D)** common reference track and lateral lanes with a **dynamic slot structure**. A common spatial reference, the **airstream reference track (ASRT)** is introduced as a geometric guideline of the air corridor configuring an airstream. The adoption of such spatial reference will ease the on-board traffic separation task within an orderly traffic along this 3D reference.

5.3.1 Definition of airstream

Like classical airways, airstreams propose a common space for aircraft adopting similar navigation and guidance objectives for a portion of their flight. Here an airstream is defined as an organized flow of aircraft along lanes around and along a common 3D reference track, called here an airstream reference track (ASRT). These lanes are positioned precisely around this reference track and separated laterally according to minimum separation constraints. Each aircraft is supposed to remain in the center of a moving spatial slot which follows a lane. This center is a permanent target for its guidance system. Figure 5.6 displays an example of section for an airstream with its ASRT, a single inner layer of lanes and a layer of peripheral lanes. The idea is that any flight intend to enter or leave the airstreams will have to past through the peripheral lanes before entering the inner lanes. This allows the aircraft to exit and enter the airstreams at any points given that any restrictions or constraints along the airstream are followed.

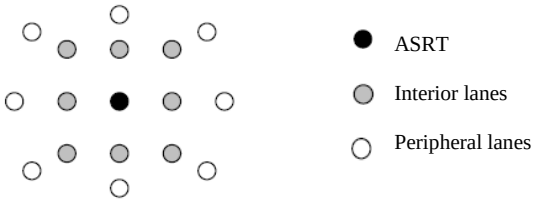

Figure 5.6 : Example of cross-section of an airstream

Airstreams have no predefined dimensions (width, height or radius) and their section will depend of the number of lanes attached to the ASRT. The ASRTs may present turns and may be changed periodically according to different factors such as expected traffic demand and next day forecasted weather conditions. Aircraft with different performances or adopted cost indexes and speeds can be present in the same airstream.

To be allowed in an airstream, aircraft equipment requirements are similar to that of airspace flow corridors where transportation aircraft must be equipped with required navigation performance (RNP), self-separation capability and on-board automated separation assurance. Self-separation on a lane is performed by dynamic position adjustments where the ADS-B technology can provide position and speed

information. Lane change maneuvers within the airstream are performed without intervention by a central controller when an aircraft adopts new reference airspeed. The on-board automated separation assurance system incorporates different levels of protection against a collision, including conflict detection and resolution, where the last protection against a collision is the Traffic Collision Avoidance System (TCAS). In airstreams, the pilots will remain responsible in ensuring the safe separation with nearby aircraft by maintaining situational awareness, performing standard maneuvers and reacting to conflict resolution advices.

5.3.2 Reference Tracks and Frames

Since an airstream is built around a common reference track, it appears of importance to define in detail the frames and tracks used to position lanes and aircraft with respect to assigned lanes. Here it is considered that the common reference track of the airstream, the ASRT, is a 3D curve given by a smooth parametric mapping which produces the geocentric coordinates of its points:

$$s \in [s_1, s_2] \subset \mathrm{R}^+ \rightarrow (L(s), M(s), R(s)) \in [0, 2\pi] \times [-\frac{\pi}{2}, +\frac{\pi}{2}] \times \Re^+ \qquad (5.1)$$

where L(s), M(s) and R(s) are respectively the geocentric longitude and latitude and the distance to the center of the Earth of the corresponding track point. Here s is defined as the curvilinear abscissa along the ASRT, then:

$$s - s_1 = \int_{track} \sqrt{(dx^2 + dy^2 + dz^2)} = \int_{track} \sqrt{dR^2 + R^2 \cdot (dM^2 + \cos M^2 \cdot dL^2)} \qquad (5.2)$$

where s_1=0 is the initial point of the airstream reference track. It is supposed that functions L, M and R are smooth, injective functions and correspond to a flyable trajectory for a transport aircraft. Typical examples of such curves are orthodrome and loxodrome curves which locally can often be assimilated with straight horizontal lines. Here it is assumed that the airstream traffic will follow trajectories positioned radially along this reference track.

5.3.3 Local Axial Reference Frames

In Figure 5.7 displays an example of airstream track as well as the Earth centered Earth fixed (ECEF) frame given in *X*, *Y* and *Z* axis, supposed here to be an inertial frame, and the local Earth frame attached to a given point *S* of this track.

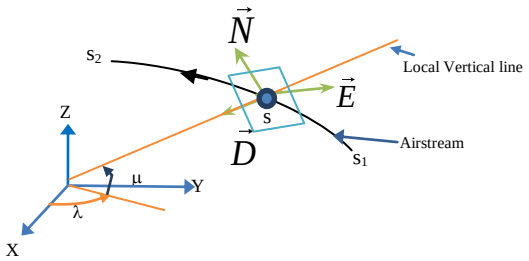

Figure 5.7: Guidance along an aircraft reference trajectory

By letting $\underline{\tau_S}$ to be the unitary tangent vector to the ASRT at point S in Figure 5.8, the intersection of the local horizontal plane with the cross section plane at this point S of the considered reference trajectory defines a local horizontal normal line to the track. Here it is assumed that this direction is positively oriented when pointing to the north. Let $\underline{n_S}$, be the corresponding unitary vector. Let $\underline{r_S}$, be the local unitary vector pointing upwards at a point *S* of the ASRT and orthogonal to $\underline{\tau_S}$ .Then the triplet $(\underline{\tau_s}, \underline{u_s}, \underline{n_s})$ defines the local airstream (LAS) frame at point *S* as displayed in Figure 5.8.

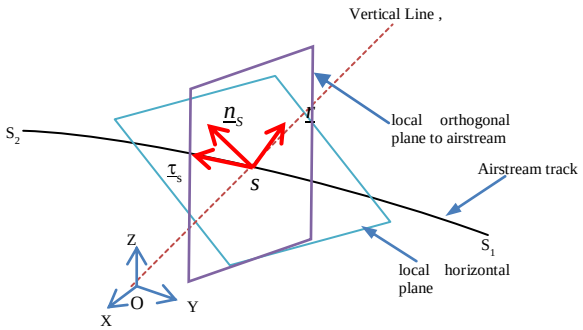

Figure 5.8 : The local airstream frame at point *S*

In many situations, it will be possible to assimilate vector $\underline{r}_S$ with the local upwards vertical direction. Point *S* and directions $\underline{n}_S$ and $\underline{r}_S$ define the cross section plane of the ASRT at some abscissa *s*.

Adopting this local frame, the position of the point *P* where the lane crosses the cross section plane $(\underline{r}_s, \underline{n}_s)$ can be given by its axial coordinates ρ and σ. In Figure 5.9, ρ is the radial distance between points *S* and *P*, σ is a local azimuth angle and *s* is the curvilinear abscissa representing the longitudinal position along the track of the airstream. Here point *S* is the mark of point *P* on the ASRT.

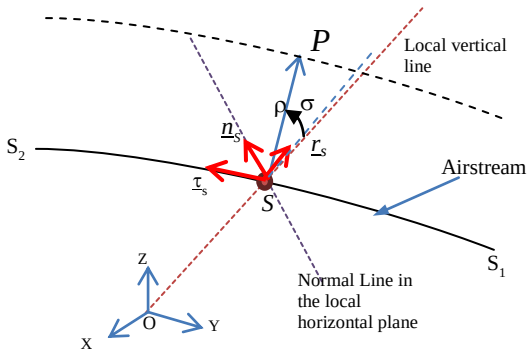

Figure 5.9 : Reference point in cross section plane

The relations between the coordinates of a point on a lane along a given ASRT, expressed in the ECEF frame and in the local airstream (LAS) frame of, are discussed in the following sections.

5.3.4 Coordinates transformation

In this section, the relationships between the coordinates of the position of an aircraft flying along an airstream expressed in the Earth Central Earth Fixed (ECEF) frame and in the local airstream frame are shown.

5.3.4.1 From LAS to ECEF Coordinates

Here the ECEF coordinates *X*, *Y* and *Z* of position *P* in Figure 5.9 are computed from its LAS coordinates *s*, ρ and σ. The reference track from S_1 to S_2, part of the airstream reference trajectory (ASRT), is given by its geocentric coordinates indexed by the curvilinear abscissa *s*: longitude *L(s)*, geocentric latitude *M(s)* and radius, *R(s)*. Then the coordinates of point S (X_S,Y_S,Z_S) on the ASRT (curvilinear abscissa $s \in [s_1, s_2]$) are given in the ECEF reference frame by:

$$X_S(s) = R(s) \cdot \cos M(s) \cdot \cos L(s) \tag{5.3}$$

$$Y_S(s) = R(s) \cdot \cos M(s) \cdot \sin L(s) \tag{5.4}$$

$$Z_S(s) = R(s) \cdot \sin M(s) \tag{5.5}$$

Here the local horizontal plane at point *S* is defined as the perpendicular plane to the local geocentric vertical line at this point, independently of the assumption about the shape of the Earth. Its equation in the ECEF frame is given by:

$$(X - X_S) \cdot x_S + (Y - Y_S) \cdot y_S + (Z - Z_S) \cdot z_S = 0 \tag{5.6}$$

Let $\underline{\tau}(s) = (\tau_x(s), \tau_y(s), \tau_z(s))'$ be the unitary direction of the tangent to the airstream track at point *S*. It is such as $\tau = d\overrightarrow{OS} / ds$. Then:

$$\tau_x(s) = \frac{dX_s}{ds} = \cos M(s) \cdot \cos L(s) \cdot \frac{dR(s)}{ds} - R(s) \cdot \sin M(s) \cdot \cos L(s) \cdot \frac{dM(s)}{ds} - R(s) \cdot \cos M(s) \cdot \sin L(s) \cdot \frac{dL(s)}{ds} \tag{5.7}$$

$$\tau_y(s) = \frac{dY_s}{ds} = \cos M(s) \cdot \sin L(s) \cdot \frac{dR(s)}{ds} - R(s) \cdot \sin M(s) \cdot \sin L(s) \cdot \frac{dM(s)}{ds} + R(s) \cdot \cos M(s) \cdot \cos L(s) \cdot \frac{dL(s)}{ds} \tag{5.8}$$

$$\tau_z(s) = \frac{dZ_s}{ds} = \sin M(s) \cdot \frac{dR(s)}{ds} + R(s) \cdot \cos M(s) \cdot \frac{dM(s)}{ds} \tag{5.9}$$

The track speed V_S (shown in Figure 5.10) is such as :

$$V_S(s) = \frac{ds_P}{dt} = < \underline{\tau}(s), \underline{\dot{P}}(s) > \tag{5.10}$$

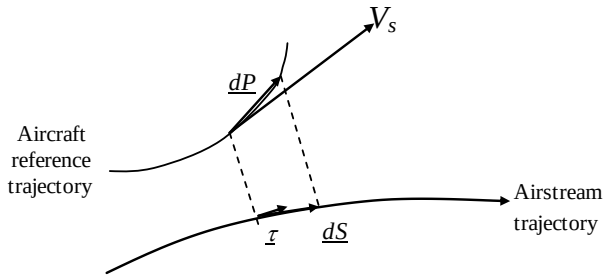

Figure 5.10: Track speed along the ASRT

The coordinates *X*, *Y*, *Z* in the ECEF frame of the points *P* belonging to the perpendicular plane to the ASRT at point *S*, satisfy the equation:

$$(X - X_S)\cdot\tau_x(s) + (Y - Y_S)\cdot\tau_y(s) + (Z - Z_S)\cdot\tau_z(s) = 0 \tag{5.11}$$

Then the normal line to the ASRT at point *S* which is in the geocentric local horizontal plane is composed of the points satisfying simultaneously Equations 5.6 and 5.11. The northbound unit vector of this line, written $\underline{n_S}$ will have its coordinates A_S, B_S and C_S in the ECEF frame such as:

$$\alpha_S \cdot X_S(s) + \beta_S \cdot Y_S(s) + \gamma_S \cdot Z_S(s) = 0 \tag{5.12}$$

$$\alpha_S \cdot \tau_x(s) + \beta_S \cdot \tau_y(s) + \gamma_S \cdot \tau_z(s) = 0 \tag{5.13}$$

$$\alpha_S^{\,2} + \beta_S^{\,2} + \gamma_S^{\,2} = 1 \tag{5.14}$$

with

$$-\sin M(s)\cdot\cos L(s)\cdot\alpha_S - \sin M(s)\cdot\sin L(s)\cdot\beta_S + \cos M(s)\cdot\gamma_S \geq 0 \tag{5.15}$$

where $-\sin M(s)\cdot\cos L(s), -\sin M(s), \sin L(s)$ and $\cos M(s)$ are the coordinates in the inertial frame of the north vector of the local frame attached to the horizontal plane at point *S*. Then $\underline{n_S}$ is such as:

$$\underline{n}_S(s) = (\alpha(s), \beta(s), \gamma(s))' \tag{5.16}$$

where

$$\alpha(s) = \frac{\varepsilon \cdot a(s)}{\left\|\underline{n}_S(s)\right\|} \qquad \beta(s) = \frac{\varepsilon \cdot b(s)}{\left\|\underline{n}_S(s)\right\|} \qquad \gamma(s) = \frac{\varepsilon}{\left\|\underline{n}_S(s)\right\|} \tag{5.17}$$

here

$$a(s) = \frac{\tau_z(s) \cdot Y_S(s) - \tau_y(s) \cdot Z_S(s)}{\tau_y(s) \cdot X_S(s) - \tau_x(s) \cdot Y_S(s)} \qquad b(s) = \frac{\tau_z(s) \cdot X_S(s) - \tau_x(s) \cdot Z_S(s)}{\tau_y(s) \cdot X_S(s) - \tau_x(s) \cdot Y_S(s)} \tag{5.18}$$

In the singular case in which:

$$\tau_y(s) \cdot X_s(s) - \tau_x(s) \cdot Y_s(s) = 0 \tag{5.19}$$

the ASRT is tangent to a meridian plane. In that case, $\underline{n}_S$ is chosen such as:

$$\underline{n}_s(s) = sign(\tau_z(s)) \cdot \underline{\tau}(s) \wedge \underline{u}(s) \tag{5.20}$$

where $\underline{u}(s)$ is the local upward vertical vector:

$$\underline{u}(s) = (X_s(s) / R(s), Y_s(s) / R(s), Z_s(s) / R(s))' \tag{5.21}$$

It is expected here that meridian reference trajectories with $\tau_z(s) = 0$ are excluded except at the Earth poles. Once $\underline{n}_S(s)$ has been obtained, the third unitary vector of the LAS direct frame will be defined by:

$$\underline{r}_s(s) = \underline{\tau}_s(s) \wedge \underline{n}(s) \tag{5.22}$$

Then a point $\underline{P}$ of coordinates *X*, *Y* and *Z* in the ECEF frame defined by the curvilinear abscissa *s* and polar coordinates ρ and σ will be such as:

$$\begin{bmatrix} X \\ Y \\ Z \end{bmatrix} = \begin{bmatrix} X_S(s) \\ Y_S(s) \\ Z_S(s) \end{bmatrix} + \rho \cdot \cos\sigma \cdot \underline{r}_S(s) + \rho \cdot \sin\sigma \cdot \underline{n}_S(s) \tag{5.23}$$

Then, for a given ASRT, the mapping:

$$s \in [s_1, s_2] \subset \mathrm{R} \rightarrow (\rho(s), \sigma(s)) \in \mathrm{R}^+ \times [0, 2\pi] \tag{5.24}$$

will define a unique trajectory within the considered airstream:

$$\begin{bmatrix} X \\ Y \\ Z \end{bmatrix} = \begin{bmatrix} X_S(s) \\ Y_S(s) \\ Z_S(s) \end{bmatrix} + \rho(s) \cdot \cos\sigma(s) \cdot \underline{r}_S(s) + \rho(s) \cdot \sin\sigma(s) \cdot \underline{n}_S(s) \tag{5.25}$$

Then, an *s*-indexed reference trajectory for a lane beside or along the considered airstream track is given when defining the functions $\rho = \rho_c(s)$ and $\sigma = \sigma_c(s)$ over [s_1, s_2].

5.3.4.2 From ECEF to LAS coordinates

Let us now consider a position *P* on a lane with *X*, *Y* and *Z* as coordinates in the ECEF frame. Here we are interested in computing the local axial coordinates (*s*, ρ, σ) of this position with respect to a nearby ASRT defined by the mapping introduced in equation 5.2 or equivalently by the mapping:

$$s \in [s_1, s_2] \subset \mathrm{R} \rightarrow (X(s), Y(s), Z(s)) \in \mathrm{R}^3 \tag{5.26}$$

This goes through the determination of the track *S* of point *P* over the ASRT. Issues such as the existence and uniqueness of the mark associated to current point *P* can be avoided by considering that the lane is close to the airstream reference trajectory (this means that its distance remains smaller than the smallest curvature radius of the track). The track is characterized by its curvilinear abscissa *s* on the ASRT. The abscissa *s* of the cross section plane to which point *P* belongs is the solution of the equation:

$$(X_s - X) \cdot \tau_x(s) + (Y_s - Y) \cdot \tau_y(s) + (Z_s - Z) \cdot \tau_z(s) = 0 \tag{5.27}$$

Let's write s_P the solution of this equation which will be a function $f(X,Y,Z)$ of the coordinates of point P in the ECEF frame ($s_P = f(X,Y,Z)$). This solution is trivial when the ASRT is a straight line. When multiple solutions exist, the one corresponding to the closest point $S(s)$ should be adopted. Then it is possible to compute the axial coordinates of point P:

$$\rho_p = \|\underline{SP}\| = \sqrt{(X - X_s(s_p))^2 + (Y - Y_s(s_p))^2 + (Z - Z_s(s_p))^2} \tag{5.28}$$

$$\sigma_p = \arctan(< \underline{SP}.\underline{n}_s(s_p) > / < \underline{SP}.\underline{r}_s(s_p) >) \pmod{2\pi} \tag{5.29}$$

with

$$s_p = f(X, Y, Z) \tag{5.30}$$

Then by considering equation 5.25 and equation 5.28, given an ASRT, there is a homeomorphism between the Cartesian representation in the ECEF frame and the ASRT axial representation:

$$(X, Y, Z) = T_S(s, \rho, \sigma) \quad \text{or} \quad \begin{cases} X = T_S^X(s, \rho, \sigma) \\ Y = T_S^Y(s, \rho, \sigma) \\ Z = T_S^Z(s, \rho, \sigma) \end{cases} \tag{5.31}$$

where T_S is a continuous function with a continuous nonsingular inverse. Observe that a point on a lane could be referenced with respect to various neighboring ASRTs, especially when the lane corresponds to the transition from an airstream to another.

5.3.5 Slot Characteristics

Each lane of an airstream gives support to a sequence of moving spatial slots. The sequence of available slots along a lane can be distributed either asynchronously (low traffic on peripheral lanes), or synchronously (high traffic on internal lanes). The dimensions of these slots must be in agreement with minimum separation standards, while their shape, considering their immersion in a common stream, may be ellipsoidal to take into account different longitudinal and lateral separation constraints. Considering that aircraft flying the same lane in an airstream are

expected to present close performance characteristics, the dimensions of these slots may be computed from the minimum separation regulations, from the current reference speed (temporal separation) and from the expected performances of the navigation (positioning accuracy) and of the guidance (spatial response length and temporal response time) systems [SESARJU, 2013].

To each point of a lane *i* with position *s* is attached a reference inertial speed $V_i(s)$, which is common to all its slots. This speed must be compatible with standard transportation aircraft performances and with wind speed predictions and should be known by the airline when constructing a flight plan. Writing $L_i(s)$ for the longitudinal length of a slot at position s of lane *i*, the current capacity of this lane is given by $V_i(s)/L_i(s)$ and the total current capacity of the airstream at section *s* is given by:

$$C = \sum_{i \in I} (V_i(s) / L_i(s)) \tag{5.32}$$

Aircraft with different performances or adopted cost indexes and speeds can be presented in the same airstream but along different lanes and can shift from one lane to another according to their evolving performances resulting mainly from mass variation. Then, one of the main role of the reference track is to provide a common spatial reference to the moving spatial slots and then to the evolving aircraft inside the airstream (shifting lanes) or around the airstream (entering the airstream or leaving it). The separation task between aircraft following a lane will be ensured once they maintain accurately the central position to their assigned slot. This should also contribute to avoid traffic conflicts between evolving aircraft by allowing the prediction of their minimum separations. It appears also of interest when defining these lanes to make them coincide as much as possible with airlines preference business trajectories as defined in [SESARJU, 2013] so that the need to shift lane will be minimized.

5.3.6 Expected benefits and challenges from airstream

The expected benefits are viewed from two perspectives, the ATC and the Pilot. From the ATC perspective, the aircraft positions are indexed to the common

spatial reference according to Local Airstream Frame (LAS) and this should ease the management of traffic separation and surveillance. The allocation of aircraft to a moving slot will ensure separation therefore the ATC workload in terms of flight surveillance can be reduced while from the pilot point of view, they are only responsible in maintaining the aircraft within the allocated slot. It is also expected that traffic collision will be reduced. The global benefits are to increase the capacity of the flight along the airstream reference trajectory while reducing delay.

Challenges perceived for the airstreams can be structured into two parts – design and adaptation. Firstly, from the design perspective, the maneuverability of the aircraft in terms of changing lane in the same direction or making a turn to move to another lane on a different airstream reference trajectory should be developed. Secondly, the adaptation of this reference airstream should be considered at which altitude should it be activated and how to ensure continuity from the Standard Instrument Departure Routes and Standard Arrival Routes (SIDs and STARs).

5.4 Conclusion

From the above it appears that new 3D+T flight guidance devices should be designed to make a more effective guidance in the context of free flight, trajectory based operations, air corridors and even airstreams. In the next chapter, the synthesis of guidance law allowing the tracking of 3D+T trajectories will be presented. In that case, to achieve the guidance function, it is considered that the guidance control law meets space indexed performances relative to the position and flyover times.

CHAPTER 6
3D+T GUIDANCE

Chapter 6: 3D+T Guidance Control

6.1 Introduction

The current evolution of ATM is based on the performance based navigation concept proposed and developed by SESAR and NEXTGEN where the aircraft needs to fly a path with high accuracy while fulfilling permanently overfly time constraint. According to the current modern guidance systems for an aircraft presented in Chapter 3, the guidance law is designed according to a time-indexed context but the flight management system (FMS) command the aircraft to follow a profile defined with respect to space and over-fly time constraints. The current flight guidance laws are not designed to follow directly a three dimensional plus time (3D+T) trajectory since they are able to perform a 3D trajectory tracking using mode-based guidance modes and a speed regulation to maintain separation with ahead traffic. Here it is supposed that the considered traffic is organized around a common reference track (an ASRT as depicted in Figure 6.1) and that aircraft should follow a given lane while maintaining their position in the middle of a moving slot.

The computations of the dimensions of these slots can be defined from the expected performances of the navigation (positioning accuracy) and of the guidance (spatial response length and temporal response time) systems [SESARJU, 2013]. Then, the tracking by aircraft of the central position in the assigned slot will ensure the separation of the aircraft following a common lane.

The main focus of this chapter is to propose a new 3D+T guidance control law which can be of interest to guide an aircraft along a lane in an airstream. The position of the aircraft along the ASRT will be taken as the independent variable for the aircraft flight guidance dynamics. The development of the reference tracking error equations with respect to the spatial variable will be considered first and transform into reference tracking error with respect to time. Using nonlinear dynamic inversion, the control law will be established to make the aircraft accurately follow 3D+T desired trajectories.

Of course the proposed guidance control law will also be of interest to track any 3D+T reference trajectory in other traffic contexts.

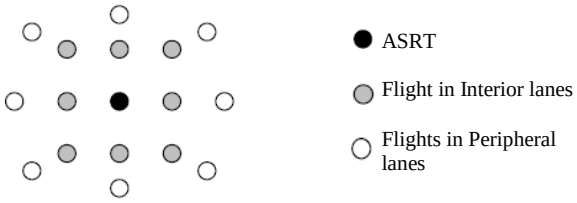

Figure 6.1: Organization of traffic around a common reference track (ASRT)

6.2 Space-Indexed versus Time-Indexed Dynamics

Considering a flight along a space-indexed reference track (ASRT), the curvilinear abscissa, s along the reference track can be adopted as an independent variable to index its nominal position using local axial coordinates. Let P_c be the current nominal position of the aircraft then the curvilinear abscissa s associated to point P_c is defined by the intersection of the orthogonal plane to the ASRT which contains point P_c (Figure 6.2).

Provided there is a bijective relation between the curvilinear abscissa and the aircraft position, any flight guidance variables can be expressed with respect to these curvilinear abscissas instead of time. This provides potential benefits such as a common spatial reference for different aircraft: overfly times become explicit control objectives, maintaining time and space separation constraints can be implemented.

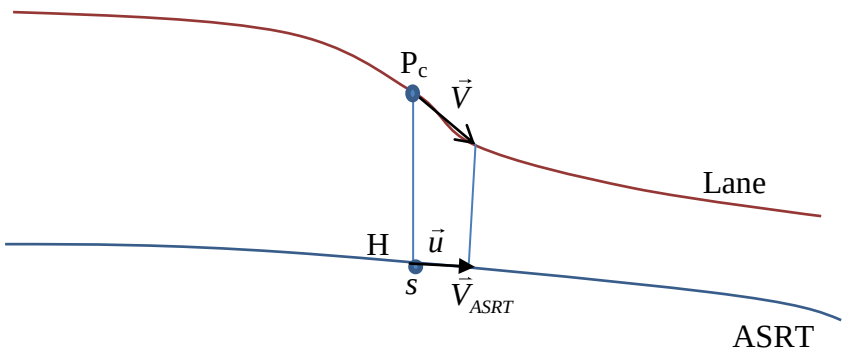

Figure 6.2: Projection of airspeed along ASRT

Let $\vec{V}_{ASRT}$ be the speed of point *H* in Figure 6.2. Figure 6.2 shows that $\vec{V}_{ASRT}$ may change even if the modulus of the inertial speed remains constant when its direction changes. Then, there is not a simple relationship between space-indexed and time-indexed derivatives of flight variables.

The expression of the rate of change of any flight variables with respect to *s* is given as:

$$\frac{d\,\mathrm{var}}{ds} = \mathrm{var}^{[1]} = \frac{d\,\mathrm{var}}{dt}\cdot\frac{dt}{ds} = \frac{1}{V_{ASRT}(s)}\cdot\frac{d\,\mathrm{var}}{dt} \tag{6.1}$$

where $\vec{V}_{ASRT} = \vec{V}\cdot\vec{u}$ is the projection of the inertial speed of the aircraft along the ASRT. $\vec{u}$ being the tangent vector along the ASRT at abscissa *s*. For the second and third derivatives of the flight variable, *var* can be rewritten as:

$$\frac{d^2\,\mathrm{var}}{ds^2} = \mathrm{var}^{[2]} = \frac{1}{V_{ASRT}^2(s)}\left(\frac{d^2(\mathrm{var})}{dt^2} + C_1\right) \tag{6.2}$$

with
$$C_1 = -\frac{\dot{V}_{ASRT}(s)}{V^3{}_{ASRT}(s)}\cdot\frac{d\,\mathrm{var}}{dt} \tag{6.3}$$

and

$$\mathrm{var}^{[3]} = \frac{1}{V_{ASRT}^3}\left(\frac{d^3}{dt^3}(\mathrm{var}) + C_2\right) \tag{6.4}$$

with
$$C_2 = \frac{1}{V_{ASRT}}\left[-3\cdot\dot{V}_{ASRT}\frac{d^2\,\mathrm{var}}{dt^2} + \frac{d\,\mathrm{var}}{dt}\cdot\left(3\frac{\dot{V}_{ASRT}^2}{V_{ASRT}} - \ddot{V}_{ASRT}\right)\right] \tag{6.5}$$

while the time equation is

$$t^{[1]} = \frac{1}{V_{ASRT}(s)} \tag{6.6}$$

6.3 Tracking control objectives

The main control objectives considered for the guidance function are to:

1. Make the aircraft to accurately follow a track along a space-indexed reference track,
2. Meet a permanent overfly time constraint,
3. Ensure the aircraft maintain its position at the center of its slot with small error tolerance.

Here the guidance problem consists of finding the adequate control variables (ϕ_c, θ_c and T_c) for the guidance dynamics so that the aircraft accurately follow its nominal 3D+T trajectory within the airstream. Here ϕ_c, θ_c and T_c are reference values sent to the autopilot (ϕ_c and θ_c) which is in charge of the rotational dynamics of the aircraft and to the auto engine control system (T_c). It is assumed that the autopilot and auto-engine control is very efficient that the piloting dynamics is assumed to be a first order dynamics. Figure 6.3 shows the resulting structure for the whole piloting and guidance dynamics. ECS means Engine Control Systems, better known as FADEC (Fuel Authority Digital Engine Control).

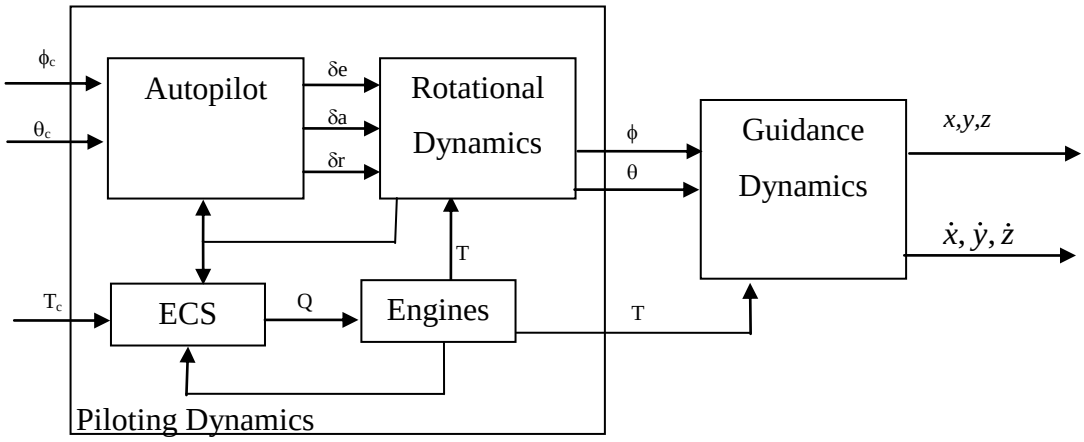

Figure 6.3: Piloting and Guidance Dynamics

There are many nonlinear controllers that have been implemented in the recent years such as back-stepping controller, sliding mode controller and nonlinear dynamic inversion (NDI) [Duan et al., 2006],[Glad and Harkegard, 2000],[Mulgund

and Stengel, 1996],[Zhi-jun et al., 2009]. The nonlinear controller adopted in this thesis to perform the tracking is the nonlinear dynamic inversion tracking. The reasons for this choice are:

1. It offers a more cost and time effective way to develop a control system in comparison to the more time consuming traditional gain scheduled controller [Campbell and Kaneshige, 2010],

2. It provides a better performance in comparison to the conventional linear and time invariant of flight control design in extreme flight conditions with high angles of attack or high angular rates [Miller, 2011],

3. The modeling aircraft forces and moments are better represented in NDI in response to large state and control perturbations [Miller, 2011],

4. It is able to directly command specific state variables.

This controller is also useful as a design of a baseline controller to evaluate the guidance control law in which later on will facilitate the development of other adaptive control systems over a large range of flight conditions. This is a first step towards building a working environment in which design changes and new research objectives can be quickly brought to flight and their real behavior ascertained [Miller, 2011].

Here the guidance problem consists in finding the adequate control variables, ϕ_c, θ_c and T_c for the guidance dynamics so that the aircraft accurately follow its nominal 3D+T trajectory within the airstream. The space guidance error tracking of the aircraft positions are given by:

$$\varepsilon_x(s) = x_{ref}(s) - x(s) \qquad \varepsilon_y(s) = y_{ref}(s) - y(s) \qquad \varepsilon_z(s) = z_{ref}(s) - z(s) \tag{6.7}$$

Where $x_{ref}(s)$, $y_{ref}(s)$ and $z_{ref}(s)$ are the coordinates of the moving slot assigned to the controlled aircraft. The nonlinear inverse control technique is used to make these guidance variables satisfy the spatial dynamics. The objective is to get asymptotically stable tracking errors with a given space interval for convergence. In [Drouin, 2013], it has been shown that to extract from these errors an effective guidance control law, a third order reference guidance errors dynamics should be considered. By

considering that the guidance dynamic is related to the input by dynamic of order three, then the reference guidance error dynamics around the track are given by the:

$$\varepsilon_i^{[3]}(s) + k_{1i}\varepsilon_i^{[2]}(s) + k_{2i}\varepsilon_i^{[1]}(s) + k_{3i}\varepsilon_i(s) = 0 \qquad i \in \{x, y, z\} \tag{6.8}$$

where the curvilinear abscissa *s* is related to the time through equation 6.6. Here *i* represents *x*, *y* or *z* and k_{1i} and k_{2i} are real parameters such that the roots of the associate polynomial are stable. Following the derivation rules of the composed functions, the guidance errors derivatives can be rewritten as:

$$\varepsilon^{[1]}(s) = \frac{\dot{\varepsilon}_i}{V_{ASRT}^2} \tag{6.9}$$

$$\varepsilon^{[2]}(s) = \frac{1}{V_{ASRT}^2}\left(\ddot{\varepsilon}_i - \dot{\varepsilon}_i.\frac{\dot{V}_{ASRT}}{V_{ASRT}}\right) \tag{6.10}$$

$$\varepsilon^{[3]}(s) = \frac{1}{V_{ASRT}^3}\left[\dddot{\varepsilon}_i - 3\ddot{\varepsilon}_i.\frac{\dot{V}_{ASRT}}{V_{ASRT}} + \dot{\varepsilon}_i\left(3\frac{\dot{V}_{ASRT}^2}{V^2_{ASRT}} - \frac{\ddot{V}_{ASRT}}{V_{ASRT}}\right)\right] \tag{6.11}$$

Then, adopting for and k_{1i}, k_{2i} and k_{3i} standard third order parameters for each coordinates we have

$$k_{1i} = \alpha_i\omega_{si} \qquad k_{2i} = \beta_i{\omega_{si}}^2 \qquad \text{and} \qquad k_{3i} = {\omega_{si}}^3 \tag{6.12}$$

where $\underline{\omega_{si}}$ are spatial frequencies (rad/m). Then equation 6.8 becomes:

$$\varepsilon_i^{[3]}(s) + \alpha_i\omega_{si}\varepsilon_i^{[2]}(s) + \beta_i{\omega_{si}}^2\varepsilon_i^{[1]}(s) + {\omega_{si}}^3\varepsilon_i(s) = 0 \qquad i \in \{x, y, z\} \tag{6.13}$$

substituting equation 6.9, 6.10 and 6.11 into equation 6.13, it gives

$$\frac{\dddot{\varepsilon}_i}{V_{ASRT}^3} + \ddot{\varepsilon}_i\left(\frac{\alpha_i\omega_{si}}{V_{ASRT}^2} - 3\frac{\dot{V}_{ASRT}}{V^4_{ASRT}}\right) + \dot{\varepsilon}_i\left(3\frac{\dot{V}^2_{ASRT}}{V^5_{ASRT}} - \frac{\ddot{V}^2_{ASRT}}{V^4_{ASRT}} - \alpha_i\omega_{si}\frac{\dot{V}_{ASRT}}{V^3_{ASRT}} + \frac{\beta_i{\omega_{si}}^2}{V^2_{ASRT}}\right) + {\omega_{si}}^3\varepsilon_i(s) = 0 \quad i \in \{x, y, z\} \tag{6.14}$$

When, the rate of change of speed along the track, $\dot{V}_{ASRT}$, can be assumed small in comparison with the velocity of the track, V_{ASRT}, the term $\frac{\dot{V}_{ASRT}}{V_{ASRT}}, \frac{\dot{V}^2_{ASRT}}{V^5_{ASRT}}, \frac{\ddot{V}^2_{ASRT}}{V^4_{ASRT}}$ and $\frac{\dot{V}_{ASRT}}{V^3_{ASRT}}$ are small enough to be negligible. Then equation 6.14 will be reduced to:

$$\dddot{\varepsilon}_i + \alpha_i \omega_{si} V_{ASRT} \ddot{\varepsilon}_i + \hat{\beta}_i \omega_{si}{}^2 V_{ASRT}{}^2 \dot{\varepsilon}_i + \omega_{si}{}^3 V_{ASRT}{}^3 \varepsilon_i = 0 \qquad i \in \{x, y, z\} \tag{6.15}$$

where $\hat{\beta}_i = \frac{\beta_i}{V_{ASRT}}$

which can be seen as constant parameters linear third order dynamics. Introducing a scaled parameters such as:

$$\omega_{ni} = \omega_{si} V_{ASRT} \tag{6.16}$$

The space indexed error dynamics given by equation 6.8, is equivalent to the error time-indexed dynamics given by:

$$\dddot{\varepsilon}_i + \alpha_i \omega_{ni} \ddot{\varepsilon}_i + \hat{\beta}_i \omega_{ni}{}^2 \dot{\varepsilon}_i + \omega_{ni}{}^3 \varepsilon_i = 0 \qquad i \in \{x, y, z\} \tag{6.17}$$

where

$$\varepsilon_x(t) = x_{ref}(t) - x(t) \qquad \varepsilon_y(t) = x_{ref}(t) - x(t) \qquad \varepsilon_z(t) = z_{ref}(t) - z(t) \tag{6.18a}$$

considering that

$$x_{ref}(t) = x_{ref}(s(t)) \qquad y_{ref}(t) = y_{ref}(s(t)) \qquad z_{ref}(t) = z_{ref}(s(t)) \tag{6.18b}$$

A range of ±2% band can be used to define the desired response. The natural space frequency, ω_{si} will shape the response of the aircraft to track the given reference trajectory. Once ω_{si} is chosen, the complete third-order closed-loop transfer function can be defined. It is then possible to assign the parameters of equation 6.18 (α_i and $\hat{\beta}_i$) the values necessary to meet the requirement of a deadbeat response. The deadbeat response is defined as a response that proceeds rapidly to the desired level and holds at that level with minimal [Levine, 1999]. With respect to the overfly time

error, it is worth to observe that once the current position error is maintained small, the overfly time constraint will be satisfied.

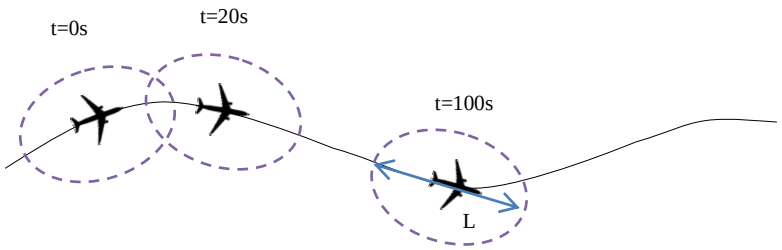

Figure 6.4: Aircraft following the center of a moving slot.

To satisfy the third objective, it will be sufficient to adopt as reference trajectory to be followed, the nominal trajectory of the assigned slot. Figure 6.4 assumes that the aircraft remains at the center of the slots as the slots move with time. The slot limits are given by the purple dashed line. L is the width of the space slot.

Adopting the design specification from [Levine, 1999], the normalized settling space response, l_i, to ensure that the system is to the center of the slot, is related to its space natural frequency. This space natural frequency can be defined from the relation:

$$l_i \cong \frac{4.04}{\omega_{si}} \tag{6.19}$$

Equation 6.19 defines the distance flown by the aircraft to be maintained within 2% of initial position error with respect to the moving position of the center of the slot. When introducing the ratio, $\upsilon_i = L/l_i$, between the slot width, L and the space response, l_i, the space natural frequency will be given by:

$$\omega_{si} \cong \frac{4.04\upsilon_i}{L} \tag{6.20}$$

In this section, the control objectives which were first expressed in space-reference have been expressed equivalently in a time-reference. This will allow using nonlinear dynamic inversion techniques to a design a time-indexed guidance control law meeting the above 3D+T requirements. Using nonlinear dynamic inversion

controller to track the control objectives along the ASRT will be discussed in the following section.

6.4 Considered aircraft Guidance Dynamics

The aircraft states representing the guidance dynamics, its adopted input generated by the aircraft fast dynamics and the wind components are given by:

$$\underline{X} = (x, y, z, \dot{x}, \dot{y}, \dot{z}, \phi, \theta, \psi, T)^T \tag{6.21}$$

$$\underline{U} = (\phi_c, \theta_c, T_c)^T \tag{6.22}$$

$$\underline{W} = (W_x\ W_y\ W_z)^T \tag{6.23}$$

Where x,y and z are the coordinates of the center of gravity of the vehicle in the local earth frame (LEF) is considered inertial. ϕ, θ and ψ are the Euler angles representing the rotation from the LEF to the Body Frame. T is the engine thrust and it is assumed that the mass of the aircraft is constant. The flight guidance dynamics of the aircraft can be written globally as:

$$\dot{\underline{X}} = f(\underline{X}, \underline{U}) \tag{6.24}$$

Where f is a tenth dimensional field and the component of aircraft accelerations is derived from Newton's second law. The components of acceleration of the center of gravity of the aircraft in the Local Earth Frame (LEF) are given by:

$$\begin{bmatrix} \ddot{x} \\ \ddot{y} \\ \ddot{z} \end{bmatrix} = \frac{1}{m}\left(R_{BL}(\phi,\theta,\psi)\left[\begin{pmatrix} T \\ 0 \\ 0 \end{pmatrix} + \begin{bmatrix} F_x(\alpha,\beta,V_a,z) \\ F_y(\alpha,\beta,V_a,z) \\ F_z(\alpha,\beta,V_a,z) \end{bmatrix}\right]\right) + \begin{bmatrix} 0 \\ 0 \\ g \end{bmatrix}_E \tag{6.25}$$

with

$$R_{BL=}\begin{bmatrix} c_\theta \cdot c_\psi & s_\phi \cdot s_\theta \cdot c_\psi - c_\phi \cdot s_\psi & c_\phi \cdot s_\theta \cdot c_\psi + s_\phi \cdot s_\psi \\ c_\theta \cdot s_\psi & s_\phi \cdot s_\theta \cdot s_\psi + c_\phi \cdot c_\psi & c_\phi \cdot s_\theta \cdot s_\psi - s_\phi \cdot c_\psi \\ -s_\theta & c_\theta \cdot s_\phi & c_\phi \cdot c_\theta \end{bmatrix} \tag{6.26}$$

Where R_{BL} is the rotation matrix from the Body Frame to the Local Earth Frame and $c_{(.)}$ and $s_{(.)}$ are cos and sin respectively. $F_{x,}$ F_y and F_z are the components of the aerodynamic forces expressed in the Body Frame. Since the aerodynamic forces are given in the Wind Frame, the transformation from the Wind Frame to the Body Frame can be performed using the following equation:

$$\begin{pmatrix} F_X \\ F_Y \\ F_Z \end{pmatrix} = R_{WB} \begin{pmatrix} -D \\ Y_F \\ -L \end{pmatrix} \tag{6.27}$$

$$R_{WB} = \begin{bmatrix} \cos\beta\cos\alpha & -\sin\beta\cos\alpha & -\sin\alpha \\ \sin\beta & \cos\beta & 0 \\ \cos\beta\sin\alpha & -\sin\beta\cos\alpha & \cos\alpha \end{bmatrix} \tag{6.28}$$

R_{WB} is the rotation matrix to transform from Wind Frame to the Body Frame. D is the drag force, Y_F is the lateral aerodynamic force and L is the lift force. These aerodynamic forces are related to the dynamic pressure $q = (1/2)\rho_a(z)V_a^2$ (in which $\rho_a(z)$ is the altitude-dependent air density and V_a is the airspeed) and the aircraft wing surface area, S_{ref} through the following equation:

$$D = \frac{1}{2}\rho_a(z)\, V_a{}^2 S_{ref} C_D \tag{6.29}$$

$$L = \frac{1}{2}\rho_a(z)\, V_a{}^2 S_{ref} C_L \tag{6.30}$$

$$Y_F = \frac{1}{2}\rho_a(z)\, V_a{}^2 S_{ref} C_Y \tag{6.31}$$

and C_D, C_Y and C_L are respectively the total summation of the dimensionless aerodynamic coefficients of the drag, the side force and the lift given by C_{Lo}, $C_{L\alpha}$, C_{D0}, C_{D1}, C_{D2} *and* $C_{Y\beta}$.

$$C_D = C_{D_0} + C_{D1}C_L + C_{D2}C_L{}^2 \tag{6.32}$$

$$C_Y = C_{Y\beta}\beta \tag{6.33}$$

$$C_L = C_{L_0} + C_{L\alpha}(\alpha - \alpha_0) \tag{6.34}$$

The airspeed V_a, angle of attack α and side slip angle β is given by

$$V_a = \sqrt{\left(\dot{x} - W_x\right)^2 + \left(\dot{y} - W_y\right)^2 + \left(\dot{z} - W_z\right)^2} \tag{6.35}$$

The angle of attack α and the sideslip angle β are angles between the airspeed to the aircraft in the Body Frame. The airspeed in the body frame is given by:

$$\begin{pmatrix} u \\ v \\ w \end{pmatrix} = R_{BL}^{-1} \begin{pmatrix} \dot{x} - W_x \\ \dot{y} - W_y \\ \dot{z} - W_z \end{pmatrix} \tag{6.36}$$

Then the angle of attack α and the sideslip angle β are given by:

$$\alpha = \arctan\left(\frac{w}{u}\right) \tag{6.37}$$

$$\beta = \arcsin\left(\frac{v}{V_a}\right) \tag{6.38}$$

When assuming that the autopilot provides a first order behavior for attitude angles ϕ and θ, we have:

$$\dot{\phi} = -\frac{1}{\tau_\phi}(\phi - \phi_c) \tag{6.39}$$

$$\dot{\theta} = -\frac{1}{\tau_\theta}(\theta - \theta_c) \tag{6.40}$$

Adopting a coordinated turn hypothesis, the rate of turn is given by:

$$\dot{\psi} = \frac{g}{GS}\tan\phi\cos\theta \tag{6.41}$$

GS is the ground speed given by the horizontal components of the inertial speed:

$$GS = \sqrt{\dot{x}^2 + \dot{y}^2} \tag{6.42}$$

For the thrust, assuming the Full Authority Digital Engine Controls (FADEC) provides a first order dynamics for the thrust given as:

$$\dot{T} = -\frac{1}{\tau_{th}}(T - T_c) \tag{6.43}$$

6.5 Inverting guidance dynamics

Feedback linearization is an approach to nonlinear control design that algebraically transforms the nonlinear systems dynamics of its output into (fully or partly) linear ones, so that linear control techniques can be finally applied. [Krstic et al., 1995],[Slotine et al., 1991] and [Khalil and Grizzle, 1996] are some references that introduce nonlinear dynamic inversion. In order to design a nonlinear dynamic inversion (NDI) controller, the outputs must be differentiated until the inputs appear in an invertible expression. The guidance output is defined as

$$\underline{Y} = (x\ y\ z)^T \tag{6.44}$$

Equation 6.25 will be differentiated again until the guidance input $\underline{U} = (\phi_c, \theta_c, T_c)^T$ appears. Then we have:

$$\begin{bmatrix} \dddot{x} \\ \dddot{y} \\ \dddot{z} \end{bmatrix} = -\frac{\dot{m}}{m^2}\left(R_{BL}\left[\begin{pmatrix} T \\ 0 \\ 0 \end{pmatrix} + \begin{bmatrix} F_x(\alpha,\beta,V_a,z) \\ F_y(\alpha,\beta,V_a,z) \\ F_z(\alpha,\beta,V_a,z) \end{bmatrix} \right] \right) + \frac{1}{m}\left(\dot{R}_{BL}\left[\begin{pmatrix} T \\ 0 \\ 0 \end{pmatrix} + \begin{bmatrix} F_x(\alpha,\beta,V_a) \\ F_y(\alpha,\beta,V_a) \\ F_z(\alpha,\beta,V_a) \end{bmatrix} \right] + R_{BL}\left[\begin{pmatrix} \dot{T} \\ 0 \\ 0 \end{pmatrix} + \begin{bmatrix} \dot{F}_x(\alpha,\beta,V_a) \\ \dot{F}_y(\alpha,\beta,V_a) \\ \dot{F}_z(\alpha,\beta,V_a) \end{bmatrix} \right] \right) + \begin{bmatrix} 0 \\ 0 \\ \dot{g} \end{bmatrix}_E \tag{6.45}$$

The mass fuel rate, $\dot{m}$ is small compared to the aircraft total mass then $\dot{m}/m^2$ is consider very small and it is neglected. The gravity is assumed constant, then $\dot{g}$ is zero. Then equation 6.45 is reduced to:

$$\begin{bmatrix} \dddot{x} \\ \dddot{y} \\ \dddot{z} \end{bmatrix} = \frac{1}{m}\left(\dot{R}_{BL}\left[\begin{pmatrix} T \\ 0 \\ 0 \end{pmatrix} + \begin{bmatrix} F_x(\alpha,\beta,V_a,z) \\ F_y(\alpha,\beta,V_a,z) \\ F_z(\alpha,\beta,V_a,z) \end{bmatrix} \right] + R_{BL}\left[\begin{pmatrix} \dot{T} \\ 0 \\ 0 \end{pmatrix} + \begin{bmatrix} \dot{F}_x(\alpha,\beta,V_a,z) \\ \dot{F}_y(\alpha,\beta,V_a,z) \\ \dot{F}_z(\alpha,\beta,V_a,z) \end{bmatrix} \right] \right) \tag{6.46}$$

The derivatives of the aerodynamic forces present in 6.46 are given by:

$$\dot{F}_x(\alpha,\beta,V_a,z)=\frac{\partial F_x}{\partial V_a}\dot{V}_a+\frac{\partial F_x}{\partial \alpha}\dot{\alpha}+\frac{\partial F_x}{\partial \beta}\dot{\beta}+\frac{\partial F_x}{\partial \rho}\dot{\rho}_a \tag{6.47}$$

$$\dot{F}_y(\alpha,\beta,V_a,z)==\frac{\partial F_y}{\partial V_a}\dot{V}_a+\frac{\partial F_y}{\partial \beta}\dot{\beta}+\frac{\partial F_y}{\partial \rho}\dot{\rho}_a \tag{6.48}$$

$$\dot{F}_z(\alpha,\beta,V_a,z)=\frac{\partial F_z}{\partial V_a}\dot{V}_a+\frac{\partial F_z}{\partial \alpha}\dot{\alpha}+\frac{\partial F_z}{\partial \beta}\dot{\beta}+\frac{\partial F_z}{\partial \rho}\dot{\rho}_a \tag{6.49}$$

The partial derivatives of each variable inside the above equations are:

$$\frac{\partial F_x}{\partial V_a}=\rho_a(z)V_aS_{ref}(-C_D\cos\alpha\cos\beta-C_Y\cos\alpha\sin\beta+C_L\sin\alpha) \tag{6.50}$$

$$\frac{\partial F_x}{\partial \alpha}=\frac{1}{2}\rho_a(z){V_a}^2S_{ref}(C_D\sin\alpha\cos\beta+C_Y\sin\alpha\sin\beta+C_L\cos\alpha) \tag{6.51}$$

$$\frac{\partial F_x}{\partial \beta}=\frac{1}{2}\rho_a(z){V_a}^2S_{ref}(C_D\cos\alpha\sin\beta-C_Y\cos\alpha\cos\beta) \tag{6.52}$$

$$\frac{\partial F_x}{\partial \rho}=\frac{1}{2}{V_a}^2S_{ref}(-C_D\cos\alpha\cos\beta-C_Y\cos\alpha\sin\beta+C_L\sin\alpha) \tag{6.53}$$

$$\frac{\partial F_y}{\partial V_a}=\rho_a(z)V_aS_{ref}(-C_D\sin\beta+C_Y\cos\beta) \tag{6.54}$$

$$\frac{\partial F_y}{\partial \beta}=\frac{1}{2}\rho_a(z){V_a}^2S_{ref}(-C_D\cos\beta-C_Y\sin\beta) \tag{6.55}$$

$$\frac{\partial F_y}{\partial \rho}=\frac{1}{2}{V_a}^2S_{ref}(-C_D\sin\beta+C_Y\cos\beta) \tag{6.56}$$

$$\frac{\partial F_z}{\partial V_a}=\rho_a(z)V_aS_{ref}(-C_D\sin\alpha\cos\beta-C_y\sin\alpha\sin\beta-C_L\cos\alpha) \tag{6.57}$$

$$\frac{\partial F_z}{\partial \alpha}=\frac{1}{2}\rho_a(z){V_a}^2S_{ref}(-C_D\cos\alpha\cos\beta-C_y\cos\alpha\sin\beta+C_L\sin\alpha) \tag{6.58}$$

$$\frac{\partial F_z}{\partial \beta}=\frac{1}{2}\rho_a(z){V_a}^2S_{ref}(C_D\sin\alpha\sin\beta-C_y\sin\alpha\cos\beta) \tag{6.59}$$

$$\frac{\partial F_x}{\partial \rho} = \frac{1}{2} V_a{}^2 S_{ref} \left(-C_D \sin\alpha \cos\beta - C_y \sin\alpha \sin\beta - C_L \cos\alpha\right) \tag{6.60}$$

The air density ρ_a is related to the air pressure, temperature and gas constant R assuming the ideal gas law. Both temperature and air pressure varies with altitude. Thus the differentiation of air density is given by:

$$\dot{\rho}_a = \frac{\partial \rho_a}{\partial P} \cdot \frac{\partial P}{\partial z} \cdot \frac{\partial z}{\partial t} + \frac{\partial \rho_a}{\partial T} \cdot \frac{\partial T}{\partial z} \cdot \frac{\partial z}{\partial t} \tag{6.61}$$

Where the derivatives of the airspeed and the flow angles are given by:

$$\dot{V}_a = \frac{\left(\dot{x} - W_x\right)\ddot{x} + \left(\dot{y} - W_y\right)\ddot{y} + \left(\dot{z} - W_z\right)\ddot{z}}{V_a} + \delta \dot{V}_a \tag{6.62}$$

with $$\delta \dot{V}_a = \frac{\left(\dot{x} - W_x\right)\dot{W}_x + \left(\dot{y} - W_y\right)\dot{W}_y + \left(\dot{z} - W_z\right)\dot{W}_z}{V_a}$$

when the wind is assume constant, C_w will be zero since the derivative of a constant wind is zero. Then differentiating equation 6.37 and 6.38, the derivatives of both angle of attack and side slip angle are given by:

$$\dot{\alpha} = \frac{u\dot{w} - \dot{u}w}{u^2 + w^2} \tag{6.63}$$

$$\dot{\beta} = \frac{V_a \dot{v} - v\dot{V}_a}{\sqrt{V_a{}^2 - v^2}} \tag{6.64}$$

The propagation of the rotation matrix is given by:

$$\dot{R}_{BL} = M_\varphi \dot{\phi} + M_\theta \dot{\theta} + M_\psi \dot{\psi} \tag{6.65}$$

where

$$M_\phi = \begin{bmatrix} 0 & c_\phi s_\theta c_\psi + s_\phi s_\psi & -s_\phi s_\theta c_\psi + c_\phi s_\psi \\ 0 & c_\phi s_\theta s_\psi - s_\phi c_\psi & -s_\phi s_\theta s_\psi - c_\phi c_\psi \\ 0 & c_\theta c_\phi & -c_\theta s_\phi \end{bmatrix} \cdot \begin{bmatrix} T + F_x \\ F_y \\ F_z \end{bmatrix} \tag{6.66}$$

$$M_\theta = \begin{bmatrix} -s_\theta c_\psi & s_\phi c_\theta c_\psi & c_\phi c_\theta c_\psi \\ -s_\theta s_\psi & s_\phi c_\theta s_\psi & c_\phi c_\theta s_\psi \\ -c_\theta & -s_\theta s_\phi & -s_\theta c_\phi \end{bmatrix} \cdot \begin{bmatrix} T + F_x \\ F_y \\ F_z \end{bmatrix} \tag{6.67}$$

$$M_\psi = \begin{bmatrix} -c_\theta s_\psi & -s_\phi s_\theta s_\psi - c_\phi c_\psi & -c_\phi s_\theta s_\psi + s_\phi c_\psi \\ c_\theta c_\psi & s_\phi s_\theta c_\psi - c_\phi s_\psi & c_\phi s_\theta c_\psi + s_\phi s_\psi \\ 0 & 0 & 0 \end{bmatrix} \cdot \begin{bmatrix} T + F_x \\ F_y \\ F_z \end{bmatrix} \tag{6.68}$$

Substituting equations 6.66 to 6.68 into equation 6.46, we can rewrite the nonlinear equation of the aircraft jerk in the inertial frame as a control-affine system such as:

$$m \begin{bmatrix} \dddot{x} \\ \dddot{y} \\ \dddot{z} \end{bmatrix} = \left(\left[\begin{array}{c|c|c} & & \cos\theta\cos\psi \\ M_\phi & M_\theta & \cos\theta\sin\psi \\ & & -\sin\theta \end{array} \right] \begin{pmatrix} \dot{\phi} \\ \dot{\theta} \\ \dot{T} \end{pmatrix} + \left(M_\psi \cdot \dot{\psi} + R_{BL} \begin{bmatrix} \dot{F}_x \\ \dot{F}_y \\ \dot{F}_z \end{bmatrix} \right) \right) \tag{6.69}$$

or, defining the aerodynamic vector by $\underline{A}=(\alpha,\beta,V_a)$

$$m \begin{bmatrix} \dddot{x} \\ \dddot{y} \\ \dddot{z} \end{bmatrix} = G(\underline{X}, \underline{A}) \begin{pmatrix} \dot{\phi} \\ \dot{\theta} \\ \dot{T} \end{pmatrix} + H(\underline{X}, \underline{A}, \dot{\underline{A}}) \tag{6.70}$$

the control matrix $G(\underline{X},\underline{A})$ is given by:

$$G(\underline{X}, \underline{A}) = \begin{bmatrix} F_y \cdot (c_\phi s_\theta c_\psi + s_\phi s_\psi) + F_z \cdot (-s_\phi s_\theta c_\psi + c_\phi s_\psi) & -(T + F_x) \cdot s_\theta c_\psi + F_y s_\phi c_\theta c_\psi + F_z c_\phi c_\theta c_\psi & c_\theta c_\psi \\ F_y \cdot (c_\phi s_\theta s_\psi - s_\phi c_\psi) + F_z \cdot (-s_\phi s_\theta s_\psi - c_\phi c_\psi) & -(T + F_x) \cdot s_\theta s_\psi + F_y s_\phi c_\theta s_\psi + F_z c_\phi c_\theta s_\psi & c_\theta s_\psi \\ F_y c_\theta c_\phi - F_z c_\theta s_\phi & -(T + F_x) \cdot c_\theta - F_y s_\theta s_\phi - F_z s_\theta c_\phi & -s_\theta \end{bmatrix} \tag{6.71}$$

and the guidance control input vector $H(\underline{X})$ is given by:

$$H(\underline{X}, \underline{A}, \dot{\underline{A}}) = \begin{bmatrix} -(T + F_x) \cdot \dot{\psi} \cdot c_\theta s_\psi + F_y \cdot \dot{\psi} \cdot (-s_\phi s_\theta s_\psi - c_\phi c_\psi) + F_z \cdot \dot{\psi} \cdot (-c_\phi s_\theta s_\psi + s_\phi c_\psi) + \dot{F}_x c_\theta c_\psi + \dot{F}_y \cdot (s_\phi s_\theta c_\psi - c_\phi s_\psi) + \dot{F}_z \cdot (c_\phi s_\theta c_\psi + s_\phi s_\psi) \\ (T + F_x) \cdot \dot{\psi} \cdot c_\theta c_\psi + F_y \cdot \dot{\psi} \cdot (s_\phi s_\theta c_\psi - c_\phi s_\psi) + F_z \cdot \dot{\psi} \cdot c_\phi s_\theta c_\psi + s_\phi s_\psi + \dot{F}_x c_\theta s_\psi + \dot{F}_y \cdot (s_\phi s_\theta s_\psi + c_\phi c_\psi) + \dot{F}_z \cdot (c_\phi s_\theta s_\psi - s_\phi c_\psi) \\ -\dot{F}_x s_\theta + \dot{F}_y c_\theta s_\phi + \dot{F}_z \cdot c_\phi c_\theta \end{bmatrix} \tag{6.72}$$

From equation 6.70 it appears that the state of the guidance dynamics is driven by the independent inputs $\dot{\phi}, \dot{\theta}$ and $\dot{T}$ which are produced respectively by the controlled rotational dynamics and controlled thrust dynamics. To meet the control objectives adopted in 6.17 the third derivatives of *x*,*y* and *z* must be such as:

$$\dddot{x} = \dddot{x}_{ref} + \alpha_y \omega_{ny}(\ddot{x}_{ref} - \ddot{x}) + \hat{\beta}_y \omega_{ny}{}^2(\dot{x}_{ref} - \dot{x}) + \omega_{ny}{}^3(x_{ref} - x) \tag{6.73a}$$

$$\dddot{y} = \dddot{y}_{ref} + \alpha_y \omega_{ny}(\ddot{y}_{ref} - \ddot{y}) + \hat{\beta}_y \omega_{ny}{}^2(\dot{y}_{ref} - \dot{y}) + \omega_{ny}{}^3(y_{ref} - y) \tag{6.73b}$$

$$\dddot{z} = \dddot{z}_{ref} + \alpha_z \omega_{nz}(\ddot{z}_{ref} - z) + \hat{\beta}_z \omega_{nz}{}^2(\dot{z}_{ref} - \dot{z}) + \omega_{nz}{}^3(z_{ref} - z) \tag{6.73c}$$

Then the required rate inputs $\dot{\phi}_r, \dot{\theta}_r$ and $\dot{T}_r$ will be given by:

$$\begin{pmatrix} \dot{\phi}_r \\ \dot{\theta}_r \\ \dot{T}_r \end{pmatrix} = G(\underline{X}, \underline{A})^{-1} \begin{bmatrix} m\left(\dddot{x}_{ref} + \alpha_y \omega_{ny}(\ddot{x}_{ref} - \ddot{x}) + \hat{\beta}_y \omega_{ny}{}^2(\dot{x}_{ref} - \dot{x}) + \omega_{ny}{}^3(x_{ref} - x)\right) - H_x(\underline{X}, \underline{A}, \dot{\underline{A}}) \\ m\left(\dddot{y}_{ref} + \alpha_y \omega_{ny}(\ddot{y}_{ref} - \ddot{y}) + \hat{\beta}_y \omega_{ny}{}^2(\dot{y}_{ref} - \dot{y}) + \omega_{ny}{}^3(y_{ref} - y)\right) - H_y(\underline{X}, \underline{A}, \dot{\underline{A}}) \\ m\left(\dddot{z}_{ref} + \alpha_z \omega_{nz}(\ddot{z}_{ref} - \ddot{z}) + \hat{\beta}_z \omega_{nz}{}^2(\dot{z}_{ref} - \dot{z}) + \omega_{nz}{}^3(z_{ref} - z)\right) - H_z(\underline{X}, \underline{A}, \dot{\underline{A}}) \end{bmatrix} \tag{6.74}$$

or

$$\begin{pmatrix} \dot{\phi}_r \\ \dot{\theta}_r \\ \dot{T}_r \end{pmatrix} = G(\underline{X}, \underline{A})^{-1} \left[m \begin{pmatrix} J_x(\underline{X}, \underline{A}) \\ J_y(\underline{X}, \underline{A}) \\ J_z(\underline{X}, \underline{A}) \end{pmatrix} - \begin{pmatrix} H_x(\underline{X}, \underline{A}, \dot{\underline{A}}) \\ H_y(\underline{X}, \underline{A}, \dot{\underline{A}}) \\ H_z(\underline{X}, \underline{A}, \dot{\underline{A}}) \end{pmatrix} \right] \tag{6.75}$$

Where $\underline{J(X,A)}$ is the jerk vector associated with the center of gravity of the aircraft or in a more summarized form:

$$\begin{pmatrix} \dot{\phi}_r \\ \dot{\theta}_r \\ \dot{T}_r \end{pmatrix} = G(\underline{X}, \underline{A})^{-1} \Gamma(\underline{X}, \underline{A}, \dot{\underline{A}}) \tag{6.76}$$

where $$\Gamma(\underline{X}, \underline{A}) = m \cdot J_x(\underline{X}, \underline{A}, \dot{\underline{A}}) + H_x(\underline{X}, \underline{A}, \dot{\underline{A}}) \tag{6.77}$$

control system of the aircraft to make it follow the proposed 3D+T trajectory can be computed by:

$$\phi_c = \dot{\phi}_r \tau_\phi + \phi \tag{6.78a}$$

$$\theta_c = \dot{\theta}_r \tau_\theta + \theta \tag{6.78b}$$

$$T_c = \dot{T}_r \tau_T + T \tag{6.78c}$$

6.6 Simulation results

The described generic transport aircraft flight dynamic model and guidance law have been implemented in the Python programming language using the Python Aerospace Toolbox [Drouin, 2013] framework. The setting of the simulation is given in the following diagram:

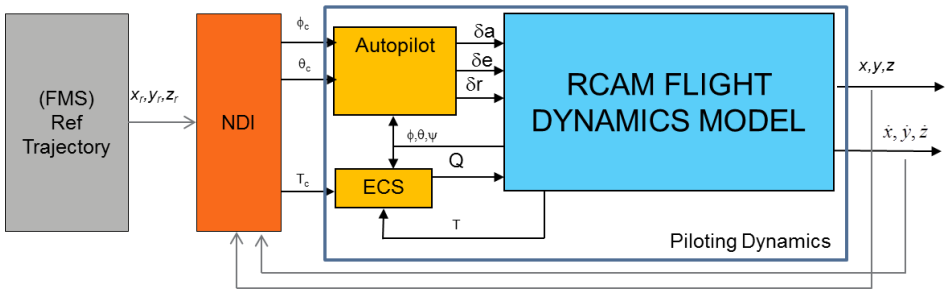

Figure 6.5: Simulation settings

The Research Civil Aviation Model is used for the plant dynamics. Then the time constants for the adopted autopilot and auto-throttle are given as:

$$\tau_\phi = 0.33s \qquad \tau_\theta = 0.33s \qquad \tau_T = 2s \tag{6.79}$$

To test the effectiveness of the space-indexed guidance controller, a nominal value for the speed and altitude is taken to perform the simulation. A number of simulations are presented in order to verify that the control objectives are actually met and to illustrate specific behaviors of the presented guidance law.

6.6.1 Rejection of perturbations

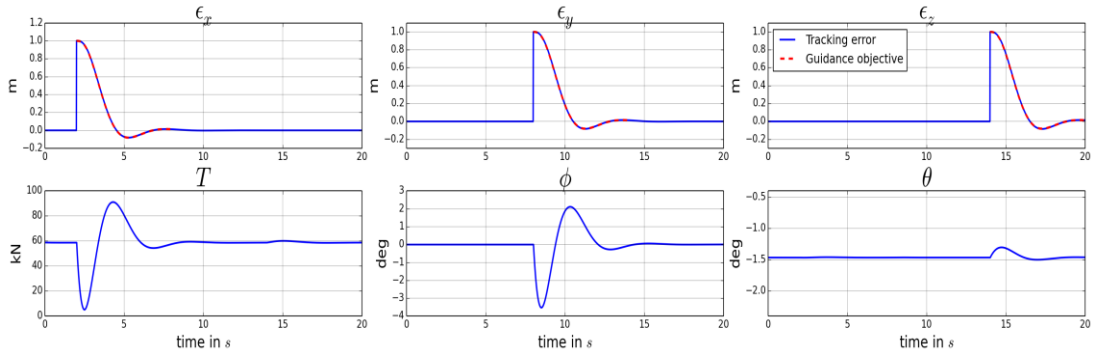

Figure 6.6: Perturbation rejection property of the guidance law

Figure 6.6 illustrates the perturbation rejection property of the guidance law. In this simulation, the aircraft is flying horizontally at an altitude of 1000m and at a constant velocity of 100m/s in the direction of the x axis. At instants t1 = 2s, t2 = 6s and t3 = 10s, perturbations in position are applied respectively on axis x, y and z. The poles of the regulator have been set in a Butterworth configuration with ω_n = 2.5rad/s (ω_s = 0.025rad/m). From this simulation when there is perturbation in the x-axis, that is the aircraft is further than the reference position, thrust will command a low value in order to make the aircraft slows and return back to the reference x-position. As for the a perturbation in the y-axis, when the aircraft is to the right of the reference y-position, then a negative bank angle will be commanded in order to make the aircraft bank to the left. While when the aircraft is below its reference z-position, the guidance pitch input will command a positive angle in order to make the aircraft climb back to its reference z-position. From here we can see that the tracking errors ε_x, ε_y, ε_z can been seen to follow the decoupled linear trajectory specified in the guidance objectives while the state variables associated with the control inputs remain free of saturation.

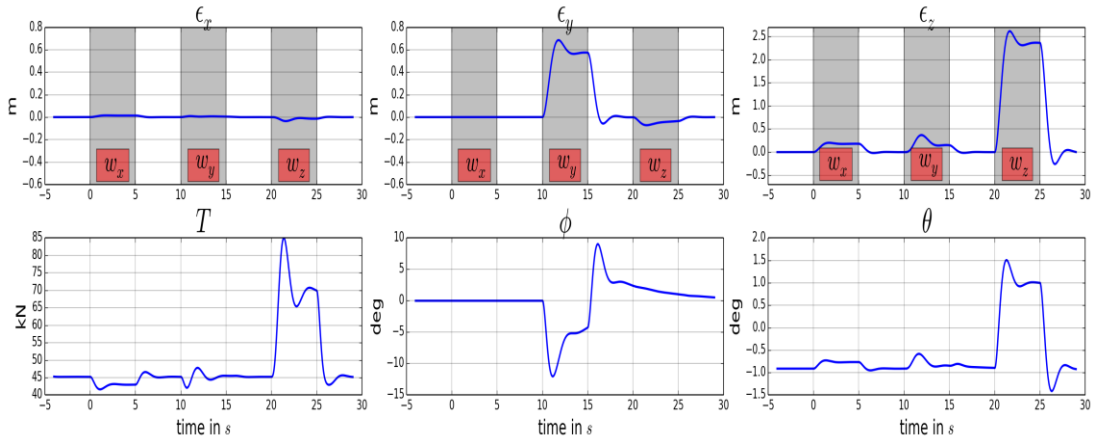

Figure 6.7: Wind gust rejection during a constant velocity horizontal trajectory

Figure 6.7 illustrates the perturbation rejection of the guidance law with a more realistic example using wind gusts. In this simulation, the aircraft is flying horizontally at an altitude of 1000m and at a constant velocity of 300m/s in the direction of the *x* axis. At instants t_1=2s, t_2=6s and t_3=10s, wind gusts of amplitude 10m/s and duration of 5s are introduced respectively on axis *x*, *y* and *z*. The poles of the regulator have been set in a Butterworth configuration with ω_n=1.5 rad/s. For the first 0-5s the wind came from the back, this will increase the aircraft speed and reduce the aircraft pitch angle, so a low input will be given by the commanded thrust and an increase in the pitch will be given by the commanded pitch angle. The correct inputs can also be seen when the aircraft is pushed to the right and pushed down. It is expected to have a bank to the left for a right side-wind and also for the down-gust, it is expected to have and increase in both thrust and pitch to make the aircraft climb. This simulation shows that the aircraft tracks its 3D+T trajectory with an accuracy of about 10cm in *x*, 70cm in *y* and 2.5m in *z* while the state variables associated with the control inputs remain free of saturation.

6.6.2 Tracking of trajectories

Figure 6.8, Figure 6.9 and Figure 6.10 are simulations illustrating the trajectory tracking feature of the proposed guidance law.

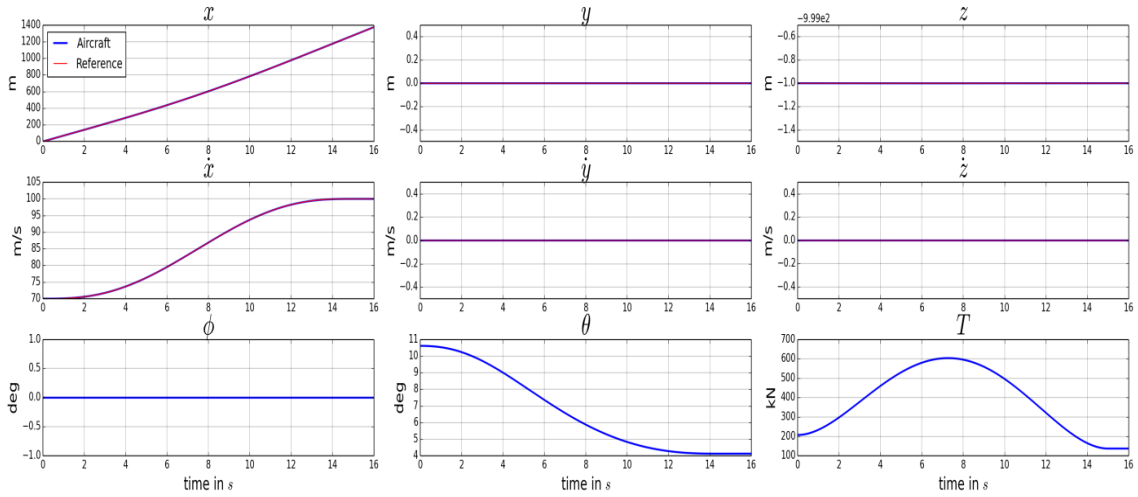

Figure 6.8: Tracking of a 3D+T trajectory consisting in a change of velocity at constant altitude and heading

Figure 6.8 shows the tracking of a trajectory consisting in a velocity change at constant altitude and heading. The fourth order reference trajectory is constructed using polynomials. The correct guidance input from the controller is shown to make the aircraft correct its' position error. We can see an increase in thrust and a decrease in pitch as the aircraft increases its' speed. From this simulation, the trajectory is accurately tracked while the guidance law generates smooth input remaining free from saturation, hence feasible.

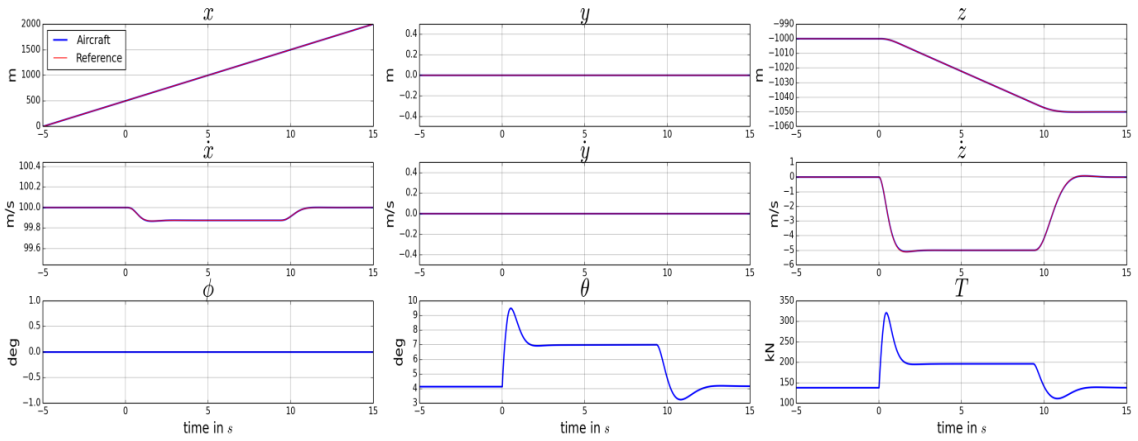

Figure 6.9: Tracking of a 3D+T trajectory consisting in a change of altitude at constant velocity

Figure 6.9 displays the tracking of a trajectory corresponding to a change of altitude at constant velocity. In this case, the fourth order reference trajectory is constructed using a nested saturations reference model [Kannan and Johnson, 2010].]. It can be seen that the modulus of the aircraft airspeed remains 100m/s during the climbing.

Here in order to perform the climb, it is expected to have an increase in both commanded pitch and commanded thrust.

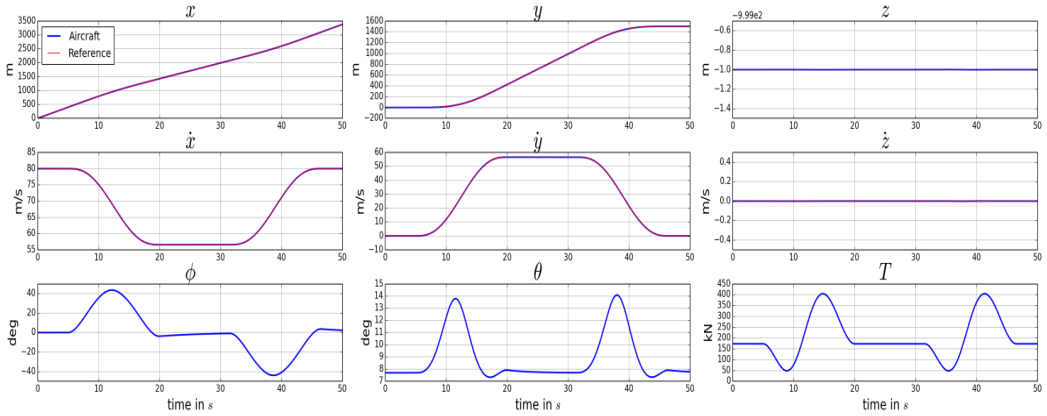

Figure 6.10: Tracking of a 3D+T lane change trajectory

Figure 6.10 illustrates the case of a shift from a lane to a parallel one at constant speed. It is the type of maneuver that will allow aircraft to shift from one lane to another, according to traffic density and aircraft performances, within airstreams. All three simulations show that the proposed guidance controller is able to track the 3D+T reference trajectory accurately with some small guidance error.

6.6.3 Comparison of time and spatial laws

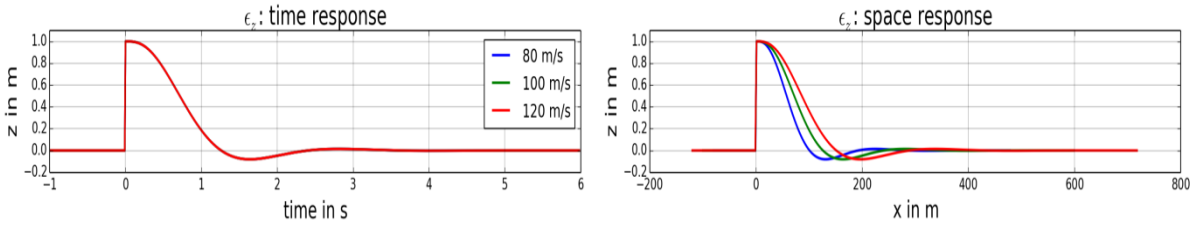

Figure 6.11: Pertubation rejection of a traditional time-indexed NLI guidance law

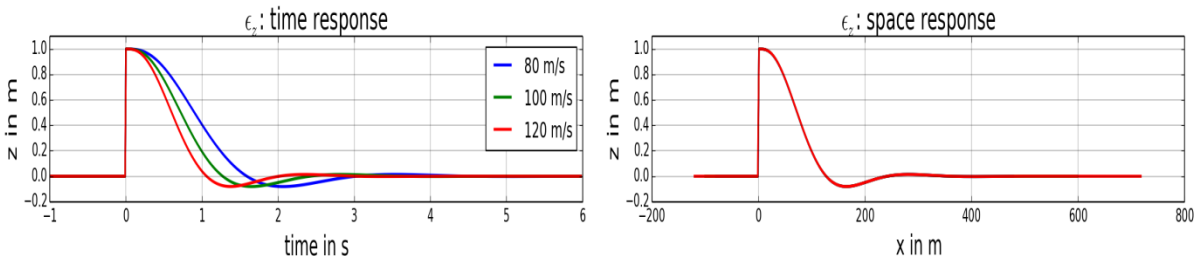

Figure 6.12: Pertubation rejection of the space-indexed NLI guidance law

Figure 6.11 and Figure 6.12 display the differentiated results obtained from time-indexed and space-indexed guidance control laws in the presence of perturbation. Their time response and space response can be set according to the chosen basis for the guidance control law independently of the adopted reference speed. In one case (time-indexed controller), the setting time will be independent of the perturbation amplitude and point of the flight domain, as represented on the left plot of Figure 6.11. In the other case (space-indexed controller), the setting distance will be independent of the perturbation amplitude and point of the flight domain as represented on the right plot of Figure 6.12.

6.7 Conclusion

In this chapter, a guidance control law compatible with accurate tracking of 3D+T trajectories has been introduced where the space-indexed and time-indexed approaches are compared. The numerical simulations, performed with a generic transportation aircraft, demonstrated that the adopted control technique, nonlinear inverse control, leads to tracking performances compatible with high density traffic situations.

However, many issues remain worthy to be investigated when considering the proposed guidance control law:

- robustness to parameter uncertainty and interest for adaptive components,
- determination of the invertibility domain bounds.
- the adoption of more realistic assumption with respect to the auto-pilot and the auto- systems.

Therefore, adoption of such guidance solution will contribute to the autonomous operation of high density traffic distributed along parallel lanes within air corridors since each aircraft will be able to remain positioned on its assigned slot. In the next chapter, the main limitations regarding the proposed guidance control law will be discussed.

CHAPTER 7
FEASIBILITY OF THE PROPOSED APPROACH

Chapter 7: Feasibility of the proposed approach

7.1 Introduction

The design of the guidance control law proposed in the previous chapter for 3D+T trajectory tracking has been developed based on different assumptions. This design particularly adopts a nonlinear dynamic inversion technique which is known to present different limitations. In this chapter these limitations are discussed and three major issues are analyzed:

1. the effect of measurement errors on the effectiveness of the control law,
2. the effect of modeling error on the effectiveness of the control law,
3. the invertibility of the control matrix, leading to bounded inputs and feasibility of the proposed control law.

Also, the compatibility of the proposed guidance system with current autopilots on-board modern aircraft is discussed.

7.2 Data accuracy

To feed in real time the proposed control law developed in the previous chapter (relations 6.70, 6.71 or 6.72) it is necessary to gather accurate estimates of the components of the state vectors, while it is well known that all these estimates are subjected to measurement and calculation errors. Errors with respect to positions (*x, y, z*) and inertial speed ($\dot{x}, \dot{y}, \dot{z}$) as well as errors with respect to the attitude angles (ϕ, θ, ψ) are related to the performance accuracy of the navigation systems which integrates inertial, GPS and magnetic measurements. The trust of the engine *T* is not directly measured on a transport aircraft but can be estimated through numerical tools such as neural networks [Maggiore et al., 2003, Shankar and Yedavalli, 2009]. In general, T will be a complex function of the fuel flow, the airspeed and the flight level. The aerodynamic data will be obtained from the air data computer systems (today often integrated into the inertial navigation system on ADIRS), the direct

measurement of angle of attack α and side slip angle β as well as the computation of the airspeed from the Pitot probes will avoid having to tackle the difficult question of estimating the local wind components in real time.

7.2.1 Current Performance of onboard sensors

The general accuracy for the aircraft instrument measurement are given in Table 7.1, Table 7.2, Table 7.3 and Table 7.4. Table 7.1 and Table 7.2 show the performance in attitude and velocity of a navigation grade INS with error correction from GPS.

Table 7.1: Attitude Performance of inertial navigation systems (INS) with GPS-updating [Schwarz, 1996]

	System Accuracy RMS	
	Pitch and Roll (arcsecond)	Azimuth (arcsecond)
1 hour	10 - 30	60-180
1 minute	5-10	15-20
1 second	3-5	3-20

Table 7.2: Velocity performance of inertial navigation systems (INS) with GPS-updating [Schwarz, 1996]

Error in Velocity	System Accuracy RMS
1 hour	0.5-1.0 m/s
1 minute	0.03-0.10 m/s
1 second	0.001-0.003m/s

Table 7.2 lists the GNSS Signal-in-Space performance according to flight operations required by ICAO. ICAO did not specify the required accuracy in the vertical position for the en-route, terminal and non-precision approach. However the actual performance of GNSS measured and analyzed by the FAA Technical Center is given in Table 7.4. According to Table 7.3, the horizontal error of the aircraft position inside a slot needs to be within the category I approach. The accuracy of the air-data is important to determine an accurate position of the aircraft in the vertical

position and also to estimate the wind velocity. Table 7.5 shows a typical accuracy performance requirement for air-data computer.

Table 7.3: ICAO GNSS Signal-in-Space Performance Requirements [Spitzer, 2001]

Operations	Horizontal Accuracy	Vertical Accuracy
En-Route (Oceanic, Remote Area)	7.4 km	-
En-Route	3.7 km	-
Terminal	0.74km	-
Nonprecision Approach	220 m	-
Approach with Vertical Guidance (APV) - I	16m	20m
Approach with Vertical Guidance (APV) - II	16m	8m
Category I approach	16m	4-6m

Table 7.4: Actual GNSS Signal-in-Space Performance [Spitzer, 2001]

	Accuracy
Nominal Horizontal Accuracy	1.6m
Maximum Horizontal Accuracy	12m
Nominal Vertical Accuracy	1.6m
Maximum Vertical Accuracy	12m

Table 7.5: A typical air-data computer accuracy requirements [Kayton and Fried, 1997]

Parameter	Accuracy
Altitude, h, Z (barometric altimeter)	±10 ft - ±15 ft sea level ±20 ft at 10000ft ±40 ft at 30000ft ±80 ft at 50000ft >±100 ft at >60000ft
Total Pressure	±0.68 mbar ≅ 109171 ft (pressure altitude)
True Air Sped, V	±4 knots for V >100 knots
Total Air Temperature, T_t	±0.5°C
Static Air temperature, T_s	±1.0°C
Angle of attack and Side Slip	±0.25°

From the above tables it appears that the accuracy of data can be a problem for the effective performance of the proposed tracking system. In the next section, a theoretical approach to assess the influence of data inaccuracy is developed.

7.2.2 Performance Analysis of the tracking system with data inaccuracy

Let us distinguish here between true values and measured/computed ones for the variables present in $\underline{X}$, $\underline{A}$, $\underline{\dot{A}}$. Then we have:

$$\underline{X}_m = \underline{X} + \delta\underline{X} \tag{7.1}$$

$$\underline{A}_m = \underline{A} + \delta\underline{A} \tag{7.2}$$

$$\underline{\dot{A}}_m = \underline{\dot{A}} + \delta\underline{\dot{A}} \tag{7.3}$$

where $\delta\underline{X}$, $\delta\underline{A}$, $\delta\underline{\dot{A}}$ are the measurement/ computation errors with respect to $\underline{X}$, $\underline{A}$, $\underline{\dot{A}}$. The computed inputs will be given by:

$$\begin{bmatrix} \dot{\phi}_{comp} \\ \dot{\theta}_{comp} \\ \dot{T}_{comp} \end{bmatrix} = G(\underline{X}_m, \underline{A}_m)^{-1}\Gamma(\underline{X}_m, \underline{A}_m, \underline{\dot{A}}_m) \tag{7.4}$$

Considering a first order development of $G(\underline{X}, \underline{A})^{-1}$ and $\Gamma(\underline{X}, \underline{A}, \underline{\dot{A}})$, the errors generated by these measurements/computations for the inputs will be such as:

$$\begin{bmatrix} \dot{\phi}_{comp} \\ \dot{\theta}_{comp} \\ \dot{T}_{comp} \end{bmatrix} = \begin{bmatrix} \dot{\phi} \\ \dot{\theta} \\ \dot{T} \end{bmatrix} + G(\underline{X}, \underline{A})^{-1}\left(\frac{\partial\Gamma}{\partial\underline{X}}\cdot\delta\underline{X} + \frac{\partial\Gamma}{\partial\underline{A}}\cdot\delta\underline{A} + \frac{\partial\Gamma}{\partial\underline{\dot{A}}}\cdot\delta\underline{\dot{A}}\right) + \left(\frac{\partial G^{-1}}{\partial\underline{X}}\cdot\delta\underline{X} + \frac{\partial G^{-1}}{\partial\underline{A}}\cdot\delta\underline{A}\right)\Gamma(\underline{X}, \underline{A}, \underline{\dot{A}}) \tag{7.5}$$

then the errors dynamics will be such as:

$$\dddot{\varepsilon}_x + \lambda_x\omega_{nx}\ddot{\varepsilon}_x + \hat{\mu}_x{\omega_{nx}}^2\dot{\varepsilon}_x + {\omega_{nx}}^3\varepsilon_x = \rho_x \tag{7.6}$$

$$\dddot{\varepsilon}_y + \lambda_y \omega_{ny} \ddot{\varepsilon}_y + \hat{\mu}_y \omega_{ny}{}^2 \dot{\varepsilon}_y + \omega_{ny}{}^3 \varepsilon_y \quad = \rho_y \tag{7.7}$$

$$\dddot{\varepsilon}_z + \lambda_z \omega_{nz} \ddot{\varepsilon}_z + \hat{\mu}_z \omega_{nz}{}^2 \dot{\varepsilon}_z + \omega_{nz}{}^3 \varepsilon_z \quad = \rho_z \tag{7.8}$$

with

$$\begin{pmatrix} \rho_x \\ \rho_y \\ \rho_z \end{pmatrix} = -\left(\frac{\partial \Gamma}{\partial \underline{X}} \cdot \delta \underline{X} + \frac{\partial \Gamma}{\partial \underline{A}} \cdot \delta \underline{A} + \frac{\partial \Gamma}{\partial \dot{\underline{A}}} \cdot \delta \dot{\underline{A}} \right) - G(\underline{X}, \underline{A}) \left(\frac{\partial G^{-1}}{\partial \underline{X}} \cdot \delta \underline{X} + \frac{\partial G^{-1}}{\partial \underline{A}} \cdot \delta \underline{A} \right) \Gamma(\underline{X}, \underline{A}, \dot{\underline{A}}) \tag{7.9}$$

or

$$\begin{pmatrix} \rho_x \\ \rho_y \\ \rho_z \end{pmatrix} = \Delta_x \cdot \delta \underline{X} + \Delta_A \cdot \delta \underline{A} + \Delta_{\dot{A}} \cdot \delta \dot{\underline{A}} \tag{7.10}$$

where

$$\Delta_x \cdot \delta \underline{X} = \begin{bmatrix} \Delta_x{}^x \\ \Delta_x{}^y \\ \Delta_x{}^z \end{bmatrix} \cdot \delta \underline{X} = -\left(\frac{\partial \Gamma}{\partial \underline{X}} \right) \cdot \delta \underline{X} - G(\underline{X}, \underline{A}) \left(\frac{\partial G^{-1}}{\partial \underline{X}} \right) \cdot \delta \underline{X} \cdot \Gamma(\underline{X}, \underline{A}, \dot{\underline{A}}) \tag{7.11}$$

$$\Delta_A \cdot \delta \underline{A} = \begin{bmatrix} \Delta_A{}^x \\ \Delta_A{}^y \\ \Delta_A{}^z \end{bmatrix} \cdot \delta \underline{A} = -\left(\frac{\partial \Gamma}{\partial \underline{A}} \right) \cdot \delta \underline{A} - G(\underline{X}, \underline{A}) \left(\frac{\partial G^{-1}}{\partial \underline{A}} \right) \cdot \delta \underline{A} \cdot \Gamma(\underline{X}, \underline{A}, \dot{\underline{A}}) \tag{7.12}$$

$$\Delta_{\dot{A}} \cdot \delta \dot{\underline{A}} = \begin{bmatrix} \Delta_{\dot{A}}{}^x \\ \Delta_{\dot{A}}{}^y \\ \Delta_{\dot{A}}{}^z \end{bmatrix} \cdot \delta \dot{\underline{A}} = -\left(\frac{\partial \Gamma}{\partial \dot{\underline{A}}} \right) \cdot \delta \dot{\underline{A}} \tag{7.13}$$

Let us consider that $\delta \underline{X}$, $\delta \underline{A}$ and $\delta \dot{\underline{A}}$ can be approximated by independent white noise vectors with covariance matrices W_x,W_A and $W_{\dot{A}}$ and supposing that the coefficients Δ_x, Δ_A and $\Delta_{\dot{A}}$ are slowly varying with respect to the current state and output variables, then the state vector composed of the tracking errors is such that:

$$\begin{pmatrix} \dot{\varepsilon}_x \\ \ddot{\varepsilon}_x \\ \dddot{\varepsilon}_x \\ \dot{\varepsilon}_y \\ \ddot{\varepsilon}_y \\ \dddot{\varepsilon}_y \\ \dot{\varepsilon}_z \\ \ddot{\varepsilon}_z \\ \dddot{\varepsilon}_z \end{pmatrix} = \begin{bmatrix} 0 & 1 & 0 & 0 & 0 & 0 & 0 & 0 & 0 \\ 0 & 0 & 1 & 0 & 0 & 0 & 0 & 0 & 0 \\ -\lambda_x\omega_{nx} & -\hat{\mu}_x\omega^2{}_{nx} & \omega^3{}_{nx} & 0 & 0 & 0 & 0 & 0 & 0 \\ 0 & 0 & 0 & 0 & 1 & 0 & 0 & 0 & 0 \\ 0 & 0 & 0 & 0 & 0 & 1 & 0 & 0 & 0 \\ 0 & 0 & 0 & -\lambda_y\omega_{ny} & -\hat{\mu}_y\omega^2{}_{ny} & \omega^3{}_{ny} & 0 & 0 & 0 \\ 0 & 0 & 0 & 0 & 0 & 0 & 1 & 0 & 0 \\ 0 & 0 & 0 & 0 & 0 & 0 & 0 & 1 & 0 \\ 0 & 0 & 0 & 0 & 0 & 0 & -\lambda_z\omega_{nz} & -\hat{\mu}_z\omega^2{}_{nz} & \omega^3{}_{nz} \end{bmatrix} \begin{pmatrix} \varepsilon_x \\ \dot{\varepsilon}_x \\ \ddot{\varepsilon}_x \\ \varepsilon_y \\ \dot{\varepsilon}_y \\ \ddot{\varepsilon}_y \\ \varepsilon_z \\ \dot{\varepsilon}_z \\ \ddot{\varepsilon}_z \end{pmatrix}$$
$$+ \begin{bmatrix} 0 & 0 & 0 \\ 0 & 0 & 0 \\ \Delta_x^x & \Delta_x^y & \Delta_x^z \\ 0 & 0 & 0 \\ 0 & 0 & 0 \\ \Delta_A^x & \Delta_A^y & \Delta_A^z \\ 0 & 0 & 0 \\ 0 & 0 & 0 \\ \Delta_{\dot{A}}^x & \Delta_{\dot{A}}^y & \Delta_{\dot{A}}^z \end{bmatrix} \begin{pmatrix} \delta\underline{X} \\ \delta\underline{A} \\ \delta\underline{\dot{A}} \end{pmatrix} \tag{7.14}$$

Equation 7.14 can be expressed simply with:

$$\dot{\underline{\varepsilon}} = S\underline{\varepsilon} + \Delta \begin{pmatrix} \delta\underline{X} \\ \delta\underline{A} \\ \delta\underline{\dot{A}} \end{pmatrix} \tag{7.15}$$

Since matrix *S* is asymptotically stable, so following the proposed assumptions, we get:

$$\lim_{t\to\infty} E\left\{\underline{\varepsilon}(t)\right\} = 0 \quad \in R^3 \tag{7.16}$$

and writing the covariance of the output vectors as Σ, this covariance follows the dynamics:

$$\dot{\Sigma} = S\Sigma + \Sigma S^T + \Delta W \Delta^T \tag{7.17}$$

which converges towards Σ_∞ given by the solution of:

$$S\Sigma_\infty + \Sigma_\infty S^T + \Delta W \Delta^T = 0 \tag{7.18}$$

When these above assumptions are not satisfied, numerical simulation applied to equations 7.6 - 7.8 will allow to assess the effect of measurement and computation errors on the performance of the proposed tracking system.

7.3 Robustness to parameters errors

When it is assumed that the aircraft plant dynamic is exactly known, a dynamic inversion control law will cancel out the nonlinearities in the output plant dynamics and substitute it with a desirable dynamics. This assumption is not met usually for most aircraft since the availability of the aircraft data, especially the aerodynamic data, are not easily obtained. Therefore in practical application, the adopted plant dynamic models cannot be perfect, presenting structural as well as parametric errors.

Because of the unavailability of the true knowledge of the aircraft plant dynamics and the variation of the aerodynamic coefficients throughout the entire flight envelope according to flight conditions there will be parameters errors in the modeling of the controller. The design of the NDI controller should be robust to these parameter uncertainties and the modeling of the parameters uncertainties should be incorporated in the controller design. Many studies have been done on the robustness of the NDI controller, to name a few [Bennani and Looye, 1998, Biannic et al., 2014, Campbell and Kaneshige, 2010, MacKunis et al., 2008, Papageorgiou and Glover, 2004].

[Campbell and Kaneshige, 2010, MacKunis et al., 2008] used a model reference adaptive control on a system having a nonparametric uncertainty. In [Biannic et al., 2014, Papageorgiou and Glover, 2004]. A linear parameter varying (LPV) model techniques is adopted in NDI controller. These approaches show a good tracking error despite uncertainty and external disturbing inputs. In [Bennani and Looye, 1998], the classical nonlinear inversion is combined with μ-synthesis containing the modeling of the parameters uncertainties to provide robust control solutions. From μ-analysis, the robust performance level of classical NDI is 16 times worse than Robust Dynamic Inversion.

In [Bouadi, 2013, Yang et al., 2014] both use a sliding mode controller to cope with the parameter's uncertainties. The robust controller in [Yang et al., 2014] is

applied to a spacecraft formation and the spacecraft is able to track the reference trajectory with position error less than 1 meter, while in [Bouadi, 2013], the controller is applied to control the flight path angle. The results obtained shows that a good path angle tracking performance is achieved and the angle of attack remains within an acceptable range for considered flight conditions with limits between the interval [-11.5^o, 18^o] .

Let us assume the true dynamic model of the system is given by the parameterized affine form:

$$m\begin{bmatrix}\dddot{x}\\ \dddot{y}\\ \dddot{z}\end{bmatrix} = g(\underline{X},\underline{A},\underline{P})\begin{pmatrix}\dot{\phi}\\ \dot{\theta}\\ \dot{T}\end{pmatrix} + h(\underline{X},\underline{A},\dot{\underline{A}},\underline{P}) \tag{7.19}$$

where $g(\underline{X},\underline{A},\underline{P})$ and $h(\underline{X},\underline{A},\dot{\underline{A}},\underline{P})$ are not exactly known as well as parameters $\underline{P}$, while the adopted synthesis model is given as:

$$m\begin{bmatrix}\dddot{x}\\ \dddot{y}\\ \dddot{z}\end{bmatrix} = G(\underline{X},\underline{A},\tilde{\underline{P}})\begin{pmatrix}\dot{\phi}\\ \dot{\theta}\\ \dot{T}\end{pmatrix} + H(\underline{X},\underline{A},\dot{\underline{A}},\tilde{\underline{P}}) \tag{7.20}$$

where $\tilde{\underline{P}}$ is the adopted value for the parameters. Then the effective guidance dynamics of the aircraft will be given by:

$$m\begin{bmatrix}\dddot{x}\\ \dddot{y}\\ \dddot{z}\end{bmatrix} = m\cdot g(\underline{X},\underline{A},\underline{P})\cdot G(\underline{X},\underline{A},\tilde{P})^{-1}\cdot J(\underline{X},\underline{A},\dot{\underline{A}},\tilde{P}) - g(\underline{X},\underline{A},\underline{P})\cdot G(\underline{X},\underline{A},\tilde{P})^{-1}\cdot H(\underline{X},\underline{A},\dot{\underline{A}}) + h(\underline{X},\underline{A},\dot{\underline{A}},\underline{P}) \tag{7.21}$$

Writing $G(\underline{X},\underline{A},\tilde{\underline{P}})^{-1} = g(\underline{X},\underline{A},\underline{P})^{-1}\cdot(\mathrm{I} + \Delta G(\underline{X},\underline{A},\underline{P},\tilde{\underline{P}}))$ we get:

$$m\begin{pmatrix} \dddot{\varepsilon}_x + \lambda_x\omega_{nx}\ddot{\varepsilon}_x + \hat{\mu}_x\omega_{nx}{}^2\dot{\varepsilon}_x + \omega_{nx}{}^3\varepsilon_x \\ \dddot{\varepsilon}_y + \lambda_y\omega_{ny}\ddot{\varepsilon}_y + \hat{\mu}_y\omega_{ny}{}^2\dot{\varepsilon}_y + \omega_{ny}{}^3\varepsilon_y \\ \dddot{\varepsilon}_z + \lambda_z\omega_{nz}\ddot{\varepsilon}_z + \hat{\mu}_z\omega_{nz}{}^2\dot{\varepsilon}_z + \omega_{nz}{}^3\varepsilon_z \end{pmatrix} = m\cdot(\mathrm{I}+\Delta G)\cdot J(\underline{X},\underline{A},\dot{\underline{A}},\tilde{P}) - (\mathrm{I}+\Delta G)\cdot H(\underline{X},\underline{A},\dot{\underline{A}}) + h(\underline{X},\underline{A},\dot{\underline{A}},\underline{P})$$

(7.22)

From the above equation, it appears that depending on the magnitude of the modeling errors, the guidance error dynamics may behave quite differently from what is to be expected.

7.4 Compatibility with current auto-pilots

In modern aircraft (Airbus and Boeing families) the primary inputs for the autopilot are not compared by the pitch and bank angles as suggested by equations (6.39) and (6.40). In the case of the Airbus family the autopilot adopts as primary inputs, the normal load factor n_z and the roll rate p, which in the case of Boeing family it adopts the normal load factor n_z with airspeed feedback to the controller integrator and also roll rate p .

In the case of roll rate control, the proposed approach in Chapter 6 computes the desired roll speed $\dot{\phi}_c$. Using the Euler equation, the corresponding desired roll rate p can be computed by:

$$p_c = \dot{\phi}_c - \dot{\psi}_c \sin\theta \tag{7.23}$$

where $\dot{\psi}_c$ is taken equal to $(g/GS)\tan\phi\cos\theta$ as the result of the equation of the yaw stability of the aircraft. Then the roll dynamics of the controlled aircraft can be supposed to be made to follow linear dynamics such as:

$$\dot{p} = \frac{1}{\tau_p}(p_c - p) \tag{7.24}$$

where τ_p is a short (<1/3s) time constant.

According to the definition of the load factor in the body frame:

$$\vec{n} = \frac{m\vec{g} + \vec{F}_i}{mg} \tag{7.25}$$

where $\vec{F}_i$ are the inertial forces, we get;

$$\vec{n} = \begin{pmatrix} n_x \\ n_y \\ n_z \end{pmatrix}_B = \begin{bmatrix} (1/g)(rv - qw) + \sin\theta \\ (1/g)(pw - ru) - \cos\theta \sin\phi \\ (1/g)(qu - pv) - \cos\phi\cos\theta \end{bmatrix} \tag{7.26}$$

The pitch control law on modern air transport aircraft is such as:

$$\dot{n}_z = \frac{1}{\tau_{n_z}}(n_{zc} - n_z) \tag{7.27}$$

where τ_{n_z} is a time constant short (<1/2s).

Here $\dot{n}_z$ is such as:

$$\dot{n}_z = (1/g)(\dot{q}u + q\dot{u} - \dot{p}v - p\dot{v}) + \dot{\phi}\sin\phi\cos\theta + \dot{\theta}\cos\phi\sin\theta \tag{7.28}$$

then relation 7.28 can be rewritten as:

$$\begin{aligned}(1/g)(\dot{q}u - \dot{p}v) = \frac{1}{\tau_{n_z}}(n_{zc} - (1/g)(qu - pv) - \cos\phi\cos\theta) - (1/g)(q\dot{u} - p\dot{v}) \\ -\dot{\phi}\sin\phi\cos\theta - \dot{\theta}\cos\phi\sin\theta\end{aligned} \tag{7.29}$$

here we adopt approximate $\dot{\phi} \cong p$ and $\dot{\theta} \cong q$ and assuming that acceleration remains small ($\dot{u}$ ~0, $\dot{v}$ ~0) while ϕ is supposed to equal zero, then we get:

$$\frac{\dot{q}u}{g} + \left(\frac{1}{g\tau_{n_z}}u + \sin\theta\right)q = \frac{1}{\tau_{n_z}}(n_{zc} + \frac{pv}{g} - \cos\theta) + \frac{\dot{p}v}{g} \tag{7.30}$$

if τ_p in equation 7.24 is chosen equal to τ_{n_z} and neglecting $sin\theta$ with respect to $u/(g\tau_{n_z})$, the above equation can be written as:

$$\frac{u}{g}\dot{q} + \frac{1}{g\tau_{n_z}}uq = \frac{1}{\tau_{n_z}}(n_{zc} - \cos\theta) + \frac{vp_c}{\tau_{n_z}g} \tag{7.31}$$

or

$$\dot{q}\tau_{n_z} + q = \frac{1}{u}(vp_c + g(n_{zc} - \cos\theta)) \tag{7.32}$$

then defining q_c as:

$$q_c = \frac{1}{u}(vp_c + g(n_{zc} - \cos\theta)) \tag{7.33}$$

it appears that the control objective represented by equation 7.27 leads to an equivalent control objective with respect to the pitch rate q where the reference value is computed from 7.33.

Then shifting the second control input in the approach proposed in chapter 6 from $\dot{\theta}$ to q, will lead to a pitch requirement from autopilot close to equation 7.27.

7.5 Invertibility

To perform NDI controller, the control matrix G($\underline{X}$) must be invertible with respect to the chosen input. If the control matrix $G(\underline{X})$ is not invertible there can be infinity of solutions or no solutions at all to the equation (6.74). Then an analysis on the invertibility of the control matrix must be performed.

7.5.1 Invertibility analysis

Matrix $G(\underline{X})$ of R^{3x3} is invertible when its determinant Δ is different from zero. When this determinant it appears that many terms vanish, so the exact expression of Δ reduces to:

$$\Delta = (F_z(\alpha,\beta,V_a,z)\cos\phi + F_y(\alpha,\beta,V_a,z)\sin\phi)(F_x(\alpha,\beta,V_a,z) + T) \tag{7.34}$$

Since the value of F_z remains during a commercial flight close to the aircraft weight, $m.g$ while lateral force F_y remains small, the first term of the left hand side of equation 7.34 will remain strictly positive during a commercial flight. Then the necessary condition for the invertibility result is:

$$F_x(\alpha,\beta,V_a,z) + T \neq 0 \tag{7.35}$$

The above equation will be written as F_x+T. It appears that the condition $F_x+T=0$ cannot be sustained when T is constant. Considering climb and descent situations as described below (where the Thrust is supposedly applied along the aircraft longitudinal axis):

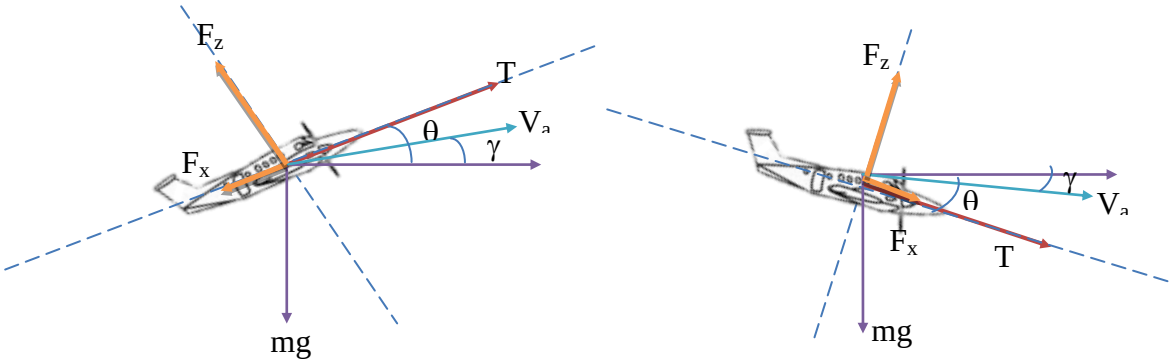

Non-invertibility climb situations

Non-invertibility descent situations

Figure 7.1: Non-invertibility situations

The sum of the external forces applied to the aircraft along its longitudinal axis is then equal to $-mgsin\theta$ in climb and $mgsin\theta$ in descent. That means that the speed along this axis will diminish in climb and increase in descent, then the longitudinal component of the aerodynamic force, F_x, will diminish in climb and increase in descent too and the non-invertibility condition ($F_x+T=0$) will no more be satisfied

The only situation in which F_x+T can be equal to zero in a permanent way is such as:

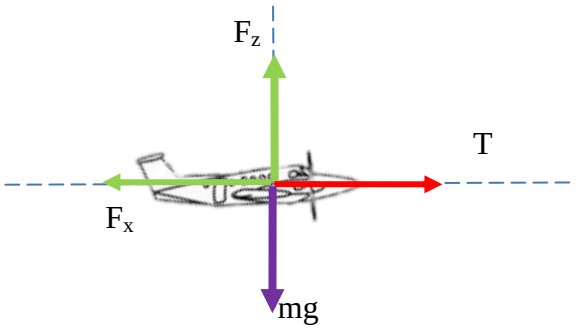

Figure 7.2: Non-invertibility situations in cruise

which shows a cruise trim condition with zero pitch angle and the aircraft airspeed, V_a is along the aircraft x-axis Body Frame which causes F_x to equal to the total aerodynamic drag. This is not the case for the majority of aircraft having static stability. So the non-invertibility can be only satisfied at singular points of time. A practical solution will be to define a threshold $\xi>0$ such that if $|F_x + T| > \xi$ then the control law (6.74) will be applied, otherwise the control rates will be taken equal to zero, freezing the bank and pitch angle, as well as the thrust, until the nonlinear inverse control law can be used again.

In the simulations presented in chapter 6, this situation appeared various times without resulting in a noticeable degradation of the tracking performance.

7.6 Conclusion

In this chapter, the main issues which can limit the applicability and effectiveness of the proposed 3D+T guidance control law have been analyzed. The nonlinearities involved in the considered flight guidance dynamics as well as the control law presents a difficulty in an analytical approach of the different identified issues (data accuracy, modeling errors, invertibility), so a simulation approach should be adopted to go deeper in this analysis. However, considering that 3D+T trajectories assigned to transportation aircraft are smooth ones, some classical control technique (integrators, adaptive elements) could be considered to turn the proposed control law more robust with respect to measurement and modeling errors.

CHAPTER 8
TOWARDS TRAFFIC MANAGEMENT ALONG AIRSTREAMS

Chapter 8: Towards Traffic Management along airstreams

8.1 Introduction

The previous chapter was designed to explain flight guidance control law to track 3D+T trajectories. In this chapter 3D+T reference trajectories built up from slots evolving along lanes in an airstream are considered. In this case, the basic maneuver will be a lane change maneuver between parallel lanes. So in this chapter a scenario to perform this basic maneuver leading to the complete parameterization of the resulting 3D+T trajectory using a common space-indexed reference is proposed. Then, synchronization conditions for merging are established and different heuristics to assign conflict free trajectories to lane changing aircraft within the airstream are considered.

8.2 Configuration inside the airstream

Within the airstream, aircraft are assumed to fly in a designated lane related with their performances. Here each lane is characterized by its flight altitude and its reference speed. Within lanes aircraft are assigned to a space slot moving at the current lane reference speed. The 3D+T guidance law makes the aircraft to remain positioned at the center of the corresponding moving slot. When an aircraft performs a lane change inside the airstream, its guidance system will make it follow a moving slot which will go to occupy a free slot in the target lane.

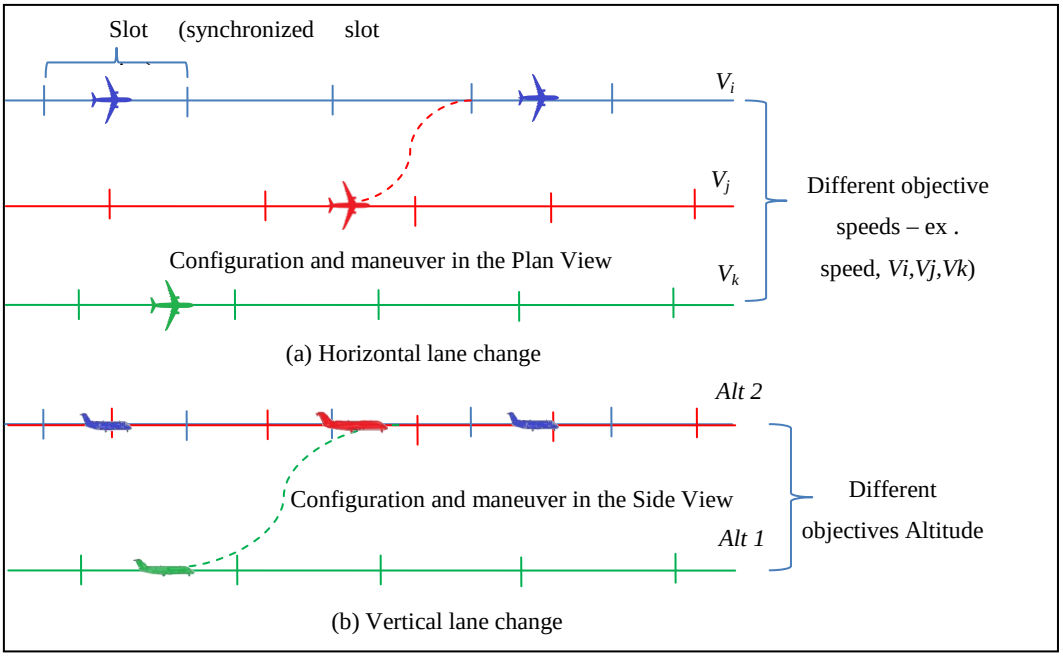

Figure 8.1: Standard shift maneuver in an airstream

From this configuration, the illustration of the shift maneuver will be done in the next section.

8.3 Reference shift maneuver between lanes

Although here only horizontal shift maneuvers are considered, the proposed approach can be easily extended to vertical ones. Then, the illustration is done in the case of a maneuver at constant altitude. Here a straight and level airstream reference trajectory is considered with several parallel lanes at the same altitude as shown in Figure 8.1. The i^{th} lane of the ASRT is composed of space slots of width Δ moving at a constant speed V_i ; Here it is assumed that two lanes i and j are separated by a constant distance D_{ij}.

Here it is considered the case when a transport aircraft flying initially along a straight lane j with a ground speed V_j , is to shift to a straight lane i by merging in a free slot of this target lane.

let $$x_j^k(t) = x_{j0}{}^k + V_j \cdot (t - t_0) \qquad (8.1)$$

be the position of the k^{th}-slot of lane j at time t where $x_{j0}{}^k$ is its initial position and V_j is the corresponding ground speed.

The position at time *t* of the following slot at time *t* on the same lane *j* is given by:

$$x_j^{k+1}(t) = x_j{}^k(t) - \Delta \tag{8.2}$$

8.3.1 Reference shift trajectories between lanes

The reference trajectory of the merging aircraft is supposed to be divided into a succession of segments denoted by s_i where only one maneuver is performed at a time. The proposed sequence is such as:

1. The aircraft waits on its original lane for the right time and position to turn towards the target lane,
2. During the straight segment after the turn, the aircraft slowly changes it speed to V_i,
3. Then it will perform another turn at constant speed to reach the center of a free slot on lane *i*.

Here, to limit the number of parameters characterizing the maneuver, the turns are supposed to be symmetrical (same radius and angle). This is described in Figure 8.2. The maneuvering aircraft is supposed to know the distance *D* between lanes *j* and *i* as well as the reference speed on the target lane. Then it can compute the length of the maneuver given by s_f-s_1 (Figure 8.2) and its duration t_f-t_1. The when there is a free slot at position $s_i(t)$ such as:

$$s_i(t) + V_i(t_f - t) = s_j(t) + (s_f - s_1) \tag{8.3}$$

the flight maneuver can start.

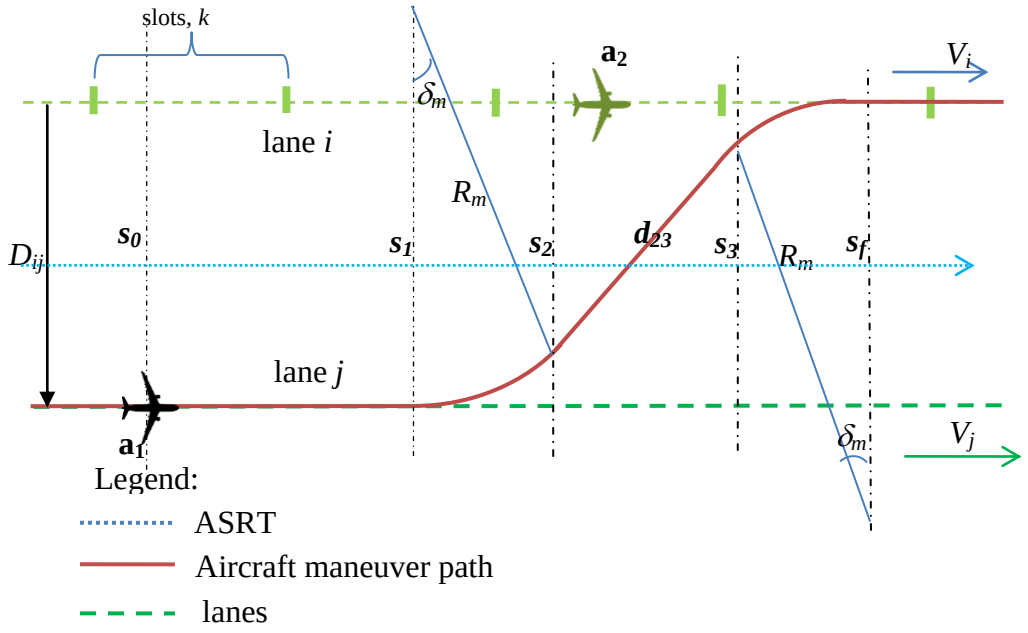

Figure 8.2: Standard shift maneuver between lanes in an ASRT

8.3.2 Characterization of the reference trajectory

Here the standard flight maneuver is parameterized using the abscissa along the airstream as independent parameter: From s_0 to s_1, the aircraft $\mathbf{a_1}$ flies a straight segment at constant speed V_j. The maneuver starts at s_1, the aircraft perform at constant speed V_j and a left equilibrated turn of angle $\delta_m (< \pi/2)$ and radius R_m such as:

$$R_m = \frac{V_j^2}{g \sin \phi_m} \tag{8.4}$$

ϕ_m is a standard turn bank angle such as $\phi_m \leq \phi_{max}$, where ϕ_{max} is a maximum bank angle value and $R_m \geq R_{min}$ with $R_{\min} > \frac{V_j^2}{g \sin \phi_{\max}}$

Then section s_2 is given by:

$$s_2 = s_1 + R_m \sin \delta_m \tag{8.5}$$

In order to merge safely into lane *i*, the aircraft performs a nominal change of speed from V_j to $V_i=V_j+\delta V_{ij}$ from s_2 to s_3. It is supposed that the nominal change of speed is characterized by a constant space rate *a* (m/s/m), such as:

$$a = \frac{\delta V_{ij} \cdot \sin \delta_m}{D_{ij} - 2R_m(1-\cos \delta_m)} \quad \text{with} \quad a_{\min} \le a \le a_{\max} \tag{8.6}$$

where a_{min} and a_{max} are the minimum and the maximum speed space rate of change. Then s_3 is given by:

$$s_3 = s_2 + \frac{D_{ij} - 2R_m(1-\cos \delta_m)}{\tan \delta_m} \tag{8.7}$$

From s_3 to the final maneuver segment, s_f, the aircraft performs at a constant speed V_i a right turn of angle δ_m and radius R_m to adopt the ASRT track at the center of a free space slot. s_3 is given by:

$$s_f = s_3 + R_m \sin \delta_m \tag{8.8}$$

with $R_m \ge R_{min}$ with $R_{\min} > \frac{V_j^{\,2}}{g \sin \phi_{\max}}$

Then s_f is parameterized by s_1, D_{ij}, δV_{ij} , V_j, R_m and δ_m where δ_m , R_m and s_1 are design parameters to be chosen. Therefore s_f is given by:

$$s_f = s_1 + D_{ij} - 2R_m(1-\cos \delta_m) / \tan \delta_m + 2R_m \sin \delta_m \tag{8.9}$$

The ground speed of the aircraft will vary along its reference merging trajectory:

$$V(s) = V_j \quad if \ s_0 \le s \le s_2 \tag{8.10a}$$

$$V(s) = V_j + \delta V_{ij} \sin \delta_m \frac{(s-s_2)}{D - 2R_m(1-\cos \delta_m)} \quad if \ s_2 \le s \le s_3 \tag{8.10b}$$

$$V(s) = V_i \quad if \ s_3 \le s \le s_f \tag{8.10c}$$

From the computed segments, the corresponding reference trajectory $(t_c(s),\rho_c(s),\sigma_c(s))$ with $s \in [\ s_0, s_f\ ]$ is given by the following expressions:

$$t_c(s) = t_1 + (R_m / V_j) \cdot \arcsin((s - s_1) / R_m) \quad if \ s_1 \le s \le s_2 \tag{8.11a}$$

$$t_c(s) = t_2 + \alpha \cdot \delta V_{ij} \cdot \ln\left(1 - \alpha \cdot (s - s_2) \cdot \delta V_{ij} / V_j\right) \quad if \ s_2 \le s \le s_3 \tag{8.11b}$$

$$t_c(s) = t_3 + (R_m / V_i) \cdot \arcsin((s - s_3) / R_m) \quad if \ s_3 \le s \le s_f \tag{8.11c}$$

with $\alpha = \dfrac{\sin \delta_m}{D_{ij} - 2R_m(1 - \cos \delta_m)}$

$$t_1 = t_0 + \left(s_1 - s_0\right) / V_j \tag{8.12a}$$

$$t_2 = t_1 + R_m \cdot \delta_m / V_j \tag{8.12b}$$

$$t_3 = t_2 + \alpha \cdot \delta V_{ij} \cdot \ln\left(1 - \cos \delta_m \cdot \delta V_{ij} / V_j\right) \tag{8.12c}$$

Therefore the final time to reach the merging position is given by:

$$t_f = t_3 + R \cdot \delta_m / V_i \tag{8.12d}$$

The distance of the aircraft to the ARST, $\rho(s)$, is given by:

$$\rho_c(s) = D_{ij} \quad if \ s_0 \le s \le s_1 \tag{8.13a}$$

$$\rho_c(s) = D_{ij} - R_m(1 - \cos \delta_m(s)) \quad if \ s_1 \le s \le s_2 \tag{8.13b}$$

$$\rho_c(s) = D_{ij} - R_m(1 - \cos \delta(s)) - (s - s_2) \tan \delta_m(s) \qquad if \ s_2 \le s \le s_3 \tag{8.13c}$$

$$\rho_c(s) = -R_m(1 + \cos \delta_m(s)) \quad if \ s_3 \le s \le s_f \tag{8.13d}$$

Since the lanes are parallel along the same flight level, the reference azimuth angle $\sigma_c(s)$ remains constant and equal to $\pi/2$. Let K_k be the set of free slots on lane i, an efficient management of the airstream will make the aircraft to merge to the center of the earliest free slot k_m on lane i such as:

$k_m = \min\{k \in K_k\}$ where $\exists R_m \le R_{\min}$ and $\exists \delta_m \in \left]0, \pi / 2\right[$ such as $s_f(s_1, R_m, \delta_m) = x_i^{k_m}$

From these calculation, the nominal shift trajectory from lane *j* to lane *i* in the airstream is completely defined from *s*, the curvilinear abscissa of the ASRT, varying from s_0 to s_f.

8.4 Traffic management along an airstream

Once an airstream and its reference parameters (reference speed on the lanes) have been designed (ASRT and parallel lanes were chosen) , the development of the traffic management to cope safely and efficiently with flights wishing to evolve from one lane to another inside the airstream can be studied. In this section, the slot assignment problem for lane shifting aircraft is tackled. An airstream composed of different parallel lanes such as those in Figure 8.3 is considered. Each lane is characterized by its position with respect to the ASRT and its reference ground speeds which take into account the wind speed so that their speed references are expressed in Mach number. To each flight is attached an aircraft with specific performances. It is considered that the ongoing traffic is composed of two kinds of flights:

1. the set of flights which are already flying their preferred lane. This is the set J_a of stable flights.

2. the set of flights which desire to perform as soon as possible a lane shift within the airstream. This is the set J_t of the transient flights.

The flights of set J_a are occupying known time-space slots along the different lanes parallel to the ASRT. Let $L=\{L_1,L_2,\ldots,L_{|L|}\}$ be the set composed of these lanes, including the ASRT and let Δ_i be the set of free slots along lane *i* where:

$$(t_i^k(s), \rho_i^k(s), \sigma_i^k(s)) \quad k \in \Delta_i \quad i \in L \tag{8.14}$$

is the reference trajectory of the k^{th} free slot of lane *i*, here with a constant speed assigned to each lane:

$$t_i^k(s) = t_i^k(s_0^{ik}) + (s - s_0^i)/V_i \tag{8.15}$$

where V_i is the reference ground speed of lane *i* and $t_i^k(s_o^i)$ is the time at which slot *k*, enters lane *i* at position (s_o^i). The problem considered here is to propose to each

transient flight a conflict free trajectory allowing it to join its preferred lane at a free slot as soon as possible. Here it is supposed that the shift trajectories are of the class considered in the previous paragraph.

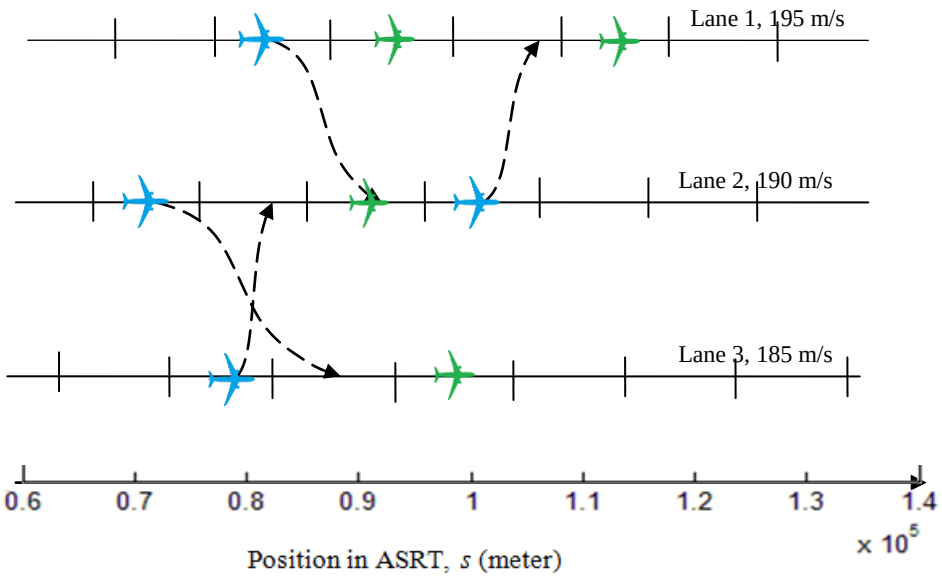

Figure 8.3: Example of transient (blue) flights and assigned (green) flight along an ASRT

Let *oj* and *dj* be the origin and the destination lanes of flight *j*, $j \in J_t$. Then let M_j be the set of feasible (conflict free trajectories with respect to the already assigned ones) merging trajectories from lane o_j to lane d_j for flight *j* and starting after position s_o^j. For a given flight, each of these trajectories, indexed by *m*, is attached to a time space moving slot on the destination lane d_j which is reached at time t_{dj}^{jm} and at the abscissa s_{dj}^{jm}.

8.4.1 Heuristic Assignment

The considered problem is an assignment problem between flights and free slots on the desired lanes where the total waiting times on the original lanes for transient flights could be a measure of the effectiveness of the management of the flights within the airstream. This assignment problem is a complex combinatorial one and its exact on-line solution may be infeasible even for rather small instances of the problem [Shen, 1995]. Then heuristic approaches seem appropriate to generate on-line assignment solutions. Different heuristics can be considered, however among

them, the greedy ones look to be the simpler to be put into operation. Either a time strategy or a space strategy can be adopted. Here two examples of greedy heuristic assignment methods according to a time strategy are considered:

The *min-time* heuristic ranks of the aircraft in set J_t increasingly with respect to m_j^f given by:

$$m_j^f = \arg\min_{m \in M_j} \{t_{d_j}^m\} \tag{8.16}$$

The index of the first flight to be assigned, j^* , is given by:

$$j^* = \arg\min_{j \in J_t} \{m_j^f\} \tag{8.17}$$

where flight j^* is assigned to the merging trajectory $m_{j^*}^f$, J_t is then updated by deleting j^*. Note that J_t must be incremented any time a new flight enters the airstream. The set of conflict free trajectories M_j are updated for $j \in Jt$.

The risk with this heuristic is that the trajectory assignment of some flights may be postponed repeatedly, making these flights support additional operations costs. Differently, the *max-wait* heuristic ranks the aircraft in set J_t decreasingly according to their waiting time within this set and assigns to the first of them, j^*, its earliest conflict free merge trajectory $m_{j^*}^f$.

Now the risk is to assign merging trajectories to flights when they have been waiting for a long time. A hybrid heuristic could be to adopt the *min-time* heuristic, but whenever the waiting time of an aircraft becomes higher than some given an upper bound, it has to be treated in priority. Similar heuristics could be proposed by adopting the spatial index $s_{d_j}^{jm}$ within a spatial strategy. Observe that the performances resulting from the temporal and the spatial strategies should not be equivalent since the speed of merging aircraft does not remain constant during the maneuver.

When considering aircraft j of set J_t, the k^{th} free slot of d_j will generate a candidate merging trajectory if there is a solution to the equations:

$$t_f = t_{d_j}^j \text{ and } s_f = s_{d_j}^j \tag{8.18}$$

where s_f is given by equation 8.9, t_f is given by equation 8.12d and:

$$t_{d_j}^k(s_{d_j}^j) = t_{d_j}^k(s_0^{d_j k}) + (s_{d_j}^j - s_0^{d_j})/V_A^{d_j} \tag{8.19}$$

This candidate trajectory will be conflict free if it remains far from any other planned trajectory in the airstream. A possible way to express this condition is such as:

$$\forall g \in J_a with \;\; s_0^{gj} s_f^{gj} : \forall s \in [s_0^{gj}, s_f^{gj}]\, d_{gj}(s) > d_{\min} \tag{8.20}$$

where

$$s_0^{gj} = \max\{s_0^g, s_0^j\} \quad \text{and} \quad s_f^{gj} = \min\{s_f^g, s_f^j\} \tag{8.21}$$

and

$$d_{gj}(s) = \sqrt{\begin{array}{c}\left(\rho_g(s)\cdot\cos(\sigma_g(s)) - \rho_j(s)\cdot\cos(\sigma_j(s))\right)^2 + \left(\rho_g(s)\cdot\sin(\sigma_g(s)) - \rho_j(s)\cdot\sin(\sigma_j(s))\right)^2 \\ + (1/4)\left(V_A^g + V_A^{d_j}\right)^2 \left(t_g(s) - t_j(s)\right)^2\end{array}} \tag{8.22}$$

and where $d_{\min}$ is a minimum safe distance.

8.4.2 Illustration of traffic assignment

Here a scenario is introduced which considers three lanes of an airstream with different reference speeds and same altitude:

1. In the considered section of the first lane there are three aircraft, one of them intending to shift to the second lane,
2. In the second lane there are also three aircraft, one of them intending to shift to the first lane and another intending to shift to the third lane,
3. In the third lane, one of the two present aircraft intend to shift to the second lane.

Table 8.1 displays the relative position of these aircraft at initial time, as well as their intentions within the airstream. The slots on the lanes are numbered backwards starting from the more engaged flight into each lane. In order to perform the assignment of the free slots to the standard shift maneuvers, a greedy heuristic based on the min-time approach is developed. The main steps of the resulting assignment algorithm are displayed below:

1. Rank increasingly the transient flights according to their minimum final maneuver time, m_j^f . Let j* the first of the list.

2. Assign to flight j* the maneuver associated to $m_{j^*}^f$ and update the sets J_a, J_t :

   $J_a = J_a \cup \{j^*\}$ and $J_t = J_t / \{j^*\}$

3. If $J_t = \varnothing$ then Exit

4. Update the sets M_j with j∈ Jt, if $\forall j \in J_t : M_j = \varnothing$ then Exit otherwise go back to step 1

Observe that when $M_j = \varnothing$, flight j has no opportunity on its target lane and must remain on its original lane. Note also that this algorithm can be run on line by adding flight entry and exit events. Firstly, the position of the aircraft will be chosen. Table 8.1 summarizes the initial position of each flight and their intensions. Then Table 8.2 shows the first calculation of the assignment without delay and their ranking. It can be seen from Table 8.2, the assignment can be done for flight 6, 7, 8. However for flight 5, since the target slot position has already been occupied by flight 3 some delay time will be proposed for the flight. To avoid any conflict during the maneuver flight 7 will be ranked third after flight 8 and there will be a delay since the assignment will be taking place after flight 8. Table 8.3 shows the final proposed assignment.

Table 8.1: Initial situation in ARST

Flight	Initial Lane	Slot position	Target Lane	Initial Lane Speed (m/s)	Target Lane Speed (m/s)	Distance between lanes (m)	Initial position s0 (m)
1	1	3	1	195	195	0	12626
2	1	1	1	195	195	0	22727
3	2	2	2	190	190	0	12626
4	3	1	3	185	185	0	22607
5	1	5	2	195	190	10000	7390
6	2	1	1	190	195	10000	17431
7	2	4	3	190	185	10000	2516
8	3	4	2	185	190	10000	7548

Table 8.2: First ranking between transient flights

Flight	Initial Lane	Initial Slot position	Target Lane	Target Slot Position	Maneuver Duration	Earliest Completion Time	Ranking of Transient Flights
1	1	3	1	3	0	-	-
2	1	1	1	1	0	-	-
3	2	2	2	2	0	-	-
4	3	1	3	1	0	-	-
5	1	4	2	3	104.28	104.28	4
6	2	1	1	2	104.28	104.28	1
7	2	4	3	4	107.07	107.07	3
8	3	3	2	3	107.07	107.07	2

From Table 8.3, it can be seen that flight 5 cannot be assigned. Even after a delay of 230.35 seconds has been proposed, flight 5 target slot 3 in lane 2 which has been occupied by flight 8. Adding to the delay might solve the problem or proposing an extra lane as a queue lane or waiting lane. This proposed lane can have a variable speed that would be adjusted to be higher or lower to assist the transient aircraft to switch lane in between maneuvers.

Table 8.3: Final proposed assignment and performance

Aircraft	Initial Lane	Initial Slot position	Final Lane	Final Slot Position	Start of Maneuver	End of Maneuver	Delay (s)
1	1	3	1	3	-	-	-
2	1	5	1	5	-	-	-
3	2	2	2	2	-	-	-
4	3	1	3	1	-	-	-
5	1	2	2	-	-	-	230.35
6	2	4	1	2	98165	118360	0
7	2	1	3	4	89307	109505	111.1
8	3	2	2	3	79838	100030	2

8.5 Conclusion

In conclusion, it appears that the proposed 3D+T guidance systems allow to perform accurately basic maneuvers within airstreams. The adoption of a spatial reference along the airstream permits to characterize completely the possible trajectories inside it as well as detects potential conflicts between aircraft. Then effective traffic management within the airstream can be performed. In this chapter, a centralized approach leading to the online solution of a slot assignment problem has been developed allowing the collective management of the flow of aircraft inside the airstream. However, once traffic rules within an airstream are defined, decentralized traffic management schemes may be developed and operated possibly under the supervision of ASAS. In the case in which only shifts between adjacent lanes are authorized, a fully decentralized approach can be foreseen.

CHAPTER 9
CONCLUSION AND PERSPECTIVES

Chapter 9: Conclusion and Perspectives

With the actual and expected increase for the next decades of air traffic all around the world, current capacity and safety levels as well as environmental conditions are at stake. A failure to provide effective solutions to this foreseeable situation would have important economic and social consequences. So, in addition to the permanent effort of Civil Aviation Authorities to improve air traffic conditions, important research programs have been launched in the last decade by national and multinational authorities to face this turnpike challenge.

It is well agreed that the more deterministic the traffic is, the more high density traffic can be managed with a given guaranteed level of safety. To turn traffic less stochastic, many different actions can be undertaken. In this thesis two of them have been developed:

- the development of a new guidance approach to cope with 3D+T flight trajectories where permanent flyover constraints have to be satisfied;
- a new organization of high density traffic flows into orderly traffic in geometric air corridors.

With respect to the first action, a nonlinear guidance control law for transportation aircraft presenting space-indexed tracking performances has been developed. This approach takes profit of the numerical invertibility of the established third order input-output flight guidance dynamics, generates reference inputs for the autopilot of the aircraft while allowing to meet 3D+T specific requirements:

- permanent dual accuracy in position and overfly time,
- safe spatial and time response to perturbations.

Onboard guidance systems are not stand alone systems and the overall guidance performance will depend on the quality of the data provided by some other onboard systems. It is the case with the navigation system which delivers on-line the estimated

aircraft position and speed information while the ADIRS (Air Data-Inertial Reference System) contributes to the estimation of wind speed components. However with the introduction of satellite technology, the performances of navigation systems have been largely enhanced allowing permanently a more precise guidance.

Anyway, the proposed guidance approach can be considered to contribute effectively to the shift from traditional Mode-Based Guidance (MBG) to the new concept of Trajectory-Based Guidance (TBG) which should give ground to Trajectory Based Operations (TBO).

Further efforts with respect to the proposed nonlinear inverse control law should be performed:

- an extended study about the points considered in chapter 7 (sensitivity, robustness and numerical inversion) for validation purpose.
- simulations should be performed to treat extensively typical 3D+T reference trajectories as well as other exceptional 3D+T reference trajectories, for certification purpose.
- Also, considering the high numerical complexity of the inversion which is the core of this control law, it appears already of interest to develop a specific tool to perform it. Earlier studies [Lu et al., 2012] point out to the neural network solution. Therefore this new flight guidance control law could be more efficiently implemented on board transport aircraft.

It is also of interest to note that the proposed flight guidance control law could be adapted to other contexts such as UAVs, helicopters and other aircraft involved in specific 3D+T missions.

With respect to the second action, the proposal to organize air corridors as a set of lanes positioned around a 3D common reference track has been introduced, giving way to the notion of airstream where the lanes are support to dynamic slots organized in

a synchronous way. The proposed 3D+T guidance approach appears to provide an adequate mean for aircraft to enter safely in such a structured airspace.

Although this second aspect of the thesis remains largely in a preliminary stage and should be much further developed, it appears already to point out to some interesting opportunities to cope with high density traffic:

- more efficient use of available capacity;
- increased automatic separation insurance and local conflict avoidance;
- collaborative local traffic monitoring and management;
- implementation of local collaborative navigation to improve the integrity of the navigation function [Monteiro, 2015],

then contributing to enhance safety as well as efficiency in high density air traffic.

Many fundamental issues remain also in that area to be analyzed and solved to validate this proposal. Among all these issues, issues like the opportunity to use airstreams, design and composition and their connection with other airspace are worth to be considered.

Finally their potential contribution to another important concept under development for Air Traffic Management, the Network Collaborative Decision Making (N-CDM), should be investigated considering the possibility of end-to-end slot assignment for commercial flights.

REFERENCES

[AIRBUS, 2009] AIRBUS (2009). getting to grips with required navigation performance with autorization required (rnp ar). Technical report, Flight Operations Support & Services.

[Amy Cavaretta and Westervelt, 2013] Amy Cavaretta, Paul Lewis, J. S. and Westervelt, M. (2013). Addressing future capacity needs in the u.s. aviation system. Technical Report 66 pp, Eno Center for Transportation (Eno).

[Anderson, 2005] Anderson, J. D. (2005). *Introduction To Flight*, volume 199. McGraw-Hill Boston.

[Ashford, 2010] Ashford, R. (2010). Nextgen trajectory-based operations status update.

[Barraci, 2010] Barraci, N. (2010). *Conflict Resolution In Autonomous Operations Area Airspace*. PhD thesis, TU Darmstadt.

[Basu, 2013] Basu, S. (2013). *Design Methods And Analysis Of Algorithms*. PHI Learning Pvt. Ltd.

[Bennani and Looye, 1998] Bennani, S. and Looye, G. (1998). Flight control law design for a civil aircraft using robust dynamic inversion. In *Proceedings of the IEEE/SMC-CESA98 Congress, Tunisia*.

[Biannic et al., 2014] Biannic, J., Burlion, L., and De Plinval, H. (2014). Robust control design over large flight envelopes: a promising approach for aerial robotics. *AerospaceLab*, (8):1–8.

[Blakelock, 1991] Blakelock, J. (1991). *Automatic Control of Aircraft and Missiles*. A Wiley-Interscience publication. Wiley.

[Blom et al., 2006] Blom, H. A., Krystul, J., Bakker, G., Klompstra, M. B., and Obbink, B. K. (2006). Free flight collision risk estimation by sequential mc simulation. *Stochastic hybrid systems*, pages 249–281.

[BOEING, 2011] BOEING, L. (2011). Boeing 787 dreamliner. *Design*, 8:022.

[Bouadi, 2013] Bouadi, H. (2013). *Contribution to Flight Control Law Design and Aircraft Trajectory Tracking*. PhD thesis, Institut National des Sciences Appliquees de Toulouse (INSA Toulouse).

[Bouadi and Mora-Camino, 2012] Bouadi, H. and Mora-Camino, F. (2012). Aircraft trajectory tracking by nonlinear spatial inversion. In *AIAA Guidance, Navigation and Control Conference, Minneapolis, Minnesota, USA*.

[Bouadi et al., 2012] Bouadi, H., Mora-Camino, F., and Choukroun, D. (2012). Aircraft time-2d longitudinal guidance based on spatial inversion of flight dynamics. In *Digital Avionics Systems Conference (DASC), 2012 IEEE/AIAA 31st*, pages 3C4–1. IEEE.

[Bowen, 2014]Bowen, D. (2014). Trajectory based operations. SESAR Joint Undertaking at 2014 ATC Global.

[Campbell and Kaneshige, 2010] Campbell, S. F. and Kaneshige, J. T. (2010). A nonlinear dynamic inversion predictor-based model reference adaptive controller for a generic transport model. In *American Control Conference (ACC), 2010*, pages 868–873. IEEE.

[Cao et al., 2011] Cao, Y., Kotegawa, T., and Post, J. (2011). Evaluation of continuous descent approach as a standard terminal airspace operation. In *Ninth USA/Europe Air Traffic Management Research and Development Seminar (ATM2011), Berlin, Germany*.

[Cate, 2013] Cate, K. T. (2013). Challenges in achieving trajectory-based operations. In *51st AIAA Aerospace Sciences Meeting including the New Horizons Forum and Aerospace Exposition, Grapevine, TX*.

[Cavcar, 2000]Cavcar, M. (2000). The international standard atmosphere (isa). *Anadolu University*, 26470.

[Christopher et al., 2010] Christopher, E., Thomas, L., and Hafid, S. (2010). Fault tolerant flight control–a benchmark challenge. *Lecture Notes in Control and Information Sciences*, 399.

[Christopher et al., 2013] Christopher, W., Mahesh, B., Paul, M., and Becher, T. (2013). 2011 trajectory based operations flight trials. In *10th USA/Europe Air Traffic Management Research and Development Seminar*.

[Collinson, 2011] Collinson, R. P. (2011). *Introduction To Avionics Systems*. Springer Science & Business Media.

[Cook, 2013] Cook, V. (2013). *Flight Dynamics Principles: A Linear Systems Approach to Aircraft Stability and Control*. Aerospace Engineering. Butterworth-Heinemann.

[Daidzic, 2015] Daidzic, N. E. (2015). Efficient general computational method for estimation of standard atmosphere parameters.

[De Prins et al., 2013] De Prins, J., Gomez Ledesma, R., and Mulder, M. (2013). Time-based arrival management concept with mixed fms equipage. In *Digital Avionics Systems Conference (DASC), 2013 IEEE/AIAA 32nd*, pages 1A3–1. IEEE.

[Ding et al., 2002] Ding, H., Lim, A., Rodrigues, B., and Zhu, Y. (2002). The airport gate assignment problem. *Dept. of Computer Science, University of Singapore*.

[Doc9750-AN/963, 2002] Doc9750-AN/963 (2002). Global air navigation plan for cns/atm systems.

[Donohue et al., 2000] Donohue, G., Brecht-Clarke, J., Fromme, W., Guffey, D., Lebron, J., Martel, N., Schonfield, P., Rakas, J., and Yazdani, A. (2000). Airspace and airports: Critical issues for the 21st century. *Transportation in the New Millennium*.

[Drouin, 2013]Drouin, A. (2013). Python aerospace toolbox. "Accessed on June 1st 2015".

[Duan et al., 2006] Duan, L., Lu, W., Mora-Camino, F., and Miguel, T. (2006). Flight-path tracking control of a transportation aircraft: Comparison of two nonlinear design approaches. In *25th Digital Avionics Systems Conference, 2006 IEEE/AIAA*, pages 1–9. IEEE.

[Duke et al., 1988] Duke, E. L., Antoniewicz, R. F., and Krambeer, K. D. (1988). Derivation and definition of a linear aircraft model.

[Durand et al., 1999] Durand, N., Alliot, J.-M., and Granger, G. (1999). Faces: A free flight autonomous and coordinated embarked solver. *ATC Quarterly*.

[Enea and Porretta, 2012] Enea, G. and Porretta, M. (2012). A comparison of 4d-trajectory operations envisioned for nextgen and sesar, some preliminary findings. In *28th Congress of the International Council of the Aeronautical Sciences*, pages 23–28.

[Etkin and Reid, 1996] Etkin, B. and Reid, L. D. (1996). *Dynamics Of Flight: Stability And Control*. Wiley New York.

[EUROCONTROL, 2010] EUROCONTROL (2010). *Airspace Concept Handbook for the Implementation of Performance Based Navigation (PBN)*. EUROCONTROL, 2 edition.

[EUROCONTROL, 2013] EUROCONTROL (2013). European airspace concept handbook for pbn implementation.

[EUROCONTROL, 2014] EUROCONTROL (2014). European route network improvement plan - part 1 european airspace design methodology - guidelines.

[EUROCONTROL, 2015a] EUROCONTROL (2015a). 2014 free route airspace target met. Access: 4 March 2015; URL: https://www.eurocontrol.int/news/2014-free-route-airspace-target-met.

[EUROCONTROL, 2015b] EUROCONTROL (2015b). European free route airspace developments. Technical Report Edition 1.0.

[EUROCONTROL, 2015c] EUROCONTROL (2015c). Free route airspace. URL: http://www.eurocontrol.int/news/free-route-airspace-sarajevo-zagreb-belgrade.

[FAA, 2012] FAA (2012). Concept of operations for nextgen alternative position, navigation, and timing (apnt). Technical report, Federal Aviation Administration.

[FAA, 2013] FAA (2013). *Pilot's Handbook Of Aeronautical Knowledge 2008*. CreateSpace Independent Publishing Platform, Lexington, KY.

[Foreman, 1998] Foreman, P. M. (1998). Proposed 'free flight' environment raises a number of pressing issues for the world's pilots. *ICAO Journal*, 53(5):9–12.

[Fr.mathworks.com, 2015] Fr.mathworks.com (2015). Implement quaternion representation of six-degrees-of-freedomequations of motion in earth-centered earth-fixed (ecef) coordinates - simulink.

[Glad and Harkegard, 2000] Glad, T. and Harkegard, O. (2000). Flight control design using backstepping.

[GPS, 2001] GPS (2001). GPWS explained. [Access: March 17, 2015], URL: http://www.boeing-727.com/Data/systems/infogpws.html.

[Hayman, 2009] Hayman, G. (2009). Trajectory based operations. [Online]Available: http://www.afceaboston.com/documents/events/cnsatm2009/Briefings/Tuesday%20Briefs/Tuesday%20Afternoon/Track%202/2 20TBO%20PresentationGeneHayman:pdf.

[Herndon, 2012] Herndon, A. A. (2012). Flight management computer (fmc) navigation database capacity. In *Integrated Communications, Navigation and Surveillance Conference (ICNS), 2012*, pages M6–1. IEEE.

[Hoekstra et al., 2001]Hoekstra, J., Ruigrok, R., and Van Gent, R. (2001). Free flight in a crowded airspace? *Progress in Astronautics and Aeronautics*, 193:533–546.

[IATA, 2014] IATA (2014). New IATA passenger forecast reveals fast-growing markets of the future. http://www.iata.org/pressroom/pr/pages/2014-10-16-01.aspx. access: Jan-Feb 2015.

[ICAO, 2013] ICAO (2013). Capacity & efficiency - pbn/cco/cdo. Access: 4 April 2015; URL: http://www.icao.int/NACC/Documents/eDOCS/ATM/ATM-Flyer_US-Letter_ANB-PBN_2013-08-26.pdf.

[ICAO, 2014] ICAO (2014). Global air navigation capacity and efficiency plan - 2013-2028. Doc 9750.

[John H. et al., 1998] John H., Anderson, J., Monique, C. A., Beverly Norwood, D., Elizabeth R., E., David B., G., and Belva M., M. (1998). National airspace system : Faa has implemented some free flight initiatives, but challenges remain. Technical Report GAO/RCED-98-246, Government Accountability Office.

[Kannan and Johnson, 2010] Kannan, S. K. and Johnson, E. N. (2010). Model reference adaptive control with a constrained linear reference model. In *Decision and Control (CDC), 2010 49th IEEE Conference on*, pages 48–53. IEEE.

[Kayton and Fried, 1997] Kayton, M. and Fried, W. (1997). *Avionics Navigation Systems*. A Wiley-Interscience publication. John Wiley & Sons.

[Khalil and Grizzle, 1996] Khalil, H. K. and Grizzle, J. (1996). *Nonlinear Systems*, volume 3. Prentice hall New Jersey.

[Kim et al., 2013] Kim, Y., Lee, S., Lee, K., and Kang, J.-Y. (2013). A development of 3-d resolution algorithm for aircraft collision avoidance. *International Journal of Aeronautical and Space Sciences*, 14(3):272–281.

[Kotecha and Hwang, 2009] Kotecha, P. and Hwang, I. (2009). Optimization based tube network design for the next generation air transportation system (nextgen). In *AIAA Guidance, Navigation, and Control Conference*, pages 10–13.

[Krstic et al., 1995] Krstic, M., Kanellakopoulos, I., and Kokotovic, P. V. (1995). *Nonlinear And Adaptive Control Design*. Wiley.

[Lee et al., 2008] Lee, P. U., Mercer, J., Gore, B., Smith, N., Lee, K., and Hoffman, R. (2008). Examining airspace structural components and configuration practices for dynamic airspace configuration. In *AIAA Guidance, Navigation, and Control Conference and Exhibit*, pages 18–21.

[Levine, 1999]Levine, W. S. (1999). *Control System Fundamentals*. CRC press.

[Lu et al., 2012] Lu, W.-C., El-Moudani, W., Revoredo, T. C., and Mora-Camino, F. (2012). Neural networks modelling for aircraft flight guidance dynamics doi 10.5028/jatm. 2012.04020712. *Journal of Aerospace Technology and Management*, 4(2):169–174.

[MacKunis et al., 2008] MacKunis, W., Kaiser, M., Patre, P., and Dixon, W. (2008). Asymptotic tracking for aircraft via an uncertain dynamic inversion method. In *American Control Conference, 2008*, pages 3482–3487. IEEE.

[Maggiore et al., 2003] Maggiore, M., Ordóñez, R., Passino, K. M., and Adibhatla, S. (2003). Estimator design in jet engine applications. *Engineering Applications of Artificial Intelligence*, 16(7):579–593.

[Meriweather, 2013] Meriweather, J. (2013). A320 flight control unit. [access: 04 June 2015]; URL: http://meriweather.com/flightdeck/320/glare/fcu.html.

[Miele, 1990] Miele, A. (1990). Optimal trajectories and guidance trajectories for aircraft flight through windshears. In *Decision and Control, 1990., Proceedings of the 29th IEEE Conference on*, pages 737–746. IEEE.

[Miller, 2011] Miller, C. J. (2011). Nonlinear dynamic inversion baseline control law: Architecture and performance predictions. *AIAA*, 6467:2011.

[Monteiro, 2015] Monteiro, J. (2015). Collaborative navigation in flow corridors. Project memoir, Adv. Master Communication, Navigation, Surveillance and Satellite Applications for Aviations, Ecole National Aviation Civile (ENAC), Toulouse.

[Mora-Camino, 2014] Mora-Camino, F. (2014). Flight control system lecture notes. ENAC/MAIAA.

[Mulgund and Stengel, 1996] Mulgund, S. S. and Stengel, R. F. (1996). Optimal nonlinear estimation for aircraft flight control in wind shear. *Automatica*, 32(1):3–13.

[Mutuel et al., 2013] Mutuel, L. H., Neri, P., and Paricaud, E. (2013). Initial 4d trajectory management concept evaluation. In *Tenth USA/Europe Air Traffic Management Research and Development Seminar (ATM2013) Airport*.

[Novacek, 2006] Novacek P. Terrain Awareness and Warning Systems—TAWS, Buyer's Guide. Pilot's Guide To Avionics Magazine. ed. 05-06.

[NASA : Virtual Skies, 2015] NASA : Virtual Skies (2015). Air traffic management. [access 10 May 2015], URL: http://virtualskies.arc.nasa.gov/atm/6.html,.

[Nelson, 1998] Nelson, R. (1998). *Flight Stability and Automatic Control*. McGraw-Hill International Editions. McGraw-Hill International Editions.

[NextGEN, 2010] NextGEN (2010). Concept of operations for the next generation air transportation system, version 3.2. Technical report, NextGen.

[Niedermeier and Lambregts, 2012] Niedermeier, D. and Lambregts, A. A. (2012). Fly-by-wire augmented manual control-basic design considerations. *SSJ*, 100:7.

[Nolan, 2010] Nolan, M. (2010). *Fundamentals Of Air Traffic Control*. Cengage Learning.

[Nolan and Ballinger, 2015] Nolan, M. and Ballinger, L. (2015). *A Career in Air Traffic Control*. eAcademicBooks LLC.

[Noureldin et al., 2013] Noureldin, A., Karamat, T. B., and Georgy, J. (2013). *Fundamentals Of Inertial Navigation, Satellite-based Positioning And Their Integration*. Springer.

[Paielli and Erzberger, 1997] Paielli, R. A. and Erzberger, H. (1997). Conflict probability for free flight. *Journal of Guidance, Control, and Dynamics*, 20(3):588–596.

[Papageorgiou and Glover, 2004] Papageorgiou, C. and Glover, K. (2004). Robustness analysis of nonlinear dynamic inversion control laws with application to flight control. In *Decision and Control, 2004. CDC. 43rd IEEE Conference on*, volume 4, pages 3485–3490. IEEE.

[Psiaki and Park, 1992] Psiaki, M. L. and Park, K. (1992). Thrust laws for microburst wind shear penetration. *Journal of Guidance, Control, and Dynamics*, 15(4):968–975.

[Radišic, 2014] Radišic, T. (2014). *The Effect of Trajectory-based Operations on Air Traffic Complexity*. PhD thesis, Fakultet prometnih znanosti, Sveucilište u Zagrebu.

[Ramalhinho Dias Lourenço and Serra, 1998] Ramalhinho Dias Lourenço, H. and Serra, D. (1998). Adaptive approach heuristics for the generalized assignment problem. *Economics Working Paper*, 288.

[Ramamoorthy et al., 2004] Ramamoorthy, K., Crassidis, J. L., and Singh, T. (2004). Potential functions for en-route air traffic management and flight planning. In *AIAA Guidance, Navigation, and Control Conference and Exhibit*, pages 1–12.

[Romeijn and Morales, 2000] Romeijn, H. E. and Morales, D. R. (2000). A class of greedy algorithms for the generalized assignment problem. *Discrete Applied Mathematics*, 103(1):209–235.

[Schwarz, 1996] Schwarz, K.-P. (1996). Aircraft position and attitude determination by gps and ins. *International Archives of Photogrammetry and Remote Sensing*, 31:67–73.

[SESARJU, 2013] SESARJU (2013). Sesar: Single european sky atm research. [ONLINE] Available: http://www.sesarju.eu/.

[Sforza, 2014] Sforza, P. M. (2014). *Commercial Airplane Design Principles*. Elsevier.

[Shankar and Yedavalli, 2009] Shankar, P. and Yedavalli, R. (2009). Neural-network-based observer for turbine engine parameter estimation. *Proceedings of the Institution of Mechanical Engineers, Part I: Journal of Systems and Control Engineering*, 223(6):821–832.

[Shen, 1995] Shen, T.-J. (1995). *Les Réseaux De Neurones Affinés Et Leur Application à La Commande Automatique Du Vol*. PhD thesis.

[Slotine et al., 1991] Slotine, J.-J. E., Li, W., et al. (1991). *Applied Nonlinear Control*, volume 60. Prentice-Hall Englewood Cliffs, NJ.

[Spitzer, 2001]Spitzer, C. (2001). *The Avionics Handbook*. The electrical engineering handbook series. CRC PressI Llc.

[STATFOR, 2013] STATFOR (2013). Task 4 report "european air traffic in 2035", challenges of growth 2013 reports.

[Stengel and Psiaki, 1985] Stengel, R. and Psiaki, M. (1985). Analysis of aircraft control strategies for microburst encounter. *Journal of Guidance, Control, and Dynamics*, 8(5):553–559.

[Stevens and Lewis, 2003] Stevens, B. L. and Lewis, F. L. (2003). *Aircraft Control And Simulation*. John Wiley & Sons.

[Takeichi et al., 2012] Takeichi, N., Nakamura, Y., and Fukuoka, K. (2012). Fundamental characteristics of decentralized air traffic flow control in high density corridor. In *28th International Congress of the Aeronautical Sciences*.

[Todorov, 2009] Todorov, T. (2009). Airspace design : Route design. ACAC ATFM Workshop.

[Tribble et al., 2002] Tribble, A. C., Lempia, D., and Miller, S. P. (2002). Software safety analysis of a flight guidance system. In *Digital Avionics Systems Conference, 2002. Proceedings. The 21st*, volume 2, pages 13C1–1. IEEE.

[Walter, 2014] Walter, W. (2014). Icao pbn concepts, benefits and objective. AFCAC/ICAO Joint Workshop.

[Wikipedia, 2015a] Wikipedia (2015a). Electronic flight instrument system. [access: 04 June 2015]; URL: https://fr.wikipedia.org/wiki/Syst%C3%A8me_de_gestion_de_vol.

[Wikipedia, 2015b] Wikipedia (2015b). Greedy algorithm. [access: 3 February 2014]; URL:https://en.wikipedia.org/wiki/Greedy_algorithm.

[Wikipedia, 2015c] Wikipedia (2015c). Primary flight display. [access: 04 June 2015]; URL: https://fr.wikipedia.org/wiki/Syst%C3%A8me_de_gestion_de_vol.

[Wikipedia, 2015d] Wikipedia (2015d). Systeme de gestion de vol. [access: 04 June 2015]; URL: https://fr.wikipedia.org/wiki/Syst%C3%A8me_de_gestion_de_vol.

[Wikipedia, 2015e] Wikipedia (2015e). Traffic collision avoidance system. [access: 04 July 2015]; URL: https://en.wikipedia.org/wiki/Traffic_collision_avoidance_system.

[Wing et al., 2008] Wing, D. J., Smith, J. C., and Ballin, M. G. (2008). Analysis of a dynamic multi-track airway concept for air traffic management.

[Xue and Kopardekar, 2009] Xue, M. and Kopardekar, P. H. (2009). High-capacity tube network design using the hough transform. *Journal of guidance, control, and dynamics*, 32(3):788–795.

[Yang et al., 2014] Yang, I., Lee, D., and Han, D. S. (2014). Designing a robust nonlinear dynamic inversion controller for spacecraft formation flying. *Mathematical Problems in Engineering*, 2014.

[Ye et al., 2014] Ye, B., Hu, M., and Shortle, J. F. (2014). Collision risk-capacity tradeoff analysis of an en-route corridor model. *Chinese Journal of Aeronautics*, 27(1):124–135.

[Yousefi et al., 2010] Yousefi, A., Lard, J., and Timmerman, J. (2010). Nextgen flow corridors initial design, procedures, and display functionalities. In *29th Digital Avionics Systems Conference*. AIAA/IEEE Salt Lake City, UT.

[Yousefi and Zadeh, 2013] Yousefi, A. and Zadeh, A. N. (2013). Dynamic allocation and benefit assessment of nextgen flow corridors. *Transportation Research Part C: Emerging Technologies*, 33:297–310.

[Zhang, 2014] Zhang, Y. (2014). Methodology for collision risk assessment of an airspace flow corridor concept.

[Zhi-jun et al., 2009] Zhi-jun, Y., Xiao-hui, Q., and Gan-lin, S. (2009). Model-following sliding mode controller design for flight control systems with wind disturbances. In *Industrial Electronics and Applications, 2009. ICIEA 2009. 4th IEEE Conference on*, pages 287–291. IEEE.

APPENDIX A
NONLINEAR DYNAMIC INVERSION

Appendix A: Nonlinear Dynamic Inversion

Feedback linearization is an approach to nonlinear control design that algebraically transforms nonlinear systems dynamics into (fully or partly) linear ones, so that linear control techniques can be applied. [Krstic et al., 1995],[Slotine et al., 1991] and [Khalil and Grizzle, 1996] are some references that introduce nonlinear dynamic inversion. Here we restrict the class of nonlinear systems which are linear with respect to the manipulated input (control-affine systems).

Before continuing to the introduction to Nonlinear Dynamic Inversion, it is important to show some mathematical tools from differential geometry and topology [Slotine et al., 1991]: Lie Derivatives and Lie Brackets.

A1. Lie Derivatives and Lie Brackets

In describing these mathematical tools, a vector function will be called $\boldsymbol{f}$**:** $\mathbf{R}^n \rightarrow \mathbf{R}^n$ a *vector field* in $\mathbf{R}^n$, to be consistent with the terminology used in differential geometry. The intuitive reason for this term is that to every vector function, $\boldsymbol{f}$ corresponds to a field of vectors in an *n*-dimensional space. In the following, we shall only be interested in *smooth* vector fields. By smoothness of a vector field, we mean that the function $\boldsymbol{f}(\mathbf{x})$ has continuous partial derivatives of any required order.

Given a smooth scalar function *h(x)* of the state x, the gradient of *h* is denoted by ∇h

$$\nabla h = \frac{\partial h}{\partial x}$$

The gradient is represented by a *row-vector* of elements $(\nabla h)_j = \partial h / \partial x_j$. Similarly, given a vector field *f(x)*, the Jacobian of $\boldsymbol{f}$ is denoted by $\nabla \boldsymbol{f}$

$$\nabla f = \frac{\partial f}{\partial x}$$

It is represented by an *n* x *n* matrix of elements $(\nabla \boldsymbol{f})_{ij} = \partial f / \partial x_j$.

Given a scalar function $h(x)$ and a vector field $f(x)$, we define a new scalar function $L_f h$, called the Lie derivative (or simply, the derivative) of h with respect to f.

Definition: Let $h : \mathbf{R}^n \rightarrow \mathbf{R}$ be a smooth scalar function, and f: $\mathbf{R}^n \rightarrow \mathbf{R}^n$ be a smooth vector field on $\mathbf{R}^n$, then the **Lie derivative** of h with respect to f is a scalar function defined by $L_f h = \nabla h f$.

Thus, the Lie derivative $L_f h$ is simply the directional derivative of h along the k direction of the vector f. Repeated Lie derivatives can be defined recursively

$$L_f{}^0 h = h$$

$$L_f{}^i h = L_f (L_f{}^{i-1} h) = \nabla (L_f{}^{i-1} h) f \qquad \text{for } i = 1, 2, \ldots$$

Similarly, if g is another vector field, then the scalar function $L_g L_f h(x)$ is

$$L_g L_f h = \nabla (L_f h) g$$

Let us move on to another important mathematical operator on vector fields, the Lie bracket.

Definition: Let f and g be two vector fields on R^n. *The **Lie bracket*** of f and g is a third vector field defined by:

$$[f, g] = \nabla g f - \nabla f g$$

The Lie bracket $[f, g]$ is commonly written as ad_f g (where *ad* stands for "adjoint").

Repeated Lie brackets can then be defined recursively by:

$$ad_f{}^0 g = g$$

$$ad_f{}^i g = [f, ad_f{}^{i-1} g] \qquad \text{for } i = 1, 2, \ldots$$

The following are Lie brackets properties which will be useful later.

(i) **bilinearity:**

$$[\alpha_1 f_1 + \alpha_2 f_2, g] = \alpha_1 [f_1, g] + \alpha_2 [f_2, g]$$

$$[f, \alpha_1 g_1 + \alpha_2 g_2] = \alpha_1 [f, g_1] + \alpha_2 [f, g_2]$$

where f ,f_1, f_2,g,g_1 and g_2 are smooth vector fields and α_1 and α_2 are constant scalars.

(ii) skew-commutativity:

$[f, g] = - [g, f]$

(iii) Jacobi identity:

$$L_{ad_f g} h = L_f L_g h - L_g L_f h$$

where $h(x)$ is a smooth scalar function of x.

A2. Nonlinear Dynamic Inversion

Nonlinear dynamic inversion is a control technique where the output, y, of the dynamic system is differentiated until the physical input, u, appears in the r^{th} derivative of y. Then u is chosen to yield a transfer function from the "synthetic input", v, to the output y. Consider an input-output linearization for a Single-Input Single-Output (SISO) nonlinear system:

$$\dot{x} = f(x) + g(x)u$$
$$y = h(x)$$

where $f(x)$ is the nonlinear state equation matrix, $g(x)$ is the controller matrix and u is the input. y is the output and $h(x)$ is the output matrix. According to the notation from the Lie derivatives, the scalar function h with respect to the vector field f is defined as

$$L_f^1 h(x) = \frac{\partial h}{\partial x} f(x)$$

if we differentiate y with respect to x, we have

$$\dot{y} = \frac{\partial h}{\partial x} \dot{x} = L_f^1 h + L_g(h)u = L_f^1 h \quad \text{if } L_g(h)u = 0$$

If $L_g h=0$, it means that the first derivative of y is not related to the input, therefore further differentiation of output y needs to be done until the input appears. We will end up with the following set of equalities such as:

$$y = h(x) = L_f^0 h$$
$$\dot{y} = L_f^1 h + L_g(h)u = L_f^1 h \quad \text{with} \quad L_g(h)u = 0$$
$$\ddot{y} = L_f^2 h + L_g(L_f^1 h)u = L_f^2 h \quad \text{with} \quad L_g(L_f^1 h)u = 0$$

continue the differentiation up to

$$y^{(r)} = L_f^r h + L_g(L_f^{(r-1)}h)u = v \quad \text{with} \quad L_g(L_f^{(r-1)}h)u \neq 0$$

r is the relative degree of $y=h(x)$ if $L_g(L_f^{(r-1)}h)u \neq 0$. $v(x)$ is the control law which is design using any linear controller design method. Then using the control input, it can cancel the nonlinearities and obtain the simple input-output relation such as:

$$u = \frac{1}{L_g(L_f^{(r-1)}h)}(v - L_f^r h)$$

The control law, v, can be chosen such as:

$$v = -\sum_{k=0}^{r-1} c_k L_f^k(h)$$

for a given guidance objectives, the output dynamic is given as:

$$y^{(r)} - v = y^{(r)} + c_{r-1}y^{(r-1)} + \cdots + c_1 y^{(1)} + c_0 y = 0$$

If r, the relative degree, is less than n, the order of the system, then there will be internal dynamics. These internal dynamics need to be bounded to ensure the stability of the systems. If $r = n$, then the system is fully observable. This method can be extended to the multi-input multi-output system such that system must be a square system, where the numbers of inputs are equal to the numbers of outputs. We shall have the following equations:

$$\dot{x} = f(x) + \sum_{i}^{m} g_i(x) u_i$$
$$y = h_i(x)$$

where *i* denotes the variables. The derivatives can be written as:

$$y_k^{r_k} = L_f^{r_k} h + \sum_{i=1}^{m} L_{g_i}(L_f^{r_k}(h_k)) u_i \qquad \text{where} \qquad L_{g_i}(L_f^{r_k}(h_k)) \neq 0$$

where r_k is the relative degree of each output. The input output linearization can be written in the form of:

$$\begin{bmatrix} \frac{d^{r_1} y_1}{dt^{r_1}} \\ \vdots \\ \frac{d^{r_m} y_m}{dt^{r_m}} \end{bmatrix} = \begin{bmatrix} L_f^{r_1}(h_1) \\ \vdots \\ L_f^{r_m}(h_m) \end{bmatrix} + \begin{bmatrix} L_{g_1}(L_f^{r_1-1}(h_1)) & \cdots & L_{g_m}(L_f^{r_1-1}(h_1)) \\ \vdots & \ddots & \vdots \\ L_{g_1}(L_f^{r_m-1}(h_m)) & \cdots & L_{g_m}(L_f^{r_m-1}(h_m)) \end{bmatrix} \begin{bmatrix} u_1 \\ \vdots \\ u_m \end{bmatrix} = \begin{bmatrix} v_1 \\ \vdots \\ v_m \end{bmatrix}$$

this can be rewritten as:

$$y^r = l(x) + J(x) \cdot u = v$$

where *J(x)* is called the input/output control matrix which should be non-singular to be able to compute. Just like in the SISO presentation, the control law *v* can be design according to any linear design method to obtain the following:

$$u = J(x)^{-1}(v - l(x))$$

The relative degree of the system is given as the total relative degree of each output:

$$r_T = \sum_{k-1}^{m} r_k$$

APPENDIX B
RESEARCH CIVIL AIRCRAFT MODEL (RCAM) DATA

APPENDIX B: Research Civil Aircraft Model (RCAM) Data

In this thesis, the model of aircraft used is taken from Research Civil Aircraft Model (RCAM) provided by GARTEUR [Bennani and Looye, 1998] and adapted to the objectives. The following tables list the aircraft configuration and aerodynamic data.

Table B.0.1: Aircraft Configuration

Symbol	Name	Default value	Unit
mass	aircraft total mass	120 000	*kg*
$\overline{c}$	mean aerodynamic chord	6.6	*m*
S	wing planform area	260.0	m^2
I_x	inertia tensor about x-axis	40.07 x *mass*	$kg.m^2$
I_y	inertia tensor about y-axis	64 x *mass*	$kg.m^2$
I_z	inertia tensor about z-axis	99.92 x *mass*	$kg.m^2$
I_{xz}	inertia tensor about xz-axis	-2.0923 x *mass*	$kg.m^2$

Table B.0.2: Aerodynamic Data

Aerodynamic Coefficient	Value
C_{lo}	1.02
$C_{l\alpha}$	6.07
C_{lq}	32.24
C_{do}	0.15
$C_{d\alpha}$	0.5
$C_{d\alpha}{}^2$	2.1175
C_{yo}	0
$C_{y\beta}$	-1.6